INVESTIGATION OF MECHANOTRANSDUCTORY MECHANISMS IN THE PATHOGENESIS OF LUNG FIBROSIS

A Dissertation

Presented to

The Academic Faculty

by

Vincent F. Fiore

In Partial Fulfillment

of the Requirements for the Degree

Doctor of Philosophy in the

School of Biomedical Engineering

Georgia Institute of Technology

May, 2014

INVESTIGATION OF MECHANOTRANSDUCTORY MECHANISMS IN THE PATHOGENESIS OF LUNG FIBROSIS

Approved by:

Dr. Thomas Barker, Advisor
Department of Biomedical Engineering
Georgia Institute of Technology

Dr. Andrés García
School of Mechanical Engineering
Georgia Institute of Technology

Dr. Philip Santangelo
Department of Biomedical Engineering
Georgia Institute of Technology

Dr. Cheng Zhu
Department of Biomedical Engineering
Georgia Institute of Technology

Dr. James Hagood
Department of Pediatrics
University of California, San Diego

Date Approved: February 14, 2014

To those who have traveled this road before, and to those who will follow.

ACKNOWLEDGEMENTS

I would like to acknowledge and thank those, without whom the completion of this Ph.D. would not have been possible. To my family, whose unconditional support helped motivate me, especially through the difficult times, thank you. I would like to acknowledge my friends, both prior to arriving in Atlanta and those throughout my time here, for keeping life outside of the lab fun, exciting, and a necessary change of pace. I would like to thank my adviser, Tom, for giving me the flexibility and independence to approach my research with passion and creativity; I will carry this, and the confidence it has instilled, with me throughout my career. I would like to thank my entire committee for their thoughtful and critical review of this work and professional guidance. Most of all, I would like to thank Alison, whose constant companionship kept me grounded, happy, and healthy throughout the most difficult years of this journey.

TABLE OF CONTENTS

LIST OF FIGURES

LIST OF SYMBOLS AND ABBREVIATIONS

2D	Two-dimensional
3D	Three-dimensional
AFM	Atomic force microscope
BSA	Bovine serum albumin
CAF	Carcinoma-associated fibroblast
COP	Cryptogenic organizing pneumonia
CDM	Cell-derived matrix
DRM	Detergent-resistant membrane
E	Young's modulus
ECM	Extracellular matrix
EDA-Fn	Extra domain A-containing fibronectin
FA	Focal adhesion
FAK	Focal adhesion kinase
Fn	Fibronectin
IPF	Idiopathic pulmonary fibrosis
IPFLF	IPF lung fibroblast
kPa	Kilopascal
NLF	Normal lung fibroblast
pAAm	Polyacrylamide
PLA	Proximity ligation assay
pMLF	Primary mouse lung fibroblast
PGE_2	Prostaglandin E_2
SFK	Src family kinase
SYF	Src/Yes/Fyn-/- fibroblasts
Thy-1^{pos}	Thy-1-positive fibroblasts
Thy-1^{neg}	Thy-1-negative fibroblasts
UIP	Usual interstitial pneumonitis

SUMMARY

Tissue fibrosis, or the formation of scar tissue, is a necessary physiological process during tissue repair. However in the pathological setting, excessive scar tissue formation disrupts tissue architecture and function, and is a major cause of mortality associated with numerous human diseases. However, the physiological processes underlying the resultant outcome of progressive and fatal fibrosis versus reparative scar tissue formation remain poorly understood.

In the process of fibrosis, remodeling and deposition of the extracellular matrix (ECM) results in stiffening of the tissue, as is commonly associated with scar tissue. Cells also respond to these changes in the stiffness of their environment through engagement of their cytoskeleton and signaling of cell-ECM contacts. Increasing ECM stiffness results in activation of fibroblasts, which are the tissue-resident cells responsible for scar tissue formation. Thus, understanding to what extent the stiffness of the cellular environment changes as a consequence of fibrotic progression, and how cells respond to this change, is critical.

In this thesis, we quantitatively measured stiffness of the lung parenchyma and its change during fibrosis. We find that the average stiffness increases by approximately 10-fold. We then investigated how changes in ECM rigidity affect the cytoskeletal phenotype of fibroblasts. We find a complex relation between expression of the glycoprotein Thy-1 (CD90) and ECM rigidity-dependent cytoskeletal phenotype (i.e. "rigidity sensing"). Finally, we investigate a mechanism for the regulation of rigidity sensing by Thy-1 and its involvement in intracellular signaling through cell-ECM contacts. Taken together, this work helps define *in vivo* parameters critical to the fibrogenesis program and to define unique cellular phenotypes that may respond or contribute to mechanical homeostasis in disease.

CHAPTER 1 INTRODUCTION

1.1 Specific aims

Fibrosis of vital organs remains one of the leading causes of death in the developed world, where it occurs predominantly in soft tissues (liver, lung, kidney, heart, skin) through fibroblast proliferation and deposition of extracellular matrix (ECM) (Bitterman and Henke 1991, Ghosh, Quaggin et al. 2013). Especially problematic are chronic fibrotic disorders, where unrelenting fibrotic remodeling disturbs normal tissue architecture and impairs organ function. Idiopathic pulmonary fibrosis (IPF) is a progressive and fatal fibrotic disorder of the lung parenchyma resulting in respiratory failure. Due to a lack of understanding of the pathogenesis of this disease, pharmacological therapies remain ineffective, with a median survival time of 3 years post-diagnosis, and whole organ transplantation is the only viable option for treatment (King, Pardo et al. 2011).

As with all fibrotic disorders, significant remodeling of the ECM results in alterations to the mechanical properties of tissue (Hinz 2010). This is of pathophysiologic interest, as alterations in extracellular mechanics (e.g. rigidity) significantly modify cell behaviors. For instance, increased ECM rigidity supports fibroblast activation to a proliferative and matrix synthetic state (Tomasek, Gabbiani et al. 2002, Liu, Mih et al. 2010, Tschumperlin, Liu et al. 2013). Thus, the extracellular matrix (ECM) exists as both a biochemical and mechanical environment; cells are able to sense and respond to the mechanical properties of the ECM, giving rise to developmentally-regulated and/or pathological processes. However, the range of tissue stiffness cells encounter in the lung *in vivo*, both during normal physiological processes and during disease progression, are unknown.

The connective tissue deposition observed in fibrosis is the result of resident fibroblasts synthesizing, assembling, and remodeling the ECM. It has long been established that subpopulations of fibroblasts exist within the lung, depending on their anatomical location, functional requirements, and gene expression profiles (Sorrell and Caplan 2009). Studies have previously demonstrated that a subpopulation of fibroblasts lacking cell surface expression of glycoprotein Thy-1 (CD90) preferentially localize to regions of ongoing fibrogenesis *in vivo* (termed fibroblastic foci) and exhibit pro-fibrotic behaviors *in vitro* (Hagood, Prabhakaran et al. 2005, Sanders, Kumbla et al. 2007). However, detailed molecular mechanisms by which Thy-1 mediates its effects on downstream signaling are still largely unknown. Intriguingly, studies have demonstrated that Thy-1 expression modulates the assembly of stress fibers and focal adhesions, structures that enable cells to transduce ECM rigidity cues into biochemical signaling in a process termed 'mechanotransduction' (Barker, Grenett et al. 2004). As fibroblasts are both responsible for and sensitive to fibrosis-associated changes in ECM rigidity, understanding how fibroblasts "sense" and "respond" to rigidity is of critical importance in understanding IPF pathophysiology.

In this thesis, our objective was to further the understanding of IPF disease pathophysiology through the specific study of fibrosis-associated ECM rigidity and the phenotypic response of fibroblasts to this parameter. This was accomplished using quantitative bioengineering methodology in combination with standard cell biological approaches in a series of three (3) specific aims:

1. **To measure the rigidity of lung parenchyma and its change as a consequence of fibrosis in both preclinical and human patient models of pulmonary fibrosis.** These studies indicate a dramatic, but spatially heterogeneous increase in tissue rigidity due to fibrosis, with average tissue

stiffness increasing by approximately an order of magnitude (from ~2 to 20 kPa).

2. **To investigate Thy-1-dependent regulation of fibroblast cytoskeletal responses to alterations in ECM rigidity.** We find that Thy-1 promotes sensitive cytoskeletal remodeling in response to changes in ECM rigidity, within the range of rigidity identified *in vivo*. Additionally, we find that Thy-1 modulates mechanosensitive activation of the cytoskeletal regulator RhoA and promotes recruitment of Fyn to cell-ECM adhesions.

3. **To investigate the molecular interactions governing Thy-1-dependent Fyn recruitment to cell-ECM adhesions and downstream mechanotransduction.** We find that Thy-1 interacts with αvβ3 integrins within the plasma membrane via its integrin-binding motif. Both Thy-1's GPI anchor and integrin-binding motif are required for Fyn recruitment to cell-ECM adhesions, force-dependent RhoA activation, and sensitive cytoskeletal remodeling in response to changes in ECM rigidity.

1.2 Significance of Research

The underlying mechanisms governing chronic fibroproliferative disorders, such as IPF, are largely unknown (King, Pardo et al. 2011). Thus, pharmacological treatments are ineffective and diseases remain a significant medical and socioeconomic burden (Wynn 2007). It has long been recognized that tissue becomes stiffer as a result of fibrosis, however only recently has it been appreciated that such physical changes in the local tissue microenvironment may participate in disease pathogenesis (Tomasek, Gabbiani et al. 2002). Therefore, describing to what degree tissue rigidity changes as a consequence of fibrosis, and how this change influences cell-level behavior is a critical

first step in understanding specific and therapeutically-targetable mechanisms underlying the physical microenvironment's involvement in fibrotic progression.

Our first undertaking is to measure the changes in tissue rigidity, or Young's modulus (*E*), at the microscale-level during lung fibrosis. These values are critical in determining the properties of the local environment that cells interact with *in vivo*. These measured values of *E* can be used to model the microenvironmental rigidity of cells *in vitro*, and as a result, these values have been used across the field of lung mechanobiology to study the impact of tissue stiffness on cell physiology (Booth, Hadley et al. 2012, Huang, Yang et al. 2012, Brown, Fiore et al. 2013). This also enables future studies on normal lung cell physiology to more closely mimic *in vivo* settings.

A second goal of this project was to investigate the phenotype of Thy-1-expressing subpopulations in physiologic microenvironments, to better evaluate the pro-fibrotic phenotype of these disease-associated fibroblasts. This is towards the ultimate goal of understanding how pro-fibrotic cellular phenotypes may contribute to the fibrogenesis program *in vivo*. This is critical because fibroblasts are the drivers of fibrotic progression, and thus understanding how they sense and respond to disease-associated cues is essential.

Lastly, we investigated the molecular mechanisms by which Thy-1 alters fibroblast phenotype *in vitro*. This is aimed towards the significant and long-term goal of discovering novel molecular pathways for therapeutic intervention in IPF. This adds to the knowledge of molecular mechanisms that may be linked to IPF pathophysiology, enabling future studies into the discovery and testing of novel therapeutics.

CHAPTER 2 LITERATURE REVIEW

2.1 Tissue Fibrosis and Idiopathic Pulmonary Fibrosis

The spatial and structural architecture of tissue is tightly controlled during development and homeostasis, enabling proper fitness of the organism. Adult tissues, especially those in higher-order multicellular and mammalian organisms, exhibit extraordinary structure-function relationships that depend on the requirements of the underlying physiological process (Fuchs and Raghavan 2002). In many human diseases, these structure-function properties are dysregulated, leading to decline of tissue function and organism fitness.

Fibrosis is a common alteration of tissue structure-function in human diseases, with chronic fibroproliferative processes broadly contributing to nearly 45% of deaths in the developed world (Wynn 2007). During fibrosis, connective tissue is assembled and remodeled by activated fibroblasts in an effort to restore tissue integrity. This is an essential process in regulated wound healing, such that wounds in the adult typically heal as scars (Gurtner, Werner et al. 2008). However, significant accumulation of such scar tissue in the parenchyma disrupts physiologic tissue architecture and results in altered tissue/organ function. Fibrosis is not only a principal cause of tissue dysfunction in major vital organs, such as the lungs, liver, and heart, but also a critical component of cancer malignancy and certain neurologic disorders (Rolls, Shechter et al. 2009). Indeed, fibrosis of tissue surrounding a primary malignant cell mass, known as the tumor stroma, plays a critical role in priming cancer cells for malignancy and metastasis (Paszek, Zahir et al. 2005, Butcher, Alliston et al. 2009). Thus, fibrosis represents a major cause of human mortality worldwide, however the mechanisms underlying fibrogenesis, especially in the context of chronic fibroproliferative disorders, are incompletely understood.

A number of pulmonary disorders are characterized by fibrotic remodeling of the lung parenchyma, including idiopathic pulmonary fibrosis (IPF), asbestosis, and cryptogenic organizing pneumonia (COP). Prominent features of these disorders are excessive fibroblast proliferation and collagen deposition in the distal airspace and lung parenchyma following lung injury (Hardie, Glasser et al. 2009, Kis, Liu et al. 2011). IPF, characterized histologically by the lesion termed usual interstitial pneumonitis (UIP), has an annual death rate higher than that of Alzheimer's disease, and about half that of HIV infection (White, Lazar et al. 2003). IPF is chronic and unrelenting fibrogenesis within the alveolar structure, what is becoming more commonly thought of as a form of disordered wound healing. What is known of the pathophysiology of IPF is complex, involving the interplay of genetic predisposition, environmental factors, activation of parenchymal and immune effector cells, and the participation of a staggering number of soluble mediators and matrix components at the local and tissue level (Crouch 1990). Traditional therapy for interstitial lung diseases, consisting of corticosteroids and other immunomodulatory agents, are ineffective as these regimens do not treat the underlying pathology (Mapel, Samet et al. 1996). A recent randomized clinical trial for the combination treatment of prednisone, azathioprine, and antioxidant N-acetylcysteine was prematurely ended due to safety concerns and lack of efficacy in the control arm (Idiopathic Pulmonary Fibrosis Clinical Research, Raghu et al. 2012). In essence, both the etiology and pathogenesis of the disease are not fully understood, making treatment of symptoms and co-morbidities prohibitively difficult, while combatting underlying disease mechanisms even more so.

Potentially adding to the complexity, numerous recent publications suggest that the physical/mechanical properties of the ECM can regulate a host of cellular processes involved in fibrosis (Engler, Griffin et al. 2004, Levental, Yu et al. 2009, Liu, Mih et al. 2010, Booth, Hadley et al. 2012, Huang, Yang et al. 2012, Brown, Fiore et al. 2013).

Specifically, cells are able to sense the mechanical properties of the ECM, such as rigidity, and engage their actinomyosin contractile machinery in a manner that facilitates mechanical homeostasis between the cell and its environment (Pelham and Wang 1997, Paszek and Weaver 2004, Solon, Levental et al. 2007). These events have implications in the progression and treatment of fibrotic diseases, as fibrosis results in profound alterations in the mechanical properties of tissues. Indeed, Barry-Hamilton *et al*. recently demonstrated successful reduction of bleomycin-induced pulmonary fibrosis in a murine model, along with a marked reduction in activated fibroblasts and decreased TGFβ signaling, by inhibiting the matrix crosslinking enzyme lysyl oxidase-like-2, which decreases tissue stiffness (Levental, Yu et al. 2009, Barry-Hamilton, Spangler et al. 2010). Further implications of mechanical properties of the microenvironment on cell phenotype and fibrosis are discussed below.

The main effector cell in IPF is the fibroblast, as is evidenced by the name "fibrosis". Activated fibroblasts within UIP lesions, termed fibroblastic foci, exhibit a highly contractile and synthetic phenotype (Katzenstein and Myers 1998, Hardie, Glasser et al. 2009). Fibroblastic foci represent regions of ongoing fibrogenesis, an increased number of which are associated with a decline in lung function and an increased risk of mortality (King, Schwarz et al. 2001, Nicholson, Fulford et al. 2002). Proliferation and recruitment of resident fibroblasts, as well as excessive deposition and remodeling of collagens and fibronectin, leads to alveolar wall expansion and distortion of epithelial structures (White, Lazar et al. 2003). This is contrasted by the normal alveolus, in which sheet-like epithelial cells lie on a laminin/collagen IV-rich basement membrane in close proximity to capillary beds, allowing for the diffusive exchange of oxygen and carbon dioxide (**Figure 1**, (Fehrenbach 2001)). As a result of ECM remodeling and cellular activation, fibrotic lesions exhibit both a biochemical and biophysical microenvironment that is distinct from its physiologic counterpart, and thus fibroblasts, as well as epithelial,

endothelial, and immune cells within this changing microenvironment are exposed to altered instructive cues.

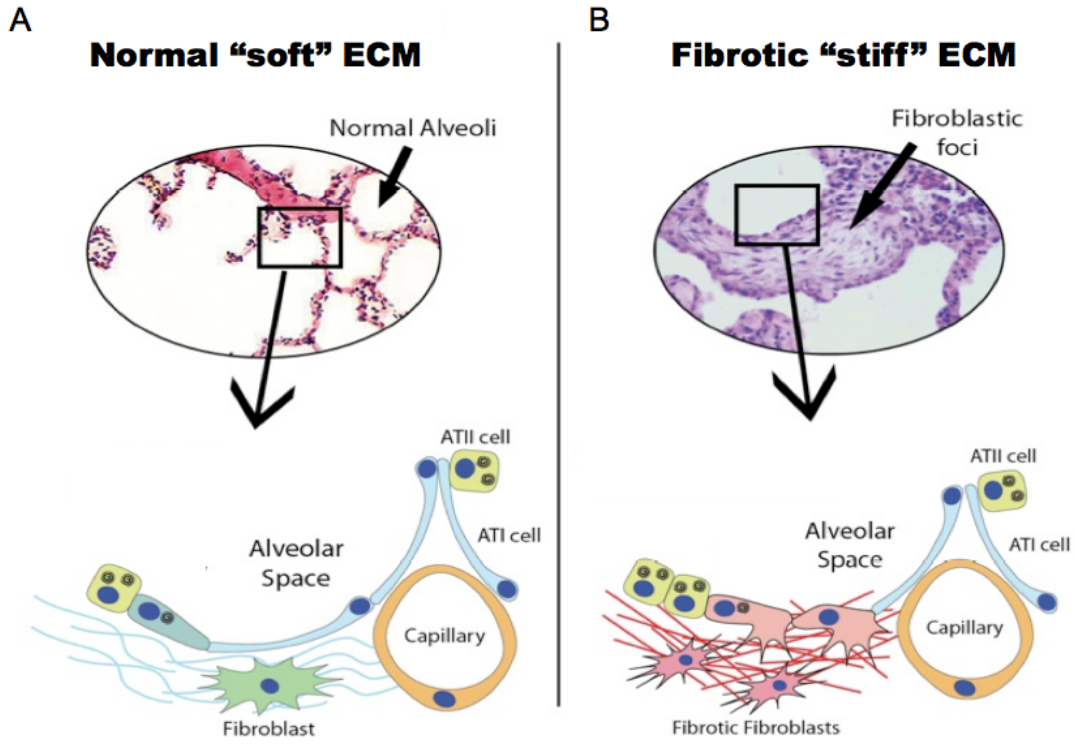

Figure 1: Schematic of fibrotic progression in the alveolar space. (A) Normal alveoli exhibit sheet-like epithelial cells on basement membrane. (B) Fibrotic regions undergo ECM remodeling and alveolar wall expansion.

2.2 Fibroblasts

2.2.1 Fibroblast function in normal physiology and pathophysiology

Fibroblasts are stroma resident cells responsible for much of the assembly and remodeling of ECM during development and adult homeostasis. Fibroblasts are defined as "cells that 1) synthesize and secrete a complex array of structural (e.g. collagens and fibronectin) and nonstructural (e.g., matricellular family of molecules such as thrombospondins, SPARC, and osteopontin) ECM molecules, 2) actively organize and

remodel the ECM through production of proteinases, and 3) converse with nearby cells through paracrine, autocrine, and other forms of communication"(Sorrell and Caplan 2009). Furthermore, fibroblasts are identified by their ability to migrate in response to directional cues and respond to the local mechanical environment (i.e. mechanotransduction). It is therefore apparent that fibroblasts are central to tissue and organ physiology.

Fibrosis is the result of aberrant and prolonged activation of fibroblasts. In IPF, the fibroblastic focus consists of fibroblasts or myofibroblasts (defined by *de novo* expression of α-smooth muscle actin and cellular fibronectin) in a fibronectin- and type I collagen-rich matrix (Kuhn and McDonald 1991). These cells proliferate and deposit ECM in the alveolar wall, supporting the primary role for this cell type in disease pathogenesis. Although studies support the general notion that IPF fibroblasts may display unique phenotypes from their normal counterparts (Miki, Mio et al. 2000, Ramos, Montano et al. 2001), large gaps in knowledge remain regarding what specific differences are responsible for progressive fibrosis versus the physiologic function of fibroblasts essential for normal lung repair. Given the distinctly heterogeneous nature of IPF, it is likely that cells from specific histological features vary in their phenotypic traits, and thus locally identifying cell phenotype with respect to disease features of interest is critical.

2.2.2 Stromal cell subpopulations *in vivo*

As the defining characteristics of fibroblasts are typically their spindle-shaped morphology, ability to adhere to plastic culture surfaces, and the absence of other lineage-specific markers, the diversity of such cells is typically slighted. Fibroblasts from distinct stromal tissues can exhibit significant phenotypic heterogeneity. For example skin fibroblasts differ from those from the lung in terms of morphology, proliferation rates, and synthesis of cytokines and ECM constituents (Sorrell and Caplan 2009).

Comparison of genome-wide mRNA expression profiles of fibroblasts from distinct anatomical locations has revealed divergence among a wide array of genes, from lipid metabolism to cell migration (Chang, Chi et al. 2002). This is perhaps unsurprising, as different anatomical locations have evolved with unique functions, and so fibroblasts within these compartments may be specialized to perform distinct roles. However, fibroblasts within the same stromal compartment can exhibit functional phenotypic differences as well. Clonal derivatives from skin, intestinal tissue, and lung have been demonstrated to differ in ECM component synthesis and assembly, epithelial-mesenchymal crosstalk, and secretion and responsiveness to cytokines (Fritsch, Orian-Rousseaul et al. 1999, Sorrell and Caplan 2009). This is further complicated by the fact that these cells can undergo phenotypic plasticity within their lifespan, dependent on microenvironmental cues. For example, carcinoma-associated fibroblasts can exhibit significant functional differences between those subpopulations promoting metastasis within tumor microenviroment versus non-malignant growth (Goetz, Minguet et al. 2011).

In the skin, distinct fibroblast lineages play unique roles in defining dermal architecture during skin development and repair. Fibroblasts arising from a single progenitor will go on to create two distinct fibroblast lineages in the mouse; one forms the upper dermis, including the dermal papilla and supports hair follicle growth and regeneration, whereas the reticular/hypodermal subpopulation will go on to synthesize the majority of fibrillar ECM and are the progenitors for pre-adipocytes within the hypodermis (Driskell, Lichtenberger et al. 2013). During wound healing, the initial wave of regeneration depends on cells of the reticular/hypodermal lineage elaborating a collagenous ECM, while upper cells become active later in the process to facilitate re-epithelialization and follicular morphogenesis.

Lung fibroblast subpopulations characterized by surface expression of Thy-1 represent an intriguing system of phenotypic subsets. *In vitro*, fibroblasts lacking expression of Thy-1 undergo enhanced proliferation and activation of pro-fibrotic cytokines in response to fibrogenic growth factors, such as platelet-derived growth factor-A (PDGF-A) and connective tissue growth factor (CTGF), and exhibit differential signaling responses to pro-inflammatory cytokines tumor necrosis factor-α (TNF-α) and interleukin-1β (IL-1β) (Hagood, Miller et al. 1999, Hagood, Lasky et al. 2001, Hagood, Mangalwadi et al. 2002, Zhou, Hagood et al. 2004). Of foremost clinical significance, Thy-1 expression is absent in fibroblasts within the fibroblastic foci IPF patients, whereas the majority of lung fibroblasts from healthy lung interstitium are Thy-1^{pos} (Hagood, Prabhakaran et al. 2005, Sanders, Pardo et al. 2008). Furthermore, Thy-1 knockout mice display more severe fibrosis in response to bleomycin challenge, a commonly used model for the induction of lung fibrosis, and regions of the interstitium undergoing fibrotic remodeling in wild-type mice are predominated by Thy-1^{neg} fibroblasts (Hagood, Prabhakaran et al. 2005). Therefore, Thy-1^{neg} fibroblasts represent a pro-fibrotic subset of cells that appear to play a central role in the pathophysiology of lung fibrosis.

2.3 Microenvironmental Changes During Fibrotic Progression

The cellular microenvironment is made up of soluble and substrate-bound macromolecules that impart strong control over resident cell phenotype. One major component of the microenvironment, apart from neighboring cells and local soluble signals, is the ECM. The ECM is a dynamic, multi-component scaffold that contains both biochemical and biophysical cues that modulate cell behavior through local interactions at the cell-ECM interface (Hynes 2009). Cells also assemble and remodel this structure in a continuous fashion during development and throughout the lifetime of

the organism (Larsen, Artym et al. 2006). Thus, cells possess the ability to communicate bidirectionally with the ECM, both instructing the local environment through modulation of ECM parameters, while also being exquisitely sensitive to these changes. To accomplish this task, cells possess a system of molecules and complexes that coordinate signaling responses from the ECM and also participate in local remodeling of the ECM (Miyamoto, Katz et al. 1998). Integrins are the major class of cell surface ECM receptors used in this process, which together with their accessory molecules, orchestrate this bidirectional communication and will be the topic of further discussion below.

As a consequence of fibrogenesis, major changes occur to the biochemical and biophysical properties of the ECM. The abundance of connective tissue deposited by fibroblasts results in an increase in the amount of fibrous ECM protein, predominantly type I-III collagens (Tomasek, Gabbiani et al. 2002), thereby altering ligand presentation and topology within the microenvironment. This is concomitant with an increase in tissue rigidity, as the amount of collagen I scales linearly with tissue rigidity over three orders of magnitude and is largely responsible for the tensile strength of tissues (Swift, Ivanovska et al. 2013). Enzymatic crosslinking of ECM fibers can further increase tissue rigidity. Both tumors and scars have long been recognized as mechanically stiffer than normal tissue, a property that has aided in the detection and resection of diseased tissue (Butcher, Alliston et al. 2009). However, it is now appreciated that changes in tissue rigidity accompanying fibrosis may provide a driving force for disease progression. During mammary tumorigenesis, stiffening of the tumor stroma, for instance due to enhanced ECM deposition and crosslinking by carcinoma-associated fibroblasts (CAFs), enhances integrin signaling in non-malignant mammary epithelial cells through extracellular-related kinase and focal adhesion kinase (FAK) (Levental, Yu et al. 2009). This can promote malignant transformation of the tumor (Paszek, Zahir et al. 2005). Furthermore, the specific adhesion- and integrin-signaling phenotype of CAFs can

regulate this cell-ECM bidirectional communication to either promote or inhibit malignancy. For example, stroma associated with breast carcinomas and metastatic melanoma is enriched in CAFs expressing high levels of caveolin-1, which promote ECM remodeling to favor directional migration and invasion of carcinoma cells (Goetz, Minguet et al. 2011).

Previous studies have demonstrated that tissue compliance decreases as a consequence of IPF disease progression. This was demonstrated at the whole organ level through lung pressure-volume measurements (i.e. plethysmography) from IPF patients, where lung compliance was seen to decrease by more than 30% and was the most strongly correlated pulmonary function parameter with the extent of fibrosis (Sansores, Ramirez-Venegas et al. 1996). Similarly, tensile-stress testing of lung tissue strips from rats after bleomycin-induced fibrosis gave quantitative values of tissue elasticity (i.e. Young's modulus), showing a significant increase as a result of fibrosis. Values for these bulk segments of tissue and were determined to increase by 2-fold, from approximately 5 to 10 kPa, between normal and bleomycin-treatment groups (Dolhnikoff, Mauad et al. 1999, Ebihara, Venkatesan et al. 2000).

In response to these increases in ECM stiffness, a number of pro-fibrotic cellular responses occur. Fibroblasts increase their expression of α-smooth muscle actin (α-SMA), which promotes further activation of cytoskeletal machinery (Hinz, Celetta et al. 2001, Goffin, Pittet et al. 2006). Enhanced polymerization of F-actin leads to translocation of the cytoplasmic G-actin-bound transcription factor MRTF-A into the nucleus, where it complexes with serum response factor and drives α-SMA gene expression (Huang, Yang et al. 2012). Both fibroblasts and type II alveolar epithelial cells activate the pro-fibrotic cytokine TGF-β to a greater extent (Wipff, Rifkin et al. 2007). We have demonstrated that ECM stiffness promotes alveolar epithelial-to-mesenchymal transition through enhanced αvβ6 integrin-mediated activation of latent

TGF-β from ECM (Brown, Fiore et al. 2013). Importantly, cytoskeletal contractility and Rho-mediated signaling are necessary for stiffness-induced EMT and latent TGF-β activation.

In fibroblasts, matrix stiffening promotes fibroblast proliferation and matrix synthesis through suppression of COX-2 and prostaglandin E_2 (PGE_2) expression, importantly linking matrix stiffness and fibroblast proliferation (Liu, Mih et al. 2010). In contrast, physiologic stiffness enhances COX-2 and PGE_2 expression, which promotes fibroblast quiescence and inhibits assembly of mature cytoskeletal structures. One of the common features of these studies is that ECM stiffening results in phenotypic changes that further promote cytoskeletal activity, pro-fibrotic ECM remodeling, and fibroblast proliferation. This demonstrates a feedback loop between the biophysical state of the ECM and the activation state of the cytoskeleton that, in the case of fibrosis, may become positive and lead to system instability, i.e. chronic fibrotic remodeling. Interestingly, how the microenvironment is initially remodeled during the wound healing/fibrotic processes that result in changes from an initially physiologic rigidity regime to a disease-associated and pro-fibrotic state is unknown. However, it must be stated the majority of studies investigating the physiology and disease-associated cell behavior *in vitro* have been performed on rigid glass or plastic materials. In fact, simply removing mesenchymal cells from their *in vivo* microenvironment results in dramatic activation of the cytoskeleton, hypertrophy, and changes in gene expression reminiscent of myofibroblast differentiation associated with fibrosis (Balestrini, Chaudhry et al. 2012).

The local rigidity of the environment of the cell is bi-directionally regulated during normal tissue homeostasis and disease progression by adhesion complexes that link that ECM to the cytoskeleton. This regulation is bi-directional: the cell (e.g. fibroblast) assembles and remodels the ECM, thereby changing its material properties, and the cell is also exquisitely sensitive to changes in the material properties of its

substratum. In other words, the cell both senses and controls the rigidity its microenvironment.

2.4 Cellular Responses to ECM Mechanics

2.4.1 Global cell phenotypic responses

Of the many parameters characterizing the material properties of biological tissue, including viscosity, strength, topology, porosity, etc., stiffness or rigidity is perhaps the most widely investigated. As a measure of the extent to which an object resists elastic deformation under an applied force, the elastic modulus has emerged as a critical regulator of cell behavior (Discher, Janmey et al. 2005). Investigation into the cellular responses to ECM rigidity has yielded multiple phenotypic outputs that are modulated by this parameter, including migration, differentiation, proliferation, and apoptosis. As may be expected, many of these phenotypes are intimately connected with the cytoskeleton, which is largely responsible for a cell's own mechanical properties and its ability to perform mechanical work (Ingber 2003, Yeung, Georges et al. 2005). Although the molecular and biophysical details of how a cell senses and responds to its mechanical environment are ongoing, a generalizable description is that a cell probes the mechanics of the ECM by generating forces within the cytoskeleton that are transmitted to the ECM through protein complexes that are also biochemically sensitive to these forces (Moore, Roca-Cusachs et al. 2010).

Tissue cells *in vitro* exhibit multiple modules of cytoskeletal contractility leading to force generation on the ECM (Ponti, Machacek et al. 2004, Hu, Ji et al. 2007). These modules are highly regulated both in space and time and are dependent on both intrinsic (eg. retrograde actin flow, myosin filament assembly and activity) and extrinsic (ECM stiffness, biochemical composition) factors. For example, under low tension, actin

filaments are not assembled into stress fibers and instead exhibit contractile network-arrays that are highly efficient in cell migration (Aratyn-Schaus, Oakes et al. 2011). This tension is controlled both by the stiffness of the underlying ECM and the ability of myosin to reorganize and tense actin filament networks. In response to a stiff ECM, contractile-network arrays can give rise to highly contractile, parallel actin stress fibers, and this in turn can generate maximal tension on the ECM. Thus, cells exhibit precisely tuned intracellular machinery, namely the actinomyosin cytoskeleton, to respond to extracellular stimuli such as changes in the mechanical microenvironment, which ultimately give rise to distinct motile or contractile phenotypes.

Cells on stiff substrates not only assemble bundles of F-actin filaments and generate larger traction forces, but also increase the size of cell-matrix adhesions, structures that can be directly correlated, during the initial stages of growth and maturation, to the cell's application of force on the matrix (Pelham and Wang 1997, Stricker, Aratyn-Schaus et al. 2011). Thusly, cells increase their applied traction forces and spread area in response to increasing substrate stiffness (Saez, Buguin et al. 2005, Yeung, Georges et al. 2005). These responses occur up to a point (~12-16 kPa), at which effective saturating levels are reached. In consequence of the assembly of cytoskeletal structures, such as stress fibers and focal adhesions, and enhanced contractility on stiff substrates, cells also increase their cortical stiffness (Solon, Levental et al. 2007, Tee, Fu et al. 2011). Therefore, there exists a range of responses, including cell spread area, stress fiber and focal assembly, traction force generation, and cortical stiffening, that result from changes in ECM stiffness and can be measured *in vitro*.

2.4.2 Integrins, focal adhesions, and associated signaling mechanisms

Integrin-based adhesions are the physical attachment sites between cells and the ECM (Hynes 2002). Cytoskeletal forces are linked to the ECM through the

transmembrane integrins and their associated molecules that cluster to form adhesions, more specifically termed focal adhesions, focal complexes, or nascent adhesions depending on their molecular composition, size, and/or historical commonplace (Geiger, Spatz et al. 2009). In this Thesis, we refer to these structures commonly as focal adhesions (FAs). The cytoplasmic tails of integrin serve as scaffolds for the binding of integrin-associated proteins, including cytoskeletal binding and adapter proteins, enzymes such as kinases and phosphatases, and small GTPases and their regulators (Gardel, Schneider et al. 2010). Thereby, adhesions serve as a macromolecular complex that physically associate the cytoskeleton and ECM with the ability to propagate biochemical signals. FAs are mechanosensitive organelles, in that they grow and change composition in response to mechanical force (Balaban, Schwarz et al. 2001, Riveline, Zamir et al. 2001). Thus, specific proteins are recruited to adhesions in a force-dependent manner, and these proteins may elicit specific downstream responses (Gardel, Schneider et al. 2010, Pasapera, Schneider et al. 2010, Kuo, Han et al. 2011). In particular, nascent complexes, including scaffolding molecules such as paxillin, form at the leading edge, while myosin II-mediated tension and structural templating lead to recruitment and activation of accessory proteins such as zyxin and α-actinin, promoting growth and "maturation" of the complex distal to the leading edge (Choi, Vicente-Manzanares et al. 2008, Pasapera, Schneider et al. 2010, Oakes, Beckham et al. 2012). Increased mechanical tension leads to activation of downstream signaling molecules such as focal adhesion kinase (FAK), Src and Rho family GEFs (Wang, Botvinick et al. 2005, Friedland, Lee et al. 2009).

Downstream of ECM ligation, a plethora of integrin-specific and tension-dependent signaling responses occur as FAs assemble and turnover (Kuo, Han et al. 2011, Schiller, Hermann et al. 2013). Intriguingly, exogenous forces applied to integrins initiate similar signaling pathways to those stimulated by internally generated forces.

Initial studies on adhesion reinforcement demonstrated that cells are able to sense the restraining force applied to Fn-coated beads and respond by a localized and proportional strengthening of cytoskeletal linkages (Choquet, Felsenfeld et al. 1997). Force-bearing FA proteins, such as vinculin, are also recruited and/or activated at the site of exogenous force application, further demonstrating the structural importance of adhesion strengthening and mechanotransduction (Galbraith, Yamada et al. 2002). These cytoskeletal rearrangements result in localized stiffening of the cell at the cell-ECM interface (Wang, Butler et al. 1993).

One of the major pathways involved in mechanotransduction signaling, or mechanosignaling, is the GTPase RhoA, a critical signaling hub in the assembly of stress fibers and FAs. RhoA is a Ras-related member of the Rho family of small GTPases that promotes the assembly of FAs and actin stress fibers, whereas inhibition with dominant-negative mutants or pharmacological inhibitors results in disassembly of stress fibers and FAs (Ridley and Hall 1992, Nobes and Hall 1995). RhoA induces stress fibers and focal adhesions by stimulating contractility, as active Rho elevates myosin light chain (MLC) phosphorylation in a Rho-associated kinase (ROCK)-dependent manner (Chrzanowska-Wodnicka and Burridge 1996). This is in contrast to other Rho family members, such as Rac and Cdc42, which have distinct, but interdependent functions with respect to cytoskeletal organization (Nobes and Hall 1995, Machacek, Hodgson et al. 2009). In addition, RhoA mediates actin assembly though an mDia-dependent pathway, both of which are necessary for the proper assembly of stress fibers (Watanabe, Madaule et al. 1997). The requirement for ROCK-mediated myosin II contraction, activated downstream of RhoA, in tension-induced adhesion assembly was demonstrated; this could be bypassed by external force application (Riveline, Zamir et al. 2001). Correspondingly, tension activates RhoA, however the molecular mechanisms upstream of this were unknown (Wozniak, Desai et al. 2003, Bhadriraju, Yang et al. 2007).

Recently two guanine nucleotide exchange factors (GEFs), LARG and GEF-H1, were demonstrated to regulate RhoA activation in response to force via their activation and recruitment to the adhesion complex (Guilluy, Swaminathan et al. 2011). These studies further illuminate the mechanochemical responses to mechanical tension that mediate cytoskeletal remodeling and cellular adaptation.

At the single molecule level, forces may alter the receptor-ligand reaction landscape or expose cryptic binding motifs to modulate the output and dynamics of downstream signaling pathways. This has been demonstrated with various structural FA- and cytoskeleton-associated proteins such as talin (del Rio, Perez-Jimenez et al. 2009), filaminA (Ehrlicher, Nakamura et al. 2011), spectrins (Johnson, Tang et al. 2007), integrin (Kong, Garcia et al. 2009, Kong, Li et al. 2013), and others. For example, force causes cryptic exposure of vinculin-binding motifs within a stretched talin molecule (del Rio et al., 2009). Force also exposes SFK-binding motifs within p130Cas, resulting in substrate phosphorylation and a potential mechanism for signal transduction (Sawada et al., 2006). However within the FAs, a multitude of proteins, binding interactions, and complex architecture make resolving mechanosignaling mechanisms at the molecular level a challenge.

2.5 Plasma membrane-associated integrin signaling

2.5.1 Lipid rafts

Lipid rafts are functional subdomains of proteins and lipids that exhibit lateral segregation within the plasma membrane (Lingwood and Simons 2010). Typically, they are enriched in cholesterol, sphingolipids, and GPI-anchored proteins and have distinct mobility characteristics within the plasma membrane (Sharma, Varma et al. 2004, Goswami, Gowrishankar et al. 2008). These domains can facilitate the clustering and

association of cooperative signaling molecules, thus organizing functional modules within the lipid bilayer. Such mechanisms have been hypothesized to facilitate protein sorting, endocytosis, transmembrane signal transduction, cell-matrix adhesion, and other critical cellular processes (Simons and Ikonen 1997). In artificial membranes, differences in lipid and/or protein composition can give rise to the coexistence of compositionally distinct equilibrium structures, such as liquid-ordered and liquid-disordered phases (van den Bogaart, Meyenberg et al. 2011); it has been hypothesized that similar segregation principles might operate in living cells, however cell membranes are composed of extremely diverse molecular constituents that are under non-equilibrium conditions (Simons and Gerl 2010). Much of the current compositional and functional understanding of these membrane subdomains stems from molecular association with detergent-resistance membrane (DRM) fractions, as defined by extraction with cold, non-ionic detergents or disruption of these subdomains by perturbation of membrane cholesterol (Lingwood and Simons 2007). However, recent advances in super-resolution microscopy and molecular imaging have demonstrated the existence of such structures within live cells and their exceptionally dynamic characteristic (Sharma, Varma et al. 2004, Goswami, Gowrishankar et al. 2008, Eggeling, Ringemann et al. 2009, van den Bogaart, Meyenberg et al. 2011).

Lipid rafts impact integrin function through localization of signaling molecules. Adhesion to the ECM promotes translocation of lipid rafts containing Rac1, enabling downstream effector activation and stimulation of actin polymerization (del Pozo, Alderson et al. 2004). Lipid rafts are also required for FAK-dependent stabilization of microtubules at the leading edge (Palazzo, Eng et al. 2004), and integrin clustering promotes the assembly of lipids into a more liquid-ordered (i.e. raft-associated) state, with the plasma membrane adjacent to mature FAs exhibiting high membrane order

(Gaus, Le Lay et al. 2006). Thus lipid rafts help regulate integrin signaling, and these two proximal cellular sub-compartments have interrelated functions.

2.5.2 Membrane-associated integrin signaling intermediates

Src family kinases (SFKs) are a family of nine related non-receptor tyrosine kinases with homology to the proto-oncogene c-Src (Thomas and Brugge 1997). SFKs are activated downstream of integrins where they play a critical role in adhesion assembly and integrin-mediated signaling (Moore, Roca-Cusachs et al. 2010). One well-characterized interaction involves the complex formation of SFKs with previously activated FAK, resulting in phosphorylation of additional tyrosine residues in FAK, serving as docking sites for subsequent proteins (Shattil 2005). SFKs play a central role in integrin signaling, regulating multiple downstream pathways including those involving phosphoinositide (PtdIns) 3-kinase, mitogen-activated protein (MAP) kinases, FAK, and Rho GTPases (Shattil 2005).

Only palmitylated SFKs associate with GPI-anchored proteins (Stefanova, Horejsi et al. 1991, Shenoy-Scaria, Gauen et al. 1993, Alland, Peseckis et al. 1994). All SFKs contain a consensus N-terminal Met-Gly-X-X-X-Ser/Thr motif enabling N-myristylation and targeting to the membrane. In addition, SrcA subfamily members Fyn, Lyn, and Lyk contain a cysteine within the N-terminal region that serves as a site for palmitylation (Resh 1994). Though reversible via palmityl thioesterases, this additional modification confers specific targeting of dually acylated SFKs. Similarly, non-myristylated versions of Fyn fail to associate with GPI-anchored proteins, demonstrating the need for both myristylation and palmitylation posttranslational modifications for targeting to subdomains containing GPI-anchored proteins (Alland, Peseckis et al. 1994).

Activation of Fyn is required for the force-dependent formation of focal complexes and reinforcement of αvβ3-integrin-cytoskeleton connections (von Wichert,

Jiang et al. 2003). This is one of the initial phases in ECM connectivity, with the activation of SFKs occurring within 300 milliseconds of force application to Fn-beads (Wang, Botvinick et al. 2005, Na, Collin et al. 2008). Furthermore, the rigidity response of enhanced spreading correlates with the leading edge recruitment of Fyn, but not c-Src. Interestingly, addition of the palmitoylation site to c-Src enables its support of this rigidity response (Kostic and Sheetz 2006). The stretch-activated substrate of Fyn, p130Cas, and its phosphorylation is dependent on substrate rigidity, and so a mechanism of force-dependent Fyn phosphorylation of p130Cas with rigidity-dependent displacement has been proposed (Jiang, Huang et al. 2006, Kostic and Sheetz 2006). However, the mechanism by which Fyn is recruitment to nascent adhesions and activated remains unknown.

2.5.3 Thy-1 structure, reactivity and function

Thy-1 is a heavily N-glycosylated single v-type immunoglobulin (Ig) domain of primordial origin within the Ig superfamily (Campbell, Gagnon et al. 1981). It is localized to the outer leaflet of the plasma membrane via an N-terminal glycophosphatidylinositol (GPI)-anchor, which specifies lateral mobility within the lipid bilayer. There it has been demonstrated to localize to specific membrane nano-/micro-domains, termed lipid rafts, to carry out transmembrane signaling functions (Tiveron, Nosten-Bertrand et al. 1994, Chen, Thelin et al. 2006). Within lipid rafts, Thy-1 may physically associate with SFKs, which, in response to a physiological stimulus, can activate downstream signals via their kinase activity. Particularly, Thy-1 partitions within similar membrane domains as dually palmitoylated and myristoylated SFKs Fyn, Lyn, and Lyk (Draberova and Draber 1993).

Thy-1 binds integrin to mediate transcellular adhesion and signaling in a variety of tissue specific contexts. Thy-1 is expressed on activated endothelial cells where it

interacts with αMβ2 (Mac-1) on leukocytes and αvβ3 on melanoma cells and participates in their extravasation from the blood stream (Wetzel, Chavakis et al. 2004, Saalbach, Wetzel et al. 2005). Within the central nervous system, Thy-1 is highly expressed on neurons where it binds αvβ3 expressed on neighboring astrocytes and mediates neurite extension inhibition in the dentate gyrus (Tiveron, Barboni et al. 1992). Interestingly, this interaction leads to signaling events in both cell type (i.e. neuron and astrocyte) that appear to be critical in the neuronal guidance (Leyton, Schneider et al. 2001, Avalos, Valdivia et al. 2009). Lung fibroblasts lacking Thy-1 are more efficient at activating matrix-bound latent TGF-β than fibroblasts expressing Thy-1 (Zhou, Hagood et al. 2010). As this process is integrin-mediated and enabled via cellular contraction, the question of whether this effect is mediated by altered contractility between Thy-1 subpopulations or a direct and inhibitory interaction with LTBP-binding integrins is warranted. Indeed, Thy-1 can interact with αvβ5 on lung fibroblasts, although the specific physical/dimensional context of this interaction is unknown. All taken together, Thy-1 exists as a cell surface glycoprotein that exhibits molecular interactions with signaling and scaffolding molecules critical to the proper form and function of cell-matrix adhesions, and it can differentiate native fibroblast cell populations with respect to their cytoskeletal phenotype.

Thy-1 regulates the activity of Rho GTPase within fibroblast subsets, leading to alterations in stress fiber and focal adhesion assembly on rigid substrates (Barker, Grenett et al. 2004). Thy-1 can negatively regulate SFK activation in quiescent cells and, through the decreased phosphorylation of p190RhoGAP, lead to elevation of active RhoA. Downstream phenotypes such as migration and cytoskeletal assembly are mediated by exogenous expression of Thy-1. Somewhat paradoxically, Thy-1^{neg} fibroblasts undergo enhanced myofibroblast differentation in response to fibrogenic cytokines, as evidenced by expression of myogenic regulatory factors MyoD and myocardin and the contracture

of collagen gels (Sanders, Kumbla et al. 2007). Interestingly, even under non-stimulated conditions, Thy-1^{neg} fibroblasts are able to more efficiently contract 3 mg/mL collagen gels than Thy-1^{pos} cells, which display Young's moduli likely in the 300-600 Pa range. Therefore, the cytoskeletal phenotype of Thy-1 fibroblast subpopulations is likely dependent on a variety external cues including fibrogenic cytokines, dimensionality, ECM ligand presentation, and ECM stiffness.

CHAPTER 3 QUANTIFICATION OF *IN VIVO* LUNG PARENCHYMA TISSUE RIGIDITY AND ITS CHANGE DURING LUNG FIBROSIS*

3.1 Introduction

One of the hallmarks of fibrosis is rigidification of the tissue microenvironment. This is a consequence of excessive synthesis, deposition, crosslinking, and contraction of ECM by fibroblastic cells within the scarring region (Hinz, Phan et al. 2012). In the case of many parenchymal fibrotic disorders (e.g. lung, liver, heart), the fibrotic remodeling that results in altered mechanical properties coincides with structural and architectural distortion of the tissue, causing tissue dysfunction and ultimately organ failure. Thus, mechanical changes to tissue are a critical parameter in the diagnosis, monitoring, and associated outcome of fibrotic pathologies.

We now appreciate that rigidity of the cellular microenvironment imparts a strong influence on residing cell phenotype. Cells sense and respond to the mechanics of their microenvironment, altering a number critical cell phenotypes including migration, differentiation, proliferation, and apoptosis (Discher, Janmey et al. 2005). Importantly, many of these phenotypes are intimately related to the cytoskeleton, which regulates ECM remodeling and fibrosis-associated fibroblast activation. Therefore, the existence of a rigid scar tissue environment is thought to be a pro-fibrotic cue, potentially resulting in a feed-forward loop of progressive fibrosis (Tomasek, Gabbiani et al. 2002, Tschumperlin, Liu et al. 2013).

In the case of pulmonary fibrosis, previous studies have demonstrated that tissue compliance decreases as a consequence of disease progression. This can be demonstrated at the whole organ level through plethysmographic measurements from IPF patients,

where lung compliance is seen to decrease by more than 30% and was the most strongly correlated pulmonary function parameter with the extent of fibrosis (Sansores, Ramirez-Venegas et al. 1996). Similarly, tensile-stress testing of lung tissue strips from rats after bleomycin-induced fibrosis established quantitative values of tissue elasticity (i.e. Young's modulus), demonstrating a significant increase due to bleomycin injury. Values for these bulk segments of tissue and were determined to increase by 2-fold, from approximately 5 to 10 kilopascal (kPa), between normal and bleomycin-treatment groups (Dolhnikoff, Mauad et al. 1999, Ebihara, Venkatesan et al. 2000).

In the case of rigidity sensing by cells, the length scales at which they measure their mechanical environment is on the order of microns, the size of individual cells or even subcellular FA organelles that locally respond to mechanical cues (Plotnikov, Pasapera et al. 2012, Trichet, Le Digabel et al. 2012). However, as the architecture of the lung is highly complex and heterogeneous, extrapolating mechanical parameters measured at the millimeter (i.e. bulk) scale to the micron scale is highly problematic (Fust, Bates et al. 2004). Therefore, it was the goal of this study to quantify the microscale rigidity of the lung parenchyma (i.e. alveolus) and its change as a consequence of fibrosis in preclinical and human patient models of pulmonary fibrosis. To do this we utilized the extremely high spatial and force resolution of the atomic force microscope (AFM) together with optical fluorescence microscopy to measure anatomical regions of interest with high spatial accuracy and precision. We also use the high spatial resolution capability of the AFM and power of sampling to obtain accurate statistical parameters regarding the distributions of mechanical properties encountered *in vivo*. These values can be then be utilized *in vitro* to assay the role of physiologic and pathophysiologic levels of microenvironmental stiffness on cellular phenotype using a reductionist approach.

*Modified from:

(1) Booth, A. J., R. Hadley, A. M. Cornett, A. A. Dreffs, S. A. Matthes, J. L. Tsui, K. Weiss, J. C. Horowitz, V. F. Fiore, T. H. Barker, B. B. Moore, F. J. Martinez, L. E. Niklason and E. S. White (2012). "Acellular normal and fibrotic human lung matrices as a culture system for in vitro investigation." Am J Respir Crit Care Med **186**(9): 866-876.

(2) Brown, A. C., V. F. Fiore, T. A. Sulchek and T. H. Barker (2013). "Physical and chemical microenvironmental cues orthogonally control the degree and duration of fibrosis-associated epithelial-to-mesenchymal transitions." J Pathol **229**(1): 25-35.

3.2 Materials and Methods

3.2.1 Murine lung tissue preparation and mechanical characteration

3.2.1.1 Animal use and bleomycin-induced fibrosis

8-10 week old C57/Bl6 mice (Charles River, MA) were intubated and 3.2 U/kg bleomycin (EMD Chemicals, NJ) was instilled intratracheally in 50 μL of sterile saline. Mice were sacrified after 14 days for tissue harvesting. All experiments were performed in accordance with guidelines set forth by the National Institutes of Health and Georgia Institute of Technology Institutional Animal Care and Use Committee-approved protocols.

3.2.1.2 Lung tissue preparation for histology

Immediately following the bronchoalveolar lavage, lungs were harvested from each time point and experimental/control group. The trachea was cannulated and left intact during the removal of the lungs from the body. Using the cannula, the lungs were inflated with 10% buffered formalin and then stored in 15 ml of 10% buffered formalin until paraffin embedding. Lungs were embedded in paraffin, sectioned, and stained with hematoxylin and eosin (H&E) for imaging.

3.2.1.3 Lung tissue preparation for fluorescence microscopy and AFM nanoindentation

Lungs were inflated using 2% ultra low-melting temperature agarose (SeaPrep, Lonza Inc.) warmed to 37°C and subsequently allowed to solidify on ice. The left lobe was dissected into approximately 1 cm^3 blocks, and 100 μm thick slices were generated using a VT100S vibratome (Leica, IL). Samples were kept in 10% FBS, 1% penicillin & streptomycin-supplemented DMEM after harvesting and during mechanical analysis. To allow for visualization of tissue architecture and type, lung slices were stained with fluorescein-labeled lectin from the Cry-Baby Tree, *Erythrina crystagalli* (ECL; Vector Laboratories) to label alveolar type I epithelial cells (ATI) and LysoTracker Red (Invitrogen) to label the lamellar bodies of alveolar type II epithelial cells (ATII). Cell nuclei were stained Hoechst 33258 (Invitrogen). Slices were incubated at 37°C for 30 minutes before washing with warm DMEM.

3.2.1.4 LIVE/DEAD assay of tissue cell viability

To study viability of resident tissue cells over the time course of mechanical characterization, the LIVE/DEAD Viability Kit for mammalian cells was used (L-3224, Invitrogen). Lung slices were incubated with 10 μM calcein AM and 5 μM EthD-1 for 1 hour prior to their corresponding time point. Samples were then fixed with 4% formaldehyde and mounted. Additionally, a dead control group was included by incubating samples with 70% methanol for 30 minutes prior to dye incubation. Samples were mounted in ProLong® Gold antifade reagent (Invitrogen) and imaged using confocal microscopy (LSM 510-META, Carl Zeiss Inc.) at 63X magnification (plan-apochromatic, 1.4 N.A. objective).

3.2.1.5 AFM nanoindentation analysis

Vital stains for ATI, ATII cells and cell nuclei were used to direct measurements to peri-alveolar regions of interest. Micrographs were acquired using the AFM base inverted microscope (TiE, Nikon) at 20X magnification (PlanFluor 20X, 0.5 NA objective) using a Nikon DS-Qi1 camera. Samples were measured in 10% FBS-supplemented DMEM at room temperature. For fibrotic regions, areas of enhanced cellularity distinct from larger airways were chosen. Using a MFP-3D-BIO AFM (Asylum Research) with a 4.74 μm diameter silica glass bead customized-silicon nitride AFM tip (Veeco), peri-alveolar regions were located and probed by force map nanoindentation at a pixel rate of 1.0 Hz, deflection set point of approximately 10 nN, and indentation rate of 22.86 μm/sec. Cantilever spring constants were determined using the thermal resonance frequency method with values ranging from 0.06-0.08 N/m (Maaloum, Muller et al. 2002). Force-indentation profiles were measured in 10x10 μm grids with approximately 600 nm spacing between points. A minimum of 10 regions were selected for each tissue slice and a minimum of 3 slices used per mouse. Force-indentation profiles were fit to a Hertz model for elastic deformation between spheres to calculate the Young's modulus for each point, assuming a Poisson's ratio of 0.4 (Butler, Nakamura et al. 1986).

3.2.2 Human lung tissue preparation and mechanical characterization

3.2.2.1 Human lung procurement

Human lungs deemed to be unsuitable for lung transplantation were obtained from beating-heart (or warm autopsy) donors through Gift of Life Michigan. Human deidentified IPF lung samples were obtained from explants of patients with IPF undergoing lung transplantation at the University of Michigan. The University of

Michigan Institutional Review Board has deemed these approaches exempt from oversight as all subjects were considered deceased.

3.2.2.2 Decellularization of lung matrices

Incubation times lasted, on average, 24 hours per step and involved instillation of solutions through both the pulmonary vasculature and the airways. In essence, lung samples were first agitated in sterile deionized, distilled water followed by incubation in 0.1% Triton X-100 to lyse cellular components. Samples were then washed 3 times with sterile PBS, followed by incubation with 2% sodium deoxycholate. Following three subsequent washes with sterile PBS, samples were incubated in 1M NaCl to lyse residual nuclei. After decanting NaCl, tissues were rinsed three times with sterile PBS and incubated with DNAse (30 μg/ml) in 1.3mM $MgSO_4$ and 2mM $CaCl_2$. The DNAse solution was decanted and tissues were washed three times with sterile PBS. This protocol was repeated three times. Resulting samples were then sterilized with a solution containing 0.18% peracetic acid and 4.8% ethanol for 20 minutes and then washed three times with sterile PBS and stored at 4°C.

3.2.2.3 AFM nanoindentation analysis

Tissue samples were dissected into strips of approximately 5 x 5 mm in length and width and 1000 μm in thickness, and were characterized using an MFP-3D-BIO atomic force microscope (AFM) (Asylum Research; Santa Barbara, CA). AFM nanoindentation tests were performed under fluid conditions (PBS, pH 7.4) using a 4.74 μm diameter spherical tipped-silicon nitride cantilever (Bruker, Camarillo, CA). Cantilever spring constants were measured prior to sample analysis using the thermal fluctuation method, with nominal values of 30-50 pN/nm (Maaloum, Muller et al. 2002). Two-dimensional force maps were taken in 30 x 30 μm grids, and force-indentation curves were individually analyzed using a Hertzian model for spherical tips, from which

Young's modulus was obtained. The sample Poisson's ratio was assumed as 0.4, and a power law of 1.5 was used to model tip geometry (Butler, Nakamura et al. 1986). All AFM measurements were made using a cantilever deflection set point of approximately 10 nN and a rate of indentation of 22.86 μm/sec.

3.3 Results

3.3.1 Characterization of lung tissue morphometry and cell viability in fresh lung tissue sections

To verify that gross tissue architecture was not perturbed during the preparation of fresh lung tissue sections for subsequent mechanical characterization, we compared vital-stained fresh tissue sections with traditional formaldehyde-fixed and paraffin-embedded histological techniques. Normal alveolar and bronchoalveolar structures are maintained in fresh tissue sections as compared to H&E stained fixed tissue (Figure 1, alveolar type I (ATI) cells stained in green). In bleomycin-treated animals, significant cellular hyperplasia, alveolar wall expansion, and overall architectural distortion are seen in both H&E and fresh tissue sections, suggesting overall maintenance of tissue structure in fresh lung tissue sections.

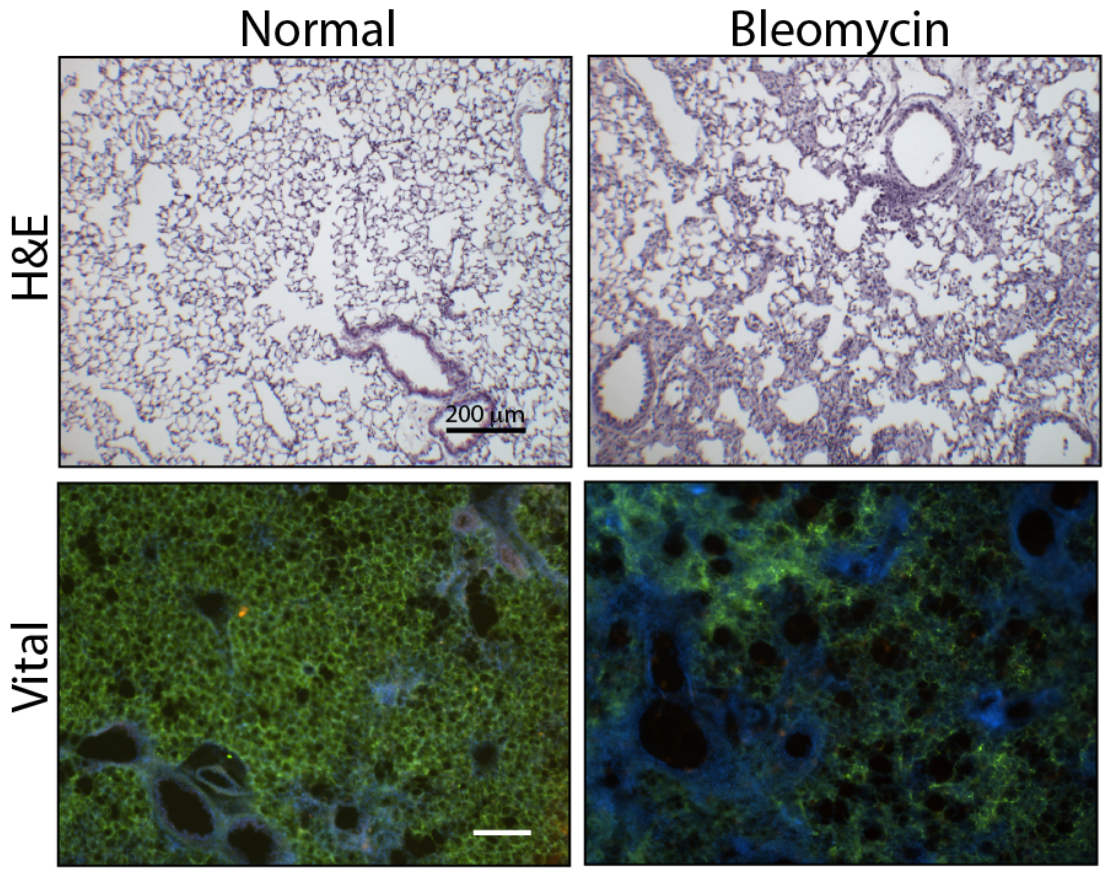

Figure 2: Histologic and vital stain characterization of mouse lung tissue. H&E-stained sections of normal lung are compared to bleomycin-treated lung. Vital stains for ATI cells (green), ATII cells (red), and cell nuclei (blue) are shown for normal and bleomycin-treated fresh tissue sections. Scale bar = 200 µm.

To investigate the preservation of cell viability within fresh tissue sections, we used a LIVE/DEAD assay over various culture times *in vitro*. Cell viability was maintained at basal levels for 3 hours in culture, after which time a 25% decrease in viability was seen, persisting to 24 hours (Figure 2). After 48 hours in culture, approximately 50% of the cells remained viable. As all AFM measurements were performed within 6 hours of tissue harvesting, this suggests that fresh tissue sections maintain proper tissue architecture and support viability in the majority of resident cells.

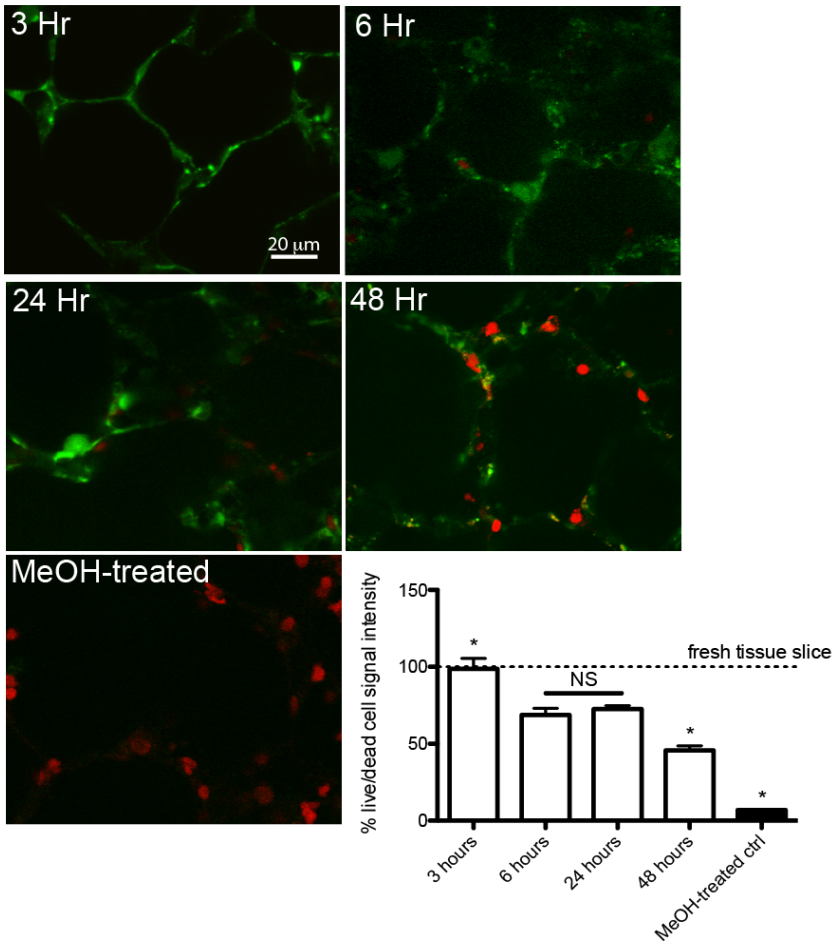

Figure 3: Cell viability characterization of fresh lung tissue sections. Fresh tissue sections were cultured for various times and stained with Calcein AM (green) and ethidium homodimer-1 (red) for detection of live and dead cells, respectively. Alveolar regions were imaged after 3, 6, 24, and 48 hours in culture. Methanol treatment was used to induce cell death. Quantification of live/dead signal intensity is depicted for various culture times; the dashed line represents freshly isolated tissue.

3.3.2 AFM measurement of mouse lung tissue Young's modulus

To ensure correct spatial and anatomical location within the lung, peri-alveolar regions (i.e. alveolar wall segments) were located based on vital staining for ATI and ATII cells and fluorescence microscopy concurrent with AFM measurements. Representative brightfield/fluorescence overlay and fluorescence-only images are shown (Figure 3A,B). AFM measurements generated force-indentation curves, from which material properties of the tissue could be derived; for our study, the Hertz model for elastic contact between two spheres was used to estimate the sample Young's modulus (*E*), a descriptive parameter for tensile stress per strain within the linear stress-strain regime (Figure 3C). Multiple regions ($\geq$ 10) and sections ($\geq$ 3) of tissue were measured to obtain Young's modulus for individual animals. Average *E* for normal lung was consistently between 1-2 kPa (Figure 3D). In contrast, bleomycin treatment to induce fibrosis dramatically increased the average *E* and variance in all samples tested. Overall mean and standard deviation values are reported for all samples (5 mice per condition, n = 180/mouse; Figure 3E). The average *E* of normal lung tissue was 1.96 ± 1.21 kPa and increased in the bleomycin-treated mouse to 17.25 ± 11.06 kPa.

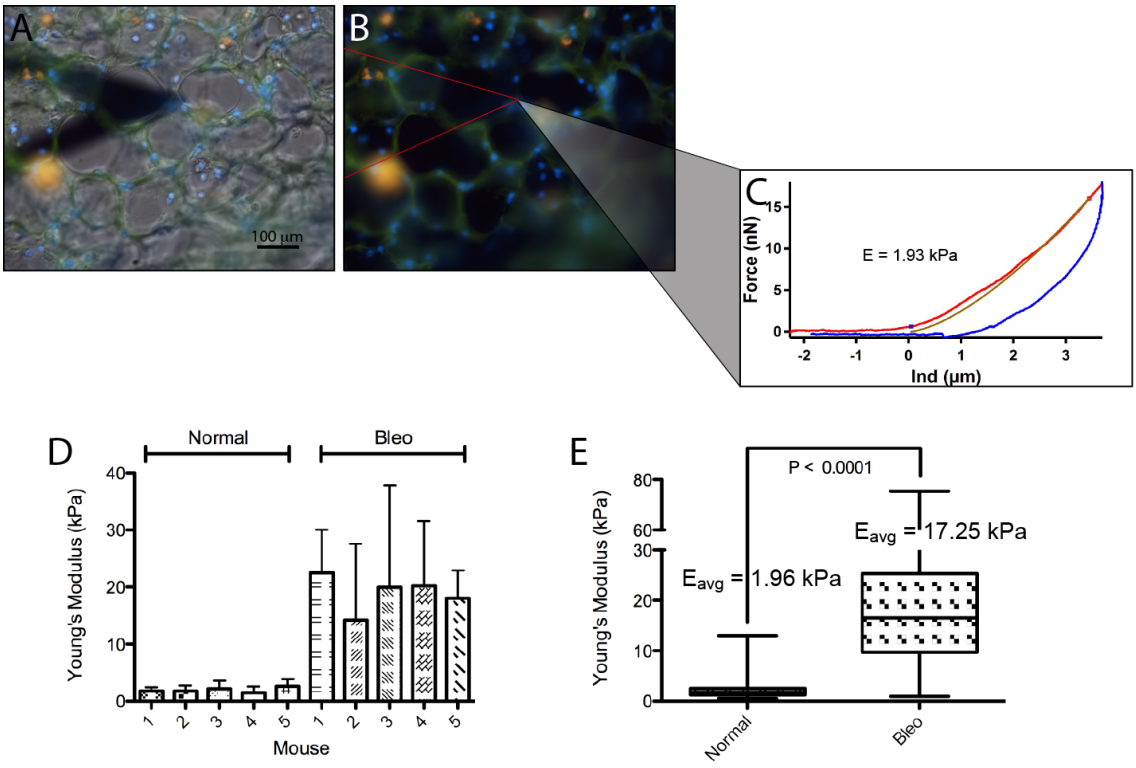

Figure 4: AFM measurement of mouse lung tissue stiffness. (A) Representative optical micrograph of vital tissue sections stained for cell nuclei (blue), ATI cells (green), and ATII cells (red) overlaid with a brightfield image depicting the AFM probe. (B) A fluorescence-only image with the AFM probe placement indicated (red dashed line). (C) A force-indentation curve for the anatomical region indicated. Approach (red) and retract (blue) curves, along with the fitted Hertz model curve (beige) are shown. (D) Average *E* ± standard deviation for individual mice from non-treated or bleomycin-treated groups. (E) Box & whisker plots of pooled average Young's modulus values for normal vs. bleomycin-treated animals. An unpaired Student's t-test was used to determine P < 0.0001.

3.3.3 Rigidity measurements of clinical IPF specimens

To extend our findings from the bleomycin model of lung fibrosis to the relevant disease pathobiology of IPF, we obtained human tissue from patients with diagnosed IPF

or otherwise healthy individuals. AFM nanoindentation measurements were made similarly to mouse lung previously described, except concurrent optical microscopy was not possible due to the sample preparation. Specifically, patient samples were not accessible for hydrogel instillation and high-precision vibratome sections, and thus light scattering due to sample thickness prohibited optical microscopy. Measurements were randomly distributed about parenchymal regions of the tissue. The average Young's modulus of native normal lung tissue was 1.92 ± 1.40 kPa, in good agreement with values obtained from normal mouse lung (Figure 4A). IPF specimens had a significantly increased average E (20.25 ± 28.49 kPa), while a significant number of measurements were distributed in the stiffness regime not dissimilar from normal lung. This is likely explained by the spatially heterogenous pathobiology of IPF, with regions of normal lung parenchyma in close proximity to mature scar tissue or regions of ongoing fibrotic remodeling.

To specifically explore the properties of the ECM during fibrotic remodeling, we used decellularized specimens from the same patient donors. After decellularization, normal lung matrices exhibited an average E of 1.66 ± 1.13 kPa, no different than native lung (Figure 4B). The rigidity of IPF lung matrices was 12.14 ± 13.24 kPa and somewhat more homogeneous in distribution, suggesting that decellularization of IPF lungs may result in a relaxation of matrix proteins that results in slightly softer tissue. However, as this tissue is significantly stiffer (approximately 5-fold greater average E) than normal decellularized tissue, this demonstrates that the ECM is significantly remodeled during fibrotic progression, resulting in localized tissue stiffening. The values for IPF tissue also qualitatively correspond to those measured in bleomycin-treated mice.

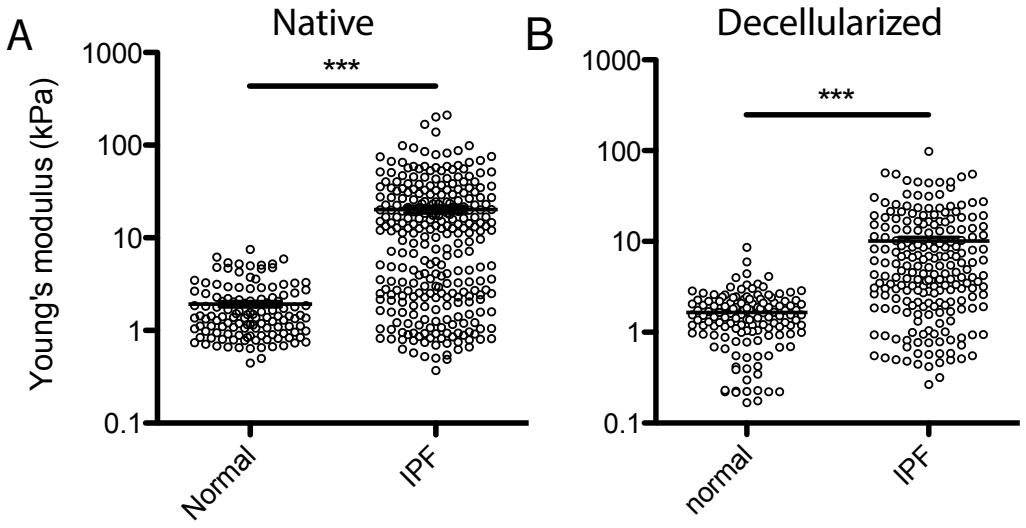

Figure 5: AFM measurement of human IPF and normal lung tissue stiffness. Young's modulus values for normal or IPF tissue is shown for both native (i.e. non-decellularized) (A) and decellularized (B) patient samples. Dot plots (mean ± S.E.M.) representing individual force-indentation measurements, and data is pooled from 2 donors per group. *** = $p < 0.001$, as assessed by the Mann-Whitney test.

Because the average values depend on the relative sampling of normal vs. distinctly stiffer histopathological regions of diseased tissue, we used frequency distributions to identify major peaks within the data. Normal tissue exhibited one major peak best fit by a log-normal distribution, with a mode of approximately 1 kPa (Figure 5A-C). When overlaid, IPF tissue exhibited a similar major peak at 1 kPa fit by the log-normal distribution, but was significantly more skewed towards higher values. Both native and decellularized tissue exhibited similar distributions with similar characteristics. Therefore, measurements from IPF tissue contained both a population of data points associated with normal lung rigidity, as well as a population unique to IPF.

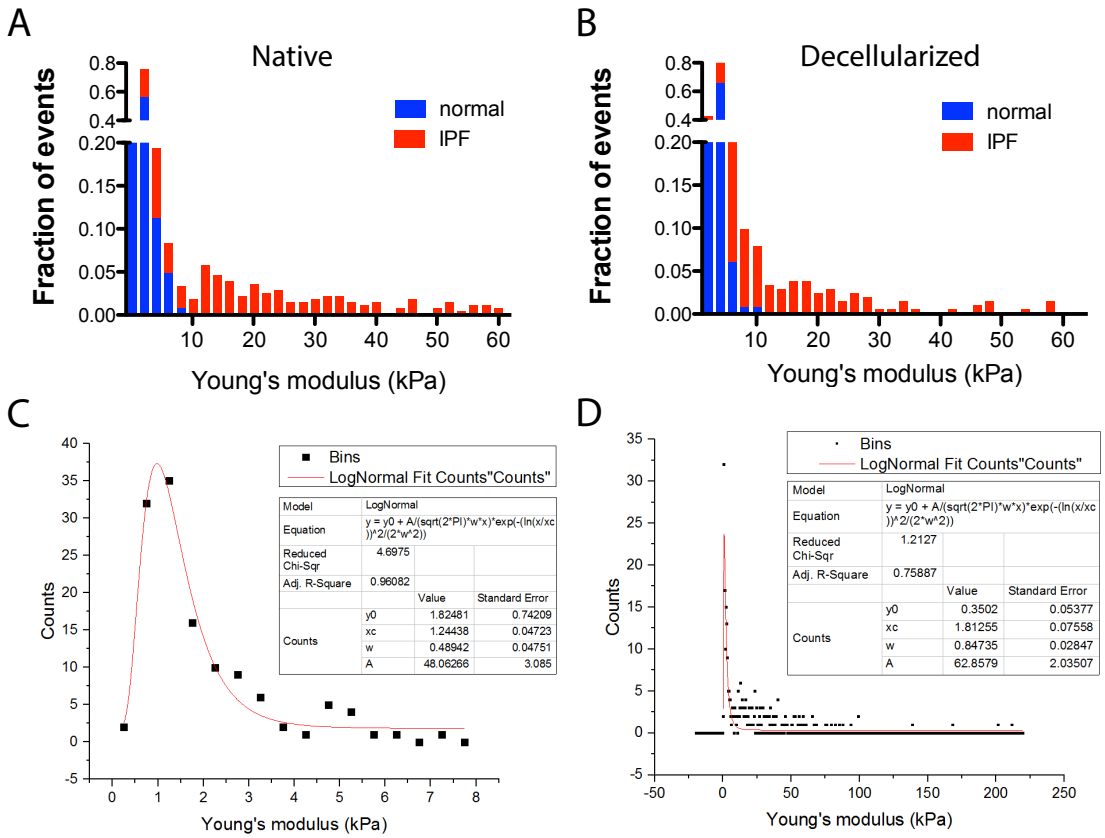

Figure 6: Histogram analysis of AFM measurements from patient samples. Young's modulus values are represented for native (A) and decellularized (B) tissue in a frequency distribution. Normal (blue) and IPF (red) datasets are overlayed. Log-normal curves fitting is shown for native normal (C) and native IPF tissue (D), along with a table of fitted parameters (inset).

3.4 Discussion

In this work we measured the Young's modulus of lung tissue from both a pre-clinical model of lung fibrosis and human IPF patients. During the completion of this study, a similar study by Liu and colleagues was published on the microscale rigidity of mouse lung during bleomycin-induced fibrosis (Liu, Mih et al. 2010). Our results are in

close agreement with theirs; further validating the findings of these two studies. However, our analysis of clinical tissue specimens from normal and IPF patients represents the first ever quantification of this critical parameter involved in the pathobiology of lung fibrosis and tissue fibrosis, in general. We find that IPF results in an enhancement of average microscale tissue rigidity by an order of magnitude (approximately 10 fold), with discrete regions of the tissue demonstrating values up to 100-fold change compared to the normal lung. This extreme change in microenvironmental stiffness is likely to have a profound impact on the phenotype of resident cells, through their ability to sense and respond to mechanical cues, as will be the investigation of subsequent chapters. As such, we have defined and quantified this important parameter as seen *in vivo*. Namely, cells rarely encounter rigidity values exceeding 4 kPa in normal lung tissue. In IPF, the average Young's modulus increases between 5-10 fold, however tissue is not globally stiffened. Instead spatially heterogenous regions are focally stiffened, in close agreement with the histopathological features. Therefore in IPF tissue, cells encounter environments (>10 kPa) never seen in normal healthy tissue, altering not only the work required for respiration but also the cytoskeletal phenotype of resident cells. This large range of values measured in IPF likely represents the spatial and temporal hierarchy of disease-associated fibrotic remodeling, as less "mature" regions of fibrosis contain less type I collagen.

In human patient samples, we compared the Young's modulus of native vs. decellularized tissue, enabling evaluation of the material properties of the non-cellular tissue compartment. The fibrotic ECM alone exhibited significant rigidification (approximately 5 fold) compared to normal decellularized tissue. This is expected as scar tissue is commonly composed of dense assemblies of ECM fibers (mainly type I collagen). Therefore, the microscale rigidity measurements made with AFM correspond to focal remodeling and stiffening of the ECM during IPF. It will be crucial in future

studies to align mechanical measurements with typical histologic classification to gain an understanding of the hierarchy of fibrotic regions within the lung and their associated mechanical properties. Likely, regions of enhanced ECM deposition and /or crosslinking will correlate to regions of elevated stiffness. However, the rigidity of fibroblastic foci (i.e. regions of active fibrogenesis), which differ from mature scar tissue in terms of their ECM composition and cellularity, remain unknown and should be the focus of future investigation.

While stiffness of the cellular microenvironment clearly plays a significant role in defining the resident cell phenotype (Paszek, Zahir et al. 2005, Engler, Sen et al. 2006, Wipff, Rifkin et al. 2007, del Rio, Perez-Jimenez et al. 2009), the origins of the increased tissue stiffness are still poorly understood. It is likely that stiffness emanates from the residential cell population and/or the over-production or activation of cross-linking enzymes. Fibroblasts that have differentiated down a contractile, myofibroblastic pathways are known to exhibit significant contractile force (Wipff, Rifkin et al. 2007). Such cell-derived forces are capable of stressing the surrounding ECM leading to increased microenvironmental stiffness. Reports have shown that lysyl oxidase in the tumor microenvironment is sufficient to crosslink and stiffen the tumor stroma (Levental, Yu et al. 2009) and transglutaminases have long been known to catalyze ECM crosslinking and recently have been shown to result in tissue stiffening (Santhanam, Tuday et al. 2010). However, the cellular mechanisms underlying how and under what external cues cells indeed stiffen their surrounding microenvironment, from a relatively compliant and physiologic state to the diseased regime seen in IPF, should be the focus of future investigation.

We characterized the distribution of Young's modulus values in normal vs. IPF tissue. Of note is the wide distribution of rigidity values in IPF tissue, while still maintaining significant "mechanically normal" regions of tissue. Thus, we define

regimes of Young's moduli corresponding to normal and fibrotic tissue. Normal lung typically yields values between 0.5-4 kPa, while fibrotic lung exceeds the normal regime in a continuous fashion (values >10 kPa are unique to IPF), extending to hundreds of kilopascals. These measurements help define the range of rigidity values seen in normal lung physiology and disease, and parameter values with which to justify *in vitro* experimentation.

CHAPTER 4 THY-1 REGULATION OF FIBROBLAST CYTOSKELETAL RESPONSES TO ALTERATIONS IN SUBSTRATE RIGIDITY

4.1 Introduction

Fibroblasts are the main ECM remodeling and maintaining cell type during normal organism homeostasis and wound healing (Sorrell and Caplan 2009). However during pathologies such as fibrosis, their aberrant and persistent activity results in the assembly of tissue structures not permissible of normal organ function (Tomasek, Gabbiani et al. 2002). These regions of scar tissue are dense, ECM-containing structures that disrupt normal tissue architecture. In IPF, fibroblasts exist within nodules of high synthetic and ECM remodeling activity, termed fibroblastic foci, which are responsible for *de novo* fibrogenesis and are the most closely associated histologic feature to disease progression and patient morbidity (King, Schwarz et al. 2001, Nicholson, Fulford et al. 2002). Thus fibroblasts, specifically those localizing to fibroblastic foci, are the major cell type of interest in IPF pathology due to their functional role of creating fibrotic tissue structures. Complicating the functional analysis of these cells *in vitro*, fibroblasts from human tissue isolates exhibit phenotypic heterogeneity (Chang, Chi et al. 2002, Sorrell and Caplan 2004); this is likely exacerbated in IPF due to the extreme spatial and temporal diversity of disease presentation and endogenous, i.e. the intermixture of normal lung parenchyma, new fibrotic tissue (i.e. fibroblastic foci), mature fibrosis, and honeycomb features within biopsied tissue segments (Visscher and Myers 2006). Further contributing to this phenotypic heterogeneity, fibroblasts constituting complex multi-cellular structures can be derived from diverse origins and exhibit functional heterogeneity. For example, the dermis is patterned by two distinct lineages of

fibroblasts from a common progenitor, with the upper dermis supported by a $Dlk^{-}/Lrig1^{+}$ subpopulation critical in regulating hair follicle formation, whereas the $Blimp1^{-}/Dlk^{+}$ reticular/hypodermal subpopulation goes on to synthesize the majority of fibrillar ECM and supply pre-adipocytes within the hypodermis. During wound healing, the initial wave of regeneration depends on cells of the reticular/hypodermal lineage elaborating a collagenous ECM, while upper cells become active during re-epithelialization and follicular morphogenesis (Driskell, Lichtenberger et al. 2013). Within the fibrotic lesions of human patients myofibroblasts lack expression of the cell-surface glycoprotein Thy-1 (CD90), whereas the majority of fibroblasts in normal interstitial spaces are Thy-1-positive ($Thy\text{-}1^{pos}$) (Hagood, Prabhakaran et al. 2005, Sanders, Pardo et al. 2008). Fibroblast subpopulations characterized by surface expression of Thy-1 also display phenotypic diversity *in vitro* (Fries, Blieden et al. 1994, Barker, Grenett et al. 2004, Rege and Hagood 2006, Hudon-David, Bouzeghrane et al. 2007, Sanders, Kumbla et al. 2007, Barker and Hagood 2009).

The previous two decades of research has identified Thy-1 as a critical modulator of fibroblast phenotype *in vitro* and *in vivo*. Thy-1 is a cell surface glycoprotein that alters fibroblast phenotype largely through modulation of intracellular signaling pathways via Src family kinases (SFKs) and Rho GTPases and regulation of inter-cellular adhesion (Rege and Hagood 2006, Barker and Hagood 2009). While it is commonly used as a marker for mesenchymal-type cells, it is not constitutively expressed on fibroblasts from rodent or human origin. Instead, Thy-1 undergoes intricate tissue-specific and spatiotemporal expression regulation via a somewhat unique combinatorial influence of control elements, dictated by the gene structure and post-transcriptional regulation (Xue, Rivero et al. 1991, Bradley, Ramirez et al. 2009). Despite the clinical relevance of this fibroblast subpopulation in IPF and the knowledge that $Thy\text{-}1^{neg}$ lung fibroblasts are hyper-proliferative (Hagood Chest 2001), differentially express growth factor receptors

(Hagood AJPhys 1999), display altered cytokine signaling (Hagood AJPCMB 2002), show enhanced myofibroblastic differentiation (Sanders AJPCMB 2007), and increasingly activate TGF-β (Yong AJP 2004, Yong JBC 2009), the molecular mechanism(s) explaining Thy-1-associated fibroblast phenotypes are still not completely defined.

Thy-1 regulates Rho activity via SFK-mediated repression of p190RhoGAP, leading to alterations in stress fiber and focal adhesion assembly on rigid two-dimensional (2D) substrates (Barker, Grenett et al. 2004). Downstream phenotypes, such as migration and cytoskeletal network assembly, can be modulated by exogenous expression of Thy-1. Somewhat paradoxically, Thy-1^{neg} fibroblasts undergo enhanced myofibroblast differentation in response to fibrogenic cytokines and are able to more efficiently contract soft three-dimensional (3D) collagen gels than Thy-1^{pos} fibroblasts, which display Young's moduli in the range of 400-600 Pa. Therefore, cytoskeletal phenotype regulated by Thy-1 expression is likely dependent on a variety of external cues including fibrogenic cytokines, ECM dimensionality, ECM ligand presentation, and ECM stiffness.

As described in the previous chapter, connective tissue fibrosis results in changes to the mechanical properties of tissue; fibrosis leads to a drastic increase in tissue rigidity. Resident stromal cells are also sensitive to the mechanics of their microenvironment, resulting in bidirectional and dynamic mechanics-driven communication. Therefore, investigating the phenotype of fibroblasts in physio- and pathophysiologically-relevant mechanical microenvironments is a critical step in linking *in vitro* cell biological studies to the cellular mechanisms of fibrogenesis *in vivo*. Furthermore, as the mechanics of the microenvironment directly influence the mechanical architecture of the cell (i.e. cytoskeleton and cell-matrix adhesions), which in turn regulate the assembly and remodeling of ECM, we focus on investigating cytoskeletal parameters in response to

changing ECM rigidity. In this chapter, we investigate the cytoskeletal phenotype of fibroblasts regulated by Thy-1 in a variety of cell systems and extracellular environments. We show that Thy-1 modulates fibroblast rigidity sensing in a complex way – Thy-1 expression enhances mechanosensitivity to matrix rigidity, while loss of Thy-1 promotes fibroblast activation in soft microenvironments, i.e. rigidity values similar to normal lung parenchyma.

4.2 Materials and Methods

4.2.1 Cells and plasmids

4.2.1.1 Isolation, sorting and RNAi treatment of human lung fibroblasts

Primary human lung fibroblasts were isolated from normal or IPF patients as described previously (White, Thannickal et al. 2003). Normal lung fibroblasts (NLFs) were obtained from patients undergoing thoracic surgery for non-fibrotic lung diseases. Written informed consent was obtained from all subjects in accordance with the University of Michigan Institutional Review Board. IPF lung fibroblasts (IPFLFs) were used from patients in whom a pathologic diagnosis of UIP was subsequently made. Briefly, under sterile conditions, lung tissue segments were minced to a fine slurry and cultured in T-75 tissue culture flasks. Media was aspirated and replaced with fresh media every 48 to 72 hours. Cells were maintained in DMEM supplemented with 10% fetal bovine serum (FBS), 100 μg/mL penicillin/streptomycin, and 1 mM sodium pyruvate. For fluorescence-activated cell sorting (FACSAria III, BD Biosciences; Franklin Lakes, New Jersey), cells were stained with FITC-labeled anti-human Thy-1 antibody (5E10, BD Pharmingen; San Jose, CA) and sorted into Thy-1^{pos} and Thy-1^{neg} subpopulations based on positive expression of normal lung fibroblasts or negative

antibody controls, respectively. Cells were sorted twice to establish >90% purity based on Thy-1 expression. Cells were used for experimentation between passages 4-9 (P4-9).

For Thy-1 knockdown experiments, CCL-210 NLFs were obtained from ATCC (Manassas, VA) and transduced with lentiviral particles (5x multiplicity of infection (M.O.I.) plus 5 μg/mL Polybrene) containing a pool of 19-25 (plus hairpin) nucleotide-encoding target-specific constructs (sc-32837-v, Santa Cruz Biotechnology; Santa Cruz, Ca) or a scrambled sequence control without specificity to any known cellular mRNA (sc-108080). After 72 hours, transduced cells were sub-cultured and selected with 1.0 μg/mL puromycin. Cells were FACS sorted once for cells exhibiting high knockdown efficiency, whereas the control shRNA construct had no effect on Thy-1 expression.

4.2.1.2 Isolation of primary mouse lung fibroblasts

Mouse lung fibroblasts were isolated from 6-8 week old C57/Bl6 mice as previously described (McIntosh, Hagood et al. 1994). Briefly, mouse lungs were lavaged with sterile PBS, the pulmonary vasculature was perfused with heparin-supplemented PBS, and then lungs were excised. Following dissection of lobes 1-5, lung parenchyma was minced and subject to enzymatic disruption (DNaseI, trypsin, collagenase; Sigma; St. Louis, MO) and plated onto tissue culture polystyrene. Early passage fibroblasts (P3-P5) were sorted for Thy-1 expression using FACS after staining with FITC-labeled anti-CD90.2 monoclonal antibody (53-2.1, BD Pharmingen). Cells were sub-cultured and re-sorted until subpopulations of >90% purity was obtained. Cells were routinely maintained and sub-cultured in DMEM supplemented with 10% FBS, 100 μg/mL penicillin/streptomycin, and 1 mM sodium pyruvate (CellGro; Herndon, VA).

4.2.1.3 Generation of RFL-6 cell lines

RFL-6 cell lines stably expressing a wild-type Thy-1.2 construct were used as previously described (Barker, Grenett et al. 2004, Rege, Pallero et al. 2006). Briefly,

RFL-6 cells were transfected with pcDNA3.1zeo+ vector with Thy-1.2 inserted into the multiple cloning site using *Eco*RI/*Xho*I or empty pcDNA3.1zeo+ vector as control and selected with 500 ug/mL Zeocin (Invitrogen; Carlsbad, CA). Following stable expression selection, cells were sorted Thy-1 expression for >95% Thy-1 expression purity and expression levels equivalent to endogenous Thy-1^{pos} fibroblasts. Cells were routinely maintained and sub-cultured in Ham's F12 (CellGro) supplemented with 10% FBS, and 100 µg/mL penicillin/streptomycin.

4.2.1.4 Sorting and transfection of c-Src/Yes/Fyn knockout cells

c-Src/Yes/Fyn-knockout MEFs (SYFs) (Klinghoffer, Sachsenmaier et al. 1999)obtained from ATCC (a generous gift of Dr. Andres Garcia, Georgia Institute of Technology) were cultured in DMEM supplemented with 10% FBS, 100 µg/mL penicillin/streptomycin, and 1 mM sodium pyruvate. SYFs were sorted for Thy-1 expression using FACS after staining with FITC-labeled anti-CD90.2 monoclonal antibody (53-2.1, BD Pharmingen). Cells were sub-cultured and re-sorted until subpopulations of >90% purity was obtained. Thy-1^{pos} and Thy-1^{neg} SYFs were transfected with EGFP-tagged c-Src or Fyn (a kind gift of Dr. Margaret Frame, Edinburgh Cancer Research Center) using Amaxa Nucleofector (Lonza; Basel, Switzerland) program U-30. After 24 hrs, cells were plated on pAAm substrates of varying stiffness, fixed, and the actin cytoskeleton was stained for quantification of cell spread area as described below.

4.2.2 ECM substrates

4.2.2.1 Preparation of cell-derived matrices (CDM)

CDMs were prepared according to Cukierman et al (Cukierman, Pankov et al. 2001). Briefly, 0.2% gelatin was adsorbed onto coverglass and crosslinked with 1.0%

glutaraldehyde. Following quenching with 1M glycine and PBS washing, NIH-3T3 cells (ATCC) were plated at $5x10^5$/mL into a 6-well plate. Cultures were maintained in DMEM supplemented with 10% FBS, 100 μg/mL penicillin/streptomycin, 1 mM sodium pyruvate, and 50 μg/mL ascorbic acid, with media changed every 48 hrs. After 8 days, cells were extracted using 0.5% TritonX-100, 20 mM Na_4OH in PBS, and DNAseI was used to digest any remaining nuclear material. CDMs were extensively washed with PBS and stored at 4°C in 100 μg/mL penicillin/streptomycin-supplemented PBS for up to 2 weeks.

4.2.2.2 Preparation of polyacryamide (pAAm) gel substrates

Polyacrylamide (pAAm) hydrogels with varying bisacrylamide concentrations were fabricated on amino-silanated coverslips, as previously described (Tse and Engler 2010, Brown, Fiore et al. 2013). Briefly, pAAm gel solutions were produced by combining acrylamide and bisacrylamide (Biorad; Hercules, CA) to final concentrations of 8% acrylamide and 0.045%, 0.102%, 0.146%, or 0.239% bisacrylamide to obtain gels with final elastic moduli of 1.8 kPa, 6.7 kPa, 10.6 kPa, or 18.7 kPa, respectively. 50 μl of each solution was polymerized by the addition of 1% (v/v) ammonium persulfate (VWR; West Chester, PA) and 0.1% (v/v) N,N,N',N'-tetramethylethylenediamine (Biorad). Human plasma fibronectin (Fn) was purified from blood plasma and covalently attached to the surface using the heterobifunctional crosslinker sulfosuccinimidyl-6-(4'-azido-2' nitrophenyl-amino)hexanoate (sulfo-SANPAH, Pierce Chemical Co.; Rockford, IL). Following overnight incubation with Fn, gels were then washed and stored in PBS.

4.2.3 Assays of cytoskeletal phenotype

4.2.3.1 Immunofluorescence staining

Thy-1 mouse lung fibroblast subpopulations or RFL-6 lines were plated on Fn-coated PAAm substrates of varying rigidity at a seeding density of 1,000 cells/cm^2. Cells plated in 10% FBS-containing growth media were allowed to attach and spread for 4 hours at 37°C, 5% CO_2. Samples were then fixed using 4% formaldehyde, permeabilized in 0.2% Triton X-100 for 5 minutes, and blocked with 10% normal goat serum (NGS). Primary antibodies including V284 (vinculin, Millipore; Billerica, MA), 8d4 (talin, Sigma), 53-2.1 (Thy-1, BD Pharmingen), 5E10 (Thy-1, BD Pharmingen), and AB2024 (Fn, Millipore) along with AlexaFluor-labeled secondary antibodies were used for staining (Invitrogen). AlexaFluor-conjugated phalloidin (Invitrogen) was used to stain F-actin, and samples were counterstained with Hoechst 33528 (Invitrogen). Images were acquired at 20x (Plan-fluor, 0.5 N.A.) or 60x (Plan-apochromat, 1.4 N.A.) magnification with a Nikon TiE epifluorescence microscope (Nikon; Tokyo, Japan) and CoolSNAP HQ2 monochromatic CCD camera (Photometrics; Tucson, AZ), or using a Zeiss LSM700 confocal microscope (Carl Zeiss, Inc.; Jena, Germany) with a variable secondary dichroic and 20x (0.8 N.A.), 60x (1.4 N.A.) objectives. Cell area was measured with an intensity-based auto-detection algorithm to detect and highlight borders and calculate pixel number. Quantitatively similar values of cell area are detected for membrane staining (DiI), actin, and vinculin immunostaining.

4.2.3.2 Quantification of cell and adhesion morphometrics

Immunostained vinculin image planes were extracted from 60x fluorescent micrographs and loaded into MATLAB. First, general background elimination was performed by averaging the intensity of a user-defined background polygon, and the average background pixel intensity was set to zero. Single cells within the field of view

were masked and remaining pixels could be converted to cell area. A second mask, applied as a function of the standard deviated of the pixel intensity distribution, was used to select and convert adhesions to a binary sequence. Connected pixels were then grouped into bins based on size, converted to units (μm^2), and saved as the focal adhesion size data to the output structure.

4.2.3.3 AFM analysis of cortical stiffness

Cells were plated as for immunofluorescent staining and measured within 4-6 hours of plating. Using an MFP-3D-BIO atomic force microscope (AFM) (Asylum Research; Santa Barbara, CA), nanoindentation tests were performed in fluid conditions (DMEM + 10 mM HEPES, 10% FBS, 1% penicillin and streptomycin, pH 7.4) using a 4.74 μm diameter spherical tipped-silicon nitride cantilever (Bruker; Camarillo, CA). Cantilever spring constants were measured prior to sample analysis using the thermal fluctuation method, with nominal values of 40-60 pN/nm. Single force points taken from at least 3 peri-nuclear regions of greater than 300 nm in height were averaged to determine a cell's average cortical stiffness. Similarly, regions of PAAm substrate surrounding measured cells were probed. Force-indentation curves were individually analyzed using the Hertz model for spherical tips, from which Young's modulus was obtained. The sample Poisson's ratio was assumed as 0.33, and a power law of 1.5 was used to model tip geometry. AFM measurements were made using a 2 nN force set point and an indentation rate of 22.85 μm/s.

4.2.3.4 Collagen gel contraction

Trypsinized cells were re-suspended at $5x10^6$ cells/mL in growth media and added to NaOH-neutralized acid-prepared rat tail collagen, type I (BD Biosciences) at a final suspension of $0.5x10^5$ cells/mL in 1.0 mg/mL collagen, type I. After polymerization for 60 min. at 37°C, gels were disassociated and growth media was added to monitor

floating contraction over 72 hrs. To obtain gel contraction values, the diameter of the well and the gel were measured using ImageJ software, and the percentage of contraction was calculated using the formula 100× (well diameter − gel diameter)/well diameter.

4.2.4 Assays of force-dependent signaling

4.2.4.1 RhoA activity assay

RFL-6 or CCL-210 cells were plated on pAAm substrates at $5x10^3/cm^2$. After 4 hours, cells were washed once with ice-cold PBS and the RhoA G-LISA assay (Cytoskeleton, Inc.; Denver, CO) was performed per manufacturer's instructions. After absorbance measurements were taken at 490 nm, buffer-only background levels were subtracted and normalized by the experimental group with lowest RhoA activity levels. For magnetic force application assays, cells were plated and subject to force application as described below and RhoA G-LISA was performed; relative RhoA activity values were obtained after normalizing to zero force RhoA activity signal per experimental group. Western blot for total RhoA protein was used to ensure protein expression of RhoA was equivalent between samples and treatment conditions.

4.2.4.2 Magnetic tweezing and complex precipitation assay

$2x10^6$ cells/dish were plated in a 10 cm tissue culture-treated polystyrene dish and made quiescent overnight in serum-free DMEM. 2.8 μm diameter magnetic beads (M280 Dynabead, Invitrogen) coated with full-length Fn, anti-transferrin receptor (CD71, H-300; Santa Cruz Biotechnology), bovine serum album (BSA) were added at a 10:1 ratio of beads per cell in serum-free plus 0.5% BSA. Following a 15 minute period to allow bead attachment, a neodymium permanent magnet with (surface field of 2451 Gauss, K & J Magnets, Inc.) was placed 6 mm from the dish surface. Following the prescribed time of magnetic force application, cells were lysed (10 mM HEPES (pH 7.6),

150 mM NaCl, 0.1% NP-40, 2 mM $MgCl_2$ plus protease inhibitor cocktail), the bead fraction was precipitated magnetically (DynaMag, Invitrogen). Following 3x wash with lysis buffer, co-precipitated proteins were either denatured in 2x Laemmli for immunoblot anaysis or stained with primary and secondary antibodies for flow cytometry. Force levels applied using this set-up were between 10-16 pN per bead as verified using COMSOL simulations and according to those published previously (Guilluy, Swaminathan et al. 2011).

4.2.4.3 Western blots

Cultured cells directly lysed in Laemmli buffer or bead-associated adhesion complexes were heat-denatured at 95°C for 5 min. Protein was separated electrophoretically on a 4-15% polyacrylamide gel (Biorad) according to standard procedures, then transferred to nitrocellulose membranes using a semi-dry transfer apparatus (Trans-Blot SD, Biorad), blocked with 5% nonfat dry milk in TBS or 5% BSA, then incubated with Thy-1 (9798, Cell Signaling Technology; Danvers, MA), αv integrin (AB1930, Millipore), α5 integrin (AB1928, Millpore), talin (8d4, Sigma), paxillin (5H11, Millipore), pY397-FAK (44-624G, Invitrogen), Fyn (1S, Millipore), c-Src (32G6, Cell Signaling Technology), and pY418-SFK (2101, Cell Signaling Technology) primary antibodies overnight at 4° C. Following washing with TBS + 0.1% Tween 20, membranes were incubated for 2 hours with IR secondary antibody (Licor; Lincoln, NE), washed, and imaged using the Odyssey IR scanner (Licor). Western blots were quantified using ImageJ image processing software and a minimum of n = 3 blots were quantified and averaged per group.

4.3 Results

4.3.1 Emergence of Thy-1^{neg} population in IPF fibroblasts

Due to the small spatial scale and heterogeneous nature of the histopathological features of IPF, isolation of cells from diseased versus normal regions of lung tissue within IPF patients has not been currently achieved. Since the predominance of normal lung fibroblasts highly express Thy-1, whereas fibroblasts within fibroblastic foci are Thy-1^{neg}, we reasoned that lung fibroblasts from IPF patients (IPFLFs) would exhibit a significant population of cells with low Thy-1 expression. Thy-1 expression was profiled in five donors with clinically diagnosed IPF (male and female between ages 28-61) and five normal healthy donors using flow cytometry (Figure 7A). Thy-1 expression was significantly lower (85% compared to 95%; P = 0.0169) (Figure 7B). This resulted in the emergence of a population of Thy-1^{neg} cells that could be sorted for using fluorescence-activated cell sorting (FACS). In contrast, all normal lung fibroblasts (NLFs) tested exhibited a single peak of high Thy-1 expression. Therefore we established Thy-1^{pos} and Thy-1^{neg} IPFLFs that were positive or negative for Thy-1, respectively.

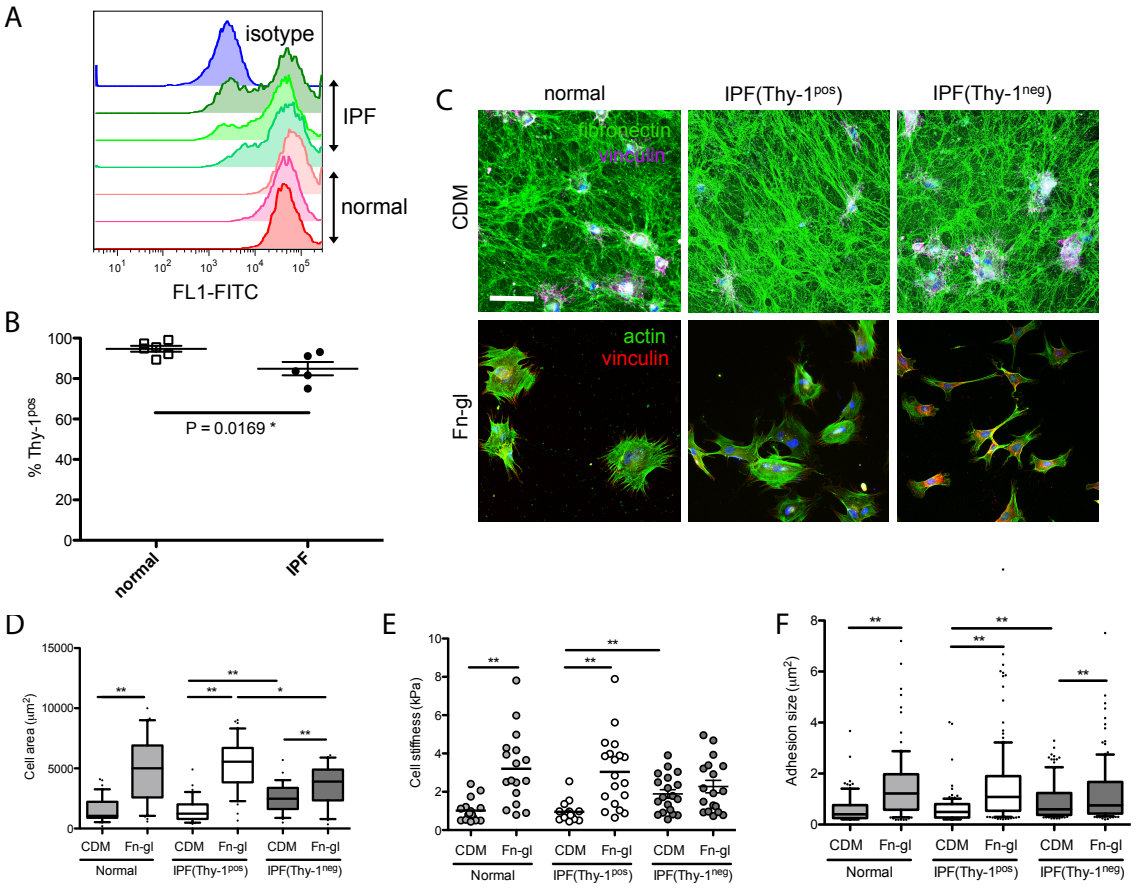

Figure 7: Thy-1 expression and cytosketetal phenotype of IPF and normal lung fibroblasts. (A) Flow cytometry histograms of Thy-1 expression for individual samples of IPF (green) and normal lung fibroblasts (red). Isotype antibody control (blue) indicates Thy-1^{neg} expression levels. (B) Quantification of the percentage of Thy-1^{pos} fibroblasts for normal and IPF fibroblasts. Mean ± S.E.M. are shown; P-value for an unpaired, two-tailed Student's t-test is shown. (C) Immunofluorescence of fibronectin and vinculin overlay (top) or vinculin and actin overlay (bottom) for IPF and normal lung fibroblasts plated on CDMs or Fn-glass. Scale bar = 100 µm. (D-F) Box or dot plots of cell area (D), cell stiffness (E), and adhesion size (F) for normal vs. Thy-1^{pos} and Thy-1^{neg} IPF fibroblasts on CDMs and Fn-glass. Boxes indicate the lower and upper quartile and whiskers are 10-90 percentile. * = p <

0.05; ** = p < 0.01; *** = p < 0.001, as assessed by unpaired, two-tailed Student's t-test for (C, D) and Mann-Whitney test (E).

4.3.2 Loss of Thy-1 enhances cytoskeleton activation in physiologic matrices

Previous studies on Thy-1 regulation of fibroblast phenotype have been performed in the context of cells adherent to ECM-coated coverglass. As this environment is known to 1) promote significant activation of most soft tissue cells, including fibroblasts (e.g. proliferation, enhanced metabolic activity, protein synthesis, cytoskeleton activation), 2) promote differentiation of normal fibroblasts into myofibroblasts (i.e. α-SMA- and EDA-Fn-expressing fibroblasts), and 3) exhibit physical properties far from those encountered during normal lung physiology, we studied cell responses to a physiologically relevant 3D cell-derived matrix (CDM). CDMs were prepared from NIH-3T3 cultures and consisted of Fn-rich fibrillar matrices of approximately 30 μm in thickness and an average Young's modulus of 670 ± 50 Pa (mean, μ ± S.E.M.; data not shown). Thy-1^{pos} IPFLFs plated on CDMs exhibited a cell spread area of 1501 ± 175 μm^2, similar to NLFs (1539 ± 164 μm^2); whereas on Fn-coated glass (Fn-glass), both Thy-1^{pos} IPFLFs and NLFs increased their spread area by approximately 3.5-fold (5373 ± 348 and 4976 ± 485 μm^2, respectively) and formed actin stress fibers, consistent with robust activation of the cell spreading response and cytoskeleton activation on rigid substrates (E ≈ 3 GPa) (Figure 7D). In contrast Thy-1^{neg} IPFLFs had a significantly higher cell area (2588 ± 222 μm^2) on CDMs, but lower on Fn-glass (3467 ± 318 μm^2) than Thy-1^{pos} IPFLFs and NLF. (Figure 7D) Atomic force microscopy (AFM) was used to measure the cell's cortical stiffness as a direct quantification of their cytoskeletal organization and contractile activity in different microenvironments (Figure 7E). Similar to cell area measurements, both Thy-1^{pos} IPFLFs and NLFs had significantly lower Young's moduli than did Thy-1^{neg} IPFLFs on CDMs (922 ±123 and 994 ± 132 vs. 1731 ± 202 Pa, respectively), whereas on Fn-glass,

Thy-1^{pos} IPFLFs and NLFs were significantly higher than Thy-1^{neg} IPFLFs (3.224 ± 0.409 and 3.111 ± 0.418 vs. 2.164 ± 0.265 kPa). Therefore, Thy-1-expressing cells from both IPF and normal patients exhibited significantly more robust cell spreading and contractile responses to rigid substrates, whereas Thy-1^{neg} cells had higher cytoskeleton activation in physiologic CDMs.

We then analyzed the morphometry of focal adhesions (FAs) via immunofluorescence staining of vinculin and quantitative image analysis. Generally, FA size is directly proportional to local traction force magnitude during initial adhesion assembly and maturation (i.e. < 10 μm from the leading edge; Stricker, Aratyn-Schaus et al. 2011). On CDMs, Thy-1^{pos} IPFLFs and NLFs had small FAs of approximately 0.5 μm^2 in size, whereas on Fn-glass a portion of FAs became significantly elongated and enlarged, indicative of adhesion maturation. The mean FA area similarly increased to 1.531 ± 0.139 and 1.552 ± 0.124 μm^2 for Thy-1^{pos} IPFLFs and NLFs, respectively (Figure 7F). In contrast, Thy-1^{neg} IPFLFs had significantly larger FAs than Thy-1-expressing cells on CDMs (0.929 ± 0.071 μm^2), indicating higher levels of adhesion maturation in physiologic ECMs.

To specifically investigate the role of Thy-1 expression on cytoskeletal responses to the ECM microenvironment, we knocked down Thy-1 expression in normal human lung fibroblasts using lentiviral-based RNA inhibition (RNAi). Control cells (cont.shRNA) displayed a phenotype consistent with NLFs and Thy-1^{pos} IPF fibroblasts, namely the spread area, cortical stiffness and adhesion size was dramatically reduced on CDMs compared to Fn-glass (Figure 8A-D). In contrast, Thy-1 knockdown (Thy-1.shRNA) increased cell area and cortical stiffness on CDMs by approximately 50% and 80%, respectively, and decreased cell area and cortical stiffness on Fn-glass by 25% and 65% compared to cont.shRNAs (Figure 8B,C). Similarly to Thy-1^{neg} IPFLFs, Thy-1.shRNAs had enlarged FAs on CDMs compared to cont.shRNAs (0.984 ± 0.072 vs.

$0.606 \pm 0.028\ \mu m^2$), but a significantly lower fraction of large FA ($\geq 1.5\ \mu m^2$) on Fn-glass (Figure 8D). Thus, Thy-1 expression confers enhanced cytoskeleton activation in microenvironments of supraphysiologic rigidity, whereas loss of Thy-1 expression results in enhanced cytoskeleton and cell-matrix adhesion activity in physiologic matrices.

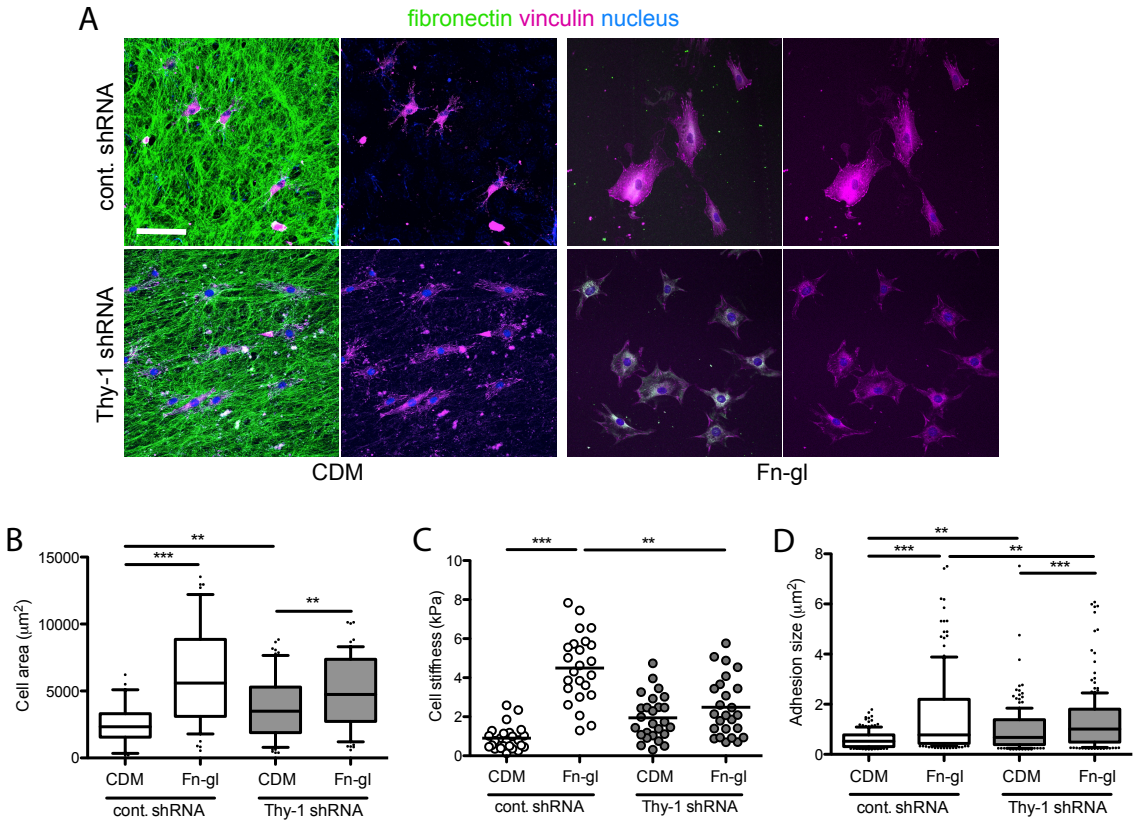

Figure 8: Thy-1 knockdown alters the cytoskeletal phenotype of normal lung fibroblasts. (A) Immunofluorescence of fibronectin and vinculin overlay (left) or vinculin only (right) for shRNA-treated NLFs plated on CDMs or Fn-glass. Scale bar = 100 μm. (B-D) Box or dot plots of cell area (B), cell stiffness (C), and adhesion size (D) for cont.shRNA- vs. Thy-1.shRNA-treated fibroblasts on CDMs and Fn-glass. Boxes indicate the lower and upper quartile and whiskers are 10-90 percentile. * = $p < 0.05$; ** = $p < 0.01$; *** = $p < 0.001$, as assessed by unpaired, two-tailed Student's t-test for (B, C) and Mann-Whitney test (D).

4.3.3 Thy-1 enhances mechanosensitivity to ECM rigidity

As rigidity is one of the parameters (including matrix biochemistry, ligand presentation/conformation, dimensionality, and surface topology and topography) different between 3D Fn-rich CDMs and Fn-glass, we investigated whether substrate rigidity sensing was directly modulated by Thy-1 expression. Polyacrylamide (pAAm) gels of variable rigidity were synthesized by varying the crosslinker, bis-acrylamide, concentration, and Fn was covalently immobilized the surface. Gel Young's modulus, *E*, was measured by AFM and controlled to approximate the *E* of normal and fibrotic lung tissue as previously determined (e.g. 2.2 kPa = normal, soft; 18.7 kPa = fibrotic, stiff). Cont.shRNAs or Thy-1^{pos} primary mouse lung fibroblasts (pMLFs) plated on soft pAAm gels exhibited a mainly cortical and diffuse actin cytoskeleton with small or unobservable adhesion plaques, whereas Thy-1.shRNA or Thy-1^{neg} pMLFs displayed larger FAs and bundled actin filaments, demonstrating enhanced cytoskeletal maturation on soft matrices (Figure 9A, Figure 10A). Consistently, Thy-1.shRNA and Thy-1^{neg} pMLFs spread area and cortical stiffness was higher than cont.shRNAs or Thy-1^{pos} pMLFs. On stiff ECM, Thy-1^{pos} displayed larger actin filament bundles (i.e. stress fibers) and larger and more elongated FAs (Figure 9B-D, Figure 10B,C). This demonstrates that Thy-1 expression is critical for efficient mechanosensitive remodeling of the cytoskeleton.

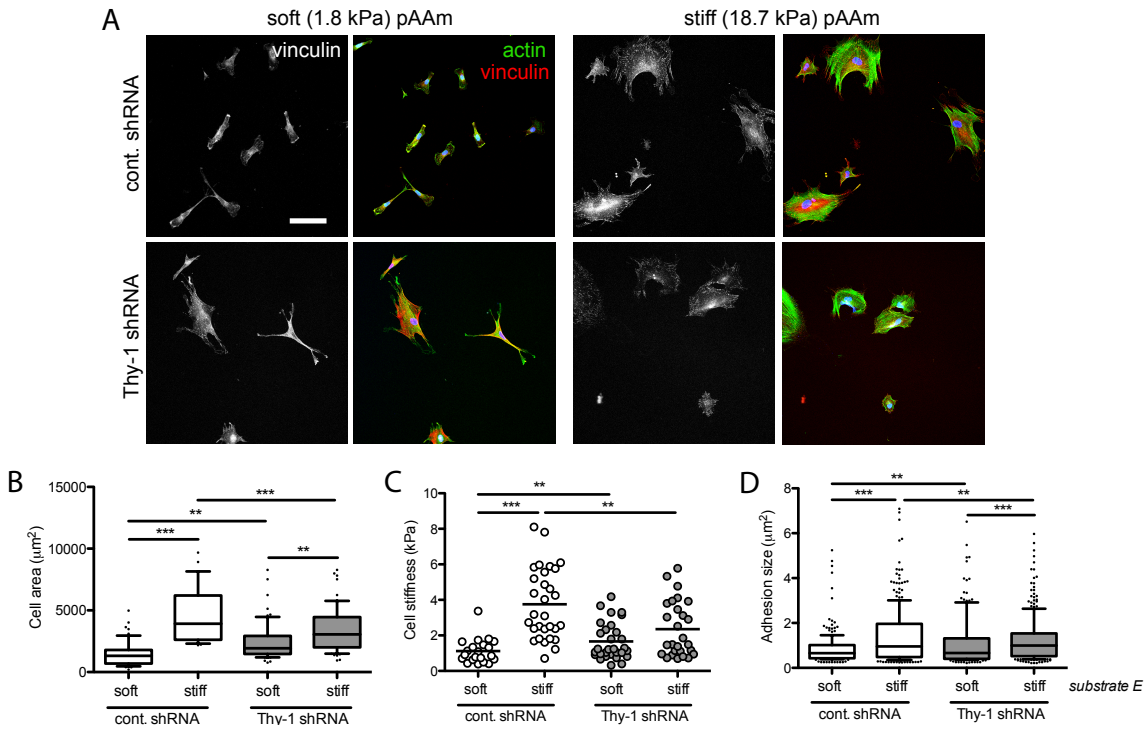

Figure 9: Analysis of Thy-1-dependent rigidity sensing in human lung fibroblasts. (A) Immunofluorescence of actin and vinculin cont.shRNA- vs. Thy-1.shRNA-treated fibroblasts on soft (1.8 kPa) vs. stiff (18.7 kPa) Fn-coated pAAm substrates. (B-D) Box or dot plots of cell area (B), cell stiffness (C), and adhesion size (D) for cont.shRNA- vs. Thy-1.shRNA-treated fibroblasts on soft and stiff pAAm substrates. Boxes indicate the lower and upper quartile and whiskers are 10-90 percentile. * = $p < 0.05$; ** = $p < 0.01$; *** = $p < 0.001$, as assessed by unpaired, two-tailed Student's t-test for (B, C) and Mann-Whitney test (D).

To further demonstrate that Thy-1 expression is sufficient to promote the mechanotransduction of ECM rigidity, we exogenously expressed wild-type Thy-1 in a rat lung cell line that is endogenously Thy-1^{neg} (RFL-6) and investigate the resulting cytoskeletal phenotypes. In agreement our previous data, monotonic growth of cortical *E* with substrate *E* up to a saturation limit of approximately 20 kPa is observed (Figure

10C). When plotted on a semi-log scale, a linear trend is observed, with which a linear least-square regression can be used to fit data. RFL-6s transfected with Thy-1 (RFL-6^{Thy-1}) exhibited enhanced substrate *E*-sensitive cortical stiffening (slope, k = 3.582 ± 0.493 kPa/kPa, r^2 = 0.615) which is statistically the same as Thy-1^{pos} pMLFs (k = 3.832 ± 0.493 kPa/kPa, r^2 = 0.598), compared with RFL-6^{EV} (k = 1.435 ± 0.493 kPa/kPa, r^2 = 0.488) and Thy-1^{neg} pMLFs (k = 1.233 ± 0.396 kPa/kPa, r^2 = 0.423) (Figure 10C). Similarly, RFL-6^{Thy-1} showed significantly enhanced substrate *E*-sensitive cell spreading (k = 1728 ± 126 μm^2/kPa, r^2 = 0.509) compared to RFL-6^{EV} (k = 798 ± 167 μm^2/kPa, r^2 = 0.668), similarly to pMLFs (k = 4081 ± 229 μm^2/kPa, r^2 = 0.72 and k = 1825 ± 232 μm^2/kPa, r^2 = 0.676 for Thy-1^{pos} and Thy-1^{neg}, respectively) (Figure 10B,D). FAs also became significantly enlarged due to increases in substrate *E* in RFL-6^{Thy-1}, whereas this effect was muted in RFL-6^{EV} (Figure 10E). Thus, exogenous Thy-1 expression is sufficient to enhance mechanotransduction of ECM rigidity, and this enhancement is similar to that observed in endogenous Thy-1-expressing cells.

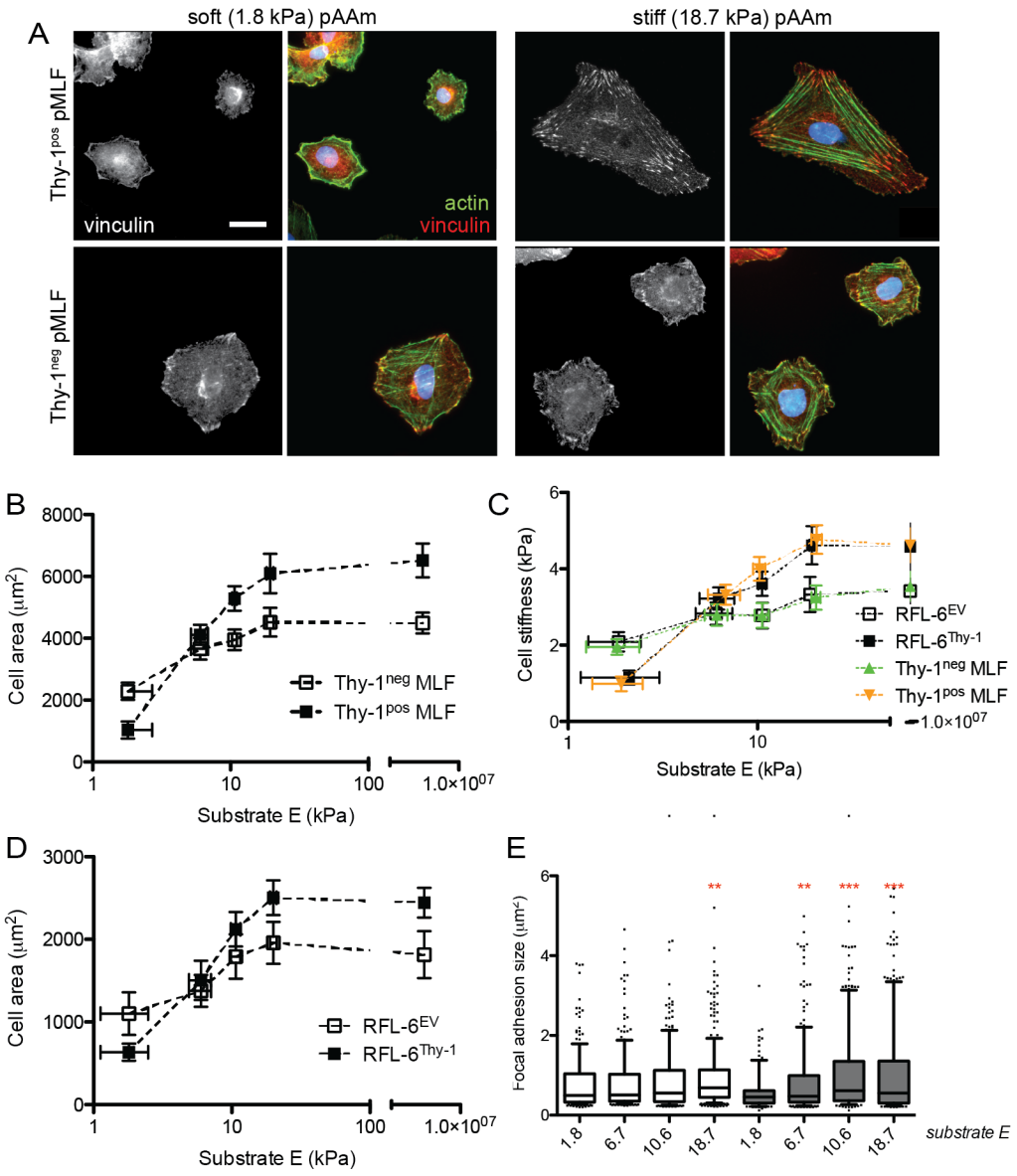

Figure 10: Analysis of Thy-1-dependent rigidity sensing in endogenous Thy-1 subpoulations and via exogenous re-expression. (A) Immunofluorescence of vinculin-only (left) or vinculin and actin overlayed (right) in Thy-1^{pos} vs. Thy-1^{neg} pMLFs on soft (top) and stiff pAAm (bottom) substrates. Scale bar = 20 μm. (B) Cell area vs. substrate *E* (mean ± S.E.M.) in Thy-1^{pos} vs. Thy-1^{neg} pMLFs. (C) Cell stiffness vs. substrate *E* (mean ± S.E.M.) for Thy-1^{pos} vs. Thy-1^{neg} pMLFs overlaid with RFL-6^{EV} vs. RFL-6^{Thy-1} cells. (D) Cell area vs. substrate *E* (mean ± S.E.M.) in RFL-6^{EV} vs. RFL-6^{Thy-1} cells. (H) Box plots of adhesion size for RFL-6^{EV} (white) and

RFL-6^{Thy-1} (gray) cells Boxes indicate the lower and upper quartile and whiskers are 10-90 percentile. * = p < 0.05; ** = p < 0.01; *** = p < 0.001, as assessed by the Mann-Whitney test.

4.3.4 Thy-1 modulates rigidity sensing via RhoA activation

Barker et al. have previously shown that Thy-1 expression modulates RhoA activity via SFK-mediated signaling through p190RhoGAP (Barker, Grenett et al. 2004). As RhoA is a major signaling hub for control of the actin cytoskeleton whose activity is modulated by ECM rigidity, we investigated whether Thy-1 expression regulated the activation state of RhoA in response to changes in substrate *E*. We performed RhoA activity assays (based on affinity pull-down of the GTP bound-specific RhoA effector rhotekin) on soft and stiff pAAm substrates. In cont.shRNA human lung fibroblasts, RhoA activity was approximately 2-fold higher on stiff vs. soft substrates (Figure 11A). This response was significantly muted in Thy-1.shRNA cells, where RhoA activity was not statistically different between soft and stiff substrates. However, RhoA activity was approximately 50% higher in Thy-1.shRNA compared to cont.shRNA on soft substrates (Figure 11A). Consistent with these results, RFL-6^{Thy-1} demonstrated enhanced substrate rigidity-dependent RhoA activation across a range of substrate *E*, whereas this response was again muted in RFL-6^{EV} (Figure 11B). Importantly, RhoA signaling was critical in the Thy-1-mediated cell spreading response to substrate *E*, as inhibition of downstream signaling effector Rho kinase (ROCK), largely abolished substrate *E*-dependent spreading in both Thy-1.shRNA- and cont.shRNA-treated NLFs (Figure 11E).

To further investigate how Thy-1 modulates RhoA activation in a substrate *E*-dependent manner, we decided to investigate whether direct force-dependent RhoA activation is affected by Thy-1 expression. It was recently demonstrated by Guilluey et al. that applying a tensile force to the cell surface via 2.8 μm-diameter Fn-coated beads,

with an approximately 15 pN constant force, is sufficient to mechanically activate RhoA (approximately 2-fold over 5 min. timescale). This contributes to the growing literature body validating RhoA as a mechanosensitive signaling element. We repeated this same experimental setup using RFL-6^{EV} and RFL-$6^{Thy\text{-}1}$ cells (schematic, Figure 11C). We found that force via Fn receptors was sufficient to activate RhoA in quiescent RFL-6 cells, however force application with an antibody to the transferrin receptor (CD71, TfR) did not activate RhoA, nor did beads coated with BSA (data not shown) (Figure 11D). RhoA activity increased with force application time in a dose-dependent manner, reaching maximal activity between 3-5 min. Intriguingly, we found that in the presence of Thy-1 expression, RhoA activity was elevated by approximately 2-fold in response to force, however this effect was diminished by approximately 50% in the absence of Thy-1. Therefore, this data demonstrates that Thy-1 modulates the direct force responsiveness of RhoA via Fn receptors.

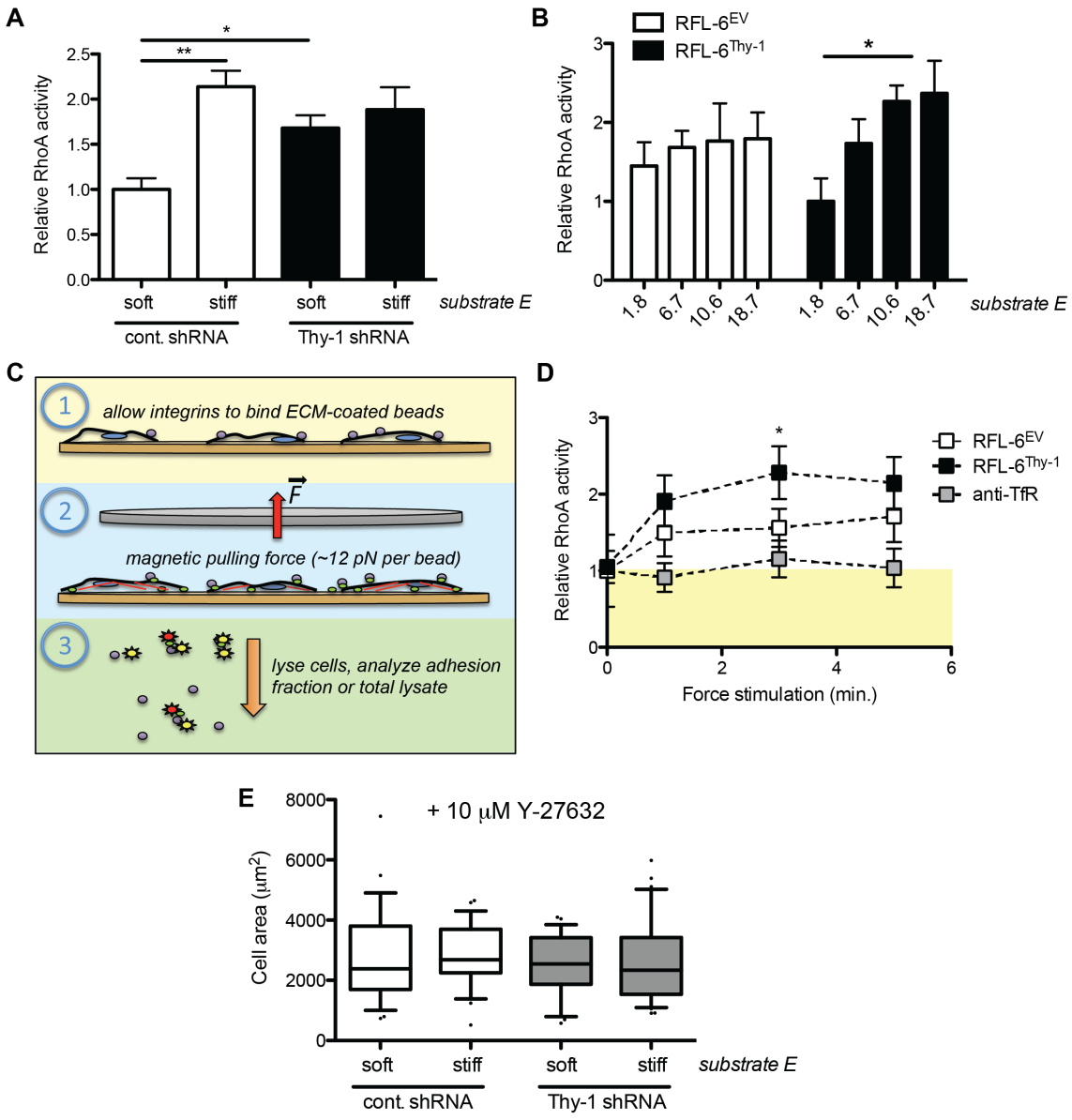

Figure 11: Analysis of substrate rigidity- and force-dependent RhoA activity. (A) RhoA activity (mean ± S.E.M.) of cont.shRNA- vs. Thy-1.shRNA-treated normal lung fibroblasts on soft (1.8 kPa) vs. stiff (18.7 kPa) Fn-coated pAAm substrates. (B) RhoA activity (mean ± S.E.M.) of RFL-6^{EV} (white) and RFL-6^{Thy-1} (black) cells on Fn-coated pAAm substrates of varying rigidity. * = $p < 0.05$ as assessed by an unpaired, two-tailed Student's t-test. (C) Cartoon schematic of the magnetic force application set-up. (D) RhoA activity (mean ± S.E.M.) of RFL-6^{EV} (white) and RFL-

6^{Thy-1} (black) probed with Fn-coated beads and RFL-6^{Thy-1} probed with anti-TfR-coated beads (gray) for varied duration of magnetic force application. Yellow box inidicates the approximate level of RhoA activity in untreated cells. (E) Box plot of cell area for cont.shRNA- vs. Thy-1.shRNA-treated normal lung fibroblasts on soft (1.8 kPa) vs. stiff (18.7 kPa) Fn-coated pAAm substrates treated with 10 μM Y-27632. Boxes indicate the lower and upper quartile and whiskers are 10-90 percentile.

4.3.5 Force-dependent adhesion signaling is modulated by Thy-1

To gain more insight into how Thy-1 may be modulating the force-dependent activation of RhoA, we investigated the complex of proteins associated with the Fn-coated beads and how they changed as a consequence of force. To accomplish this, we used magnets to pull-down bead-associated complexes, and following washing steps to promote specificity, we denatured and resolved the protein complexes via SDS-PAGE. We then took a targeted approach, looking at known adhesion-associated molecules that have been previously demonstrated to be involved in mechanotransduction and mechanosignaling via Western blot (Figure 12 A,B). The prevalence of integrin receptor subunits αv and α5 was unchanged in both the presence and absence of Thy-1 and/or 5 minute force application. The integrin-actin linking protein talin was also associated independently of Thy-1 and force, suggesting that integrin ligation is sufficient for exposure of talin binding sites within the complex, or vice versa (Figure 12 A,B). Also, the prevalence of the adapter protein paxillin was independent of Thy-1 and force. Intriguingly, the SFK member Fyn was specifically associated with the complex only in the presence of Thy-1, and largely independent of force. In contrast another SFK member c-Src was associated independently of Thy-1, demonstrating the specificity of Thy-1-mediated SFK recruitment to Fyn (Figure 12 A). Interestingly, SFK activation, as reported by phosphorylation of tyrosine 418 (pY418) within the activation loop of SFK,

exhibited both force-dependent and -independent responses, however both were critically reliant on Thy-1. However another mechanosensitive signaling molecule, FAK, was activated in response to force independently of Thy-1 (Figure 12 A,B). Importantly, Thy-1 was also associated with the adhesion complexes. Therefore, Fyn recruitment and force-dependent SFK activation was dependent on Thy-1 expression. As Fyn has been demonstrated to be a critical early mechanosensitive signaling element, an upstream component of the force-dependent RhoA activation pathway, and its localization to adhesion complexes is modulated by Thy-1 expression, this represents an intriguing effector in Thy-1-regulated mechanosignaling and rigidity sensing (von Wichert, Jiang et al. 2003, Kostic and Sheetz 2006, Na, Collin et al. 2008, Guilluy, Swaminathan et al. 2011).

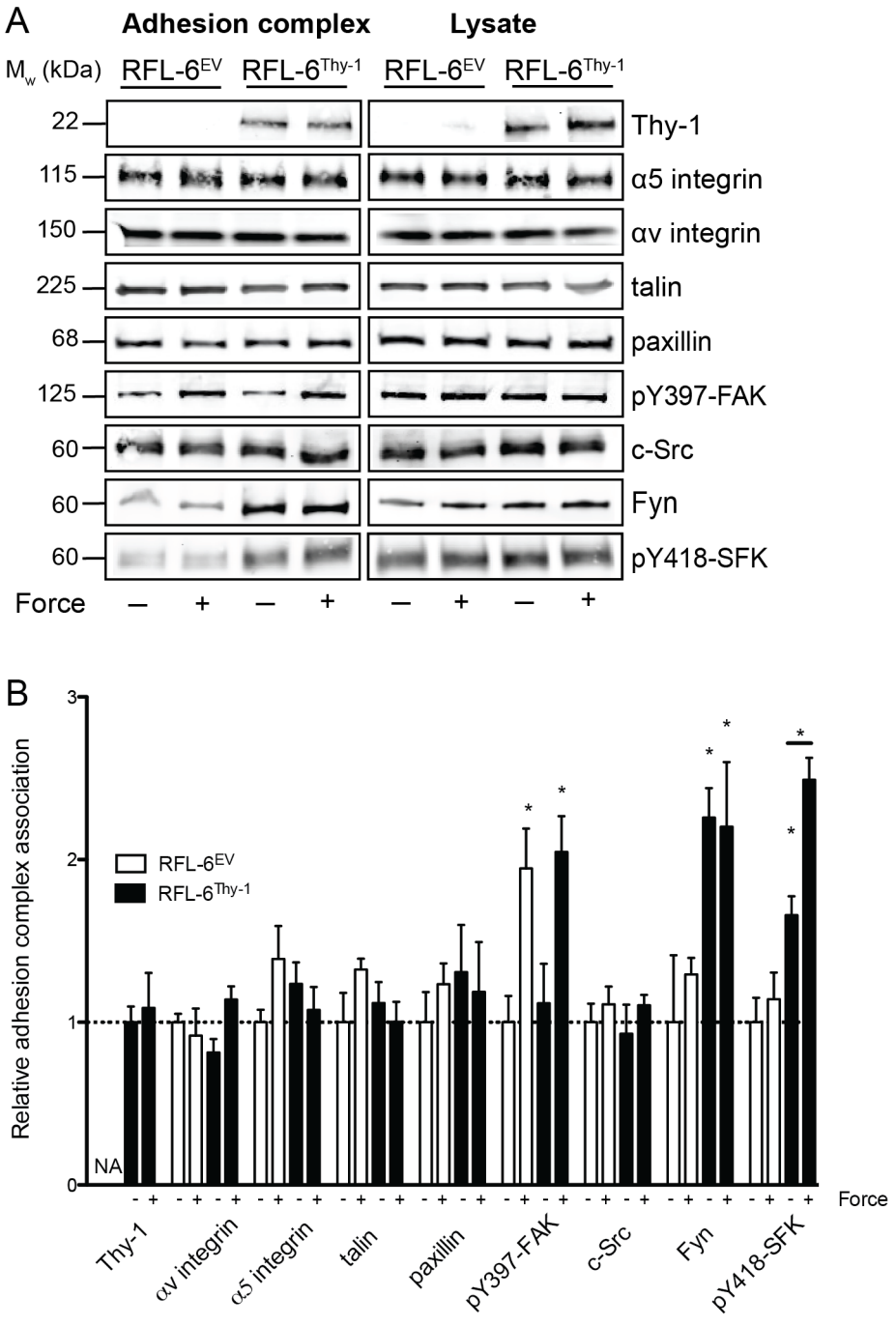

Figure 12: Analysis of Thy-1- and force-dependent adhesion complex components. (A) Western blots of indicated proteins, along with their molecular weight, within the adhesion complex or total cell lysate for RFL-6^{EV} and RFL-6^{Thy-1} cells. Absence or presence of 5 min. continual force application is indicated below individual lanes.

(B) Quantification of Western blots via densitomtery for a minimum of n = 3 blots from at least two independent experiments. Density measurements for each molecule is represented relative to the levels of RFL-6^{EV} without force application, with the exception of Thy-1, for which measurements are represented relative to RFL-6^{Thy-1} without force application. * = $p < 0.05$ as assessed by an unpaired, two-tailed Student's t-test.

4.3.6 Fyn and Thy-1 expression is required for efficient rigidity sensing

To further explore relevance of Fyn in Thy-1-regulated phenotypes, we asked the whether Fyn was a critical component of the Thy-1-dependent responses to substrate rigidity. As pharmacological inhibitors are not specific to individual SFKs, especially highly homologous members such Fyn, Lyk, c-Src, and Hck, we used a genetic approach to specifically assess the role of Fyn vs. c-Src. c-Src-Yes-Fyn triple knockout mouse embryonic fibroblasts (SYFs) were FACS sorted into Thy-1^{pos} and Thy-1^{neg} populations. Cells were then transfected with EGFP-tagged Fyn (Fyn-GFP) or c-Src (c-Src-GFP), plated on soft and stiff pAAm substrates, and the cell spreading response was assayed. In general, spreading responses were retarded in these cells, as has been previously demonstrated (Klinghoffer, Sachsenmaier et al. 1999). Non-transfected SYFs did not spread to significantly different areas on soft (1.8 kPa) vs. stiff (18.7 kPa) pAAm gels, consistent with data previously observed (Kostic and Sheetz 2006) (Figure 13 B). In contrast, Thy-1^{pos} SYFs transfected with Fyn-GFP spread and assembled actin stress fibers to a significantly greater extent on stiff substrates, whereas this did not happen in Thy-1^{neg} SYFs transfected with Fyn-GFP (Figure 13 A,B). Furthermore, Thy-1^{pos} SYFs expressing Fyn-GFP spread significantly less on soft substrates, compared to Thy-1^{pos} SYFs expressing c-Src-GFP; this affect was not observed in Thy-1^{neg} SYFs. This data demonstrates that indeed both Thy-1 and Fyn expression are required in these fibroblasts for sensitive cytoskeletal remodeling in response to changes in substrate rigidity.

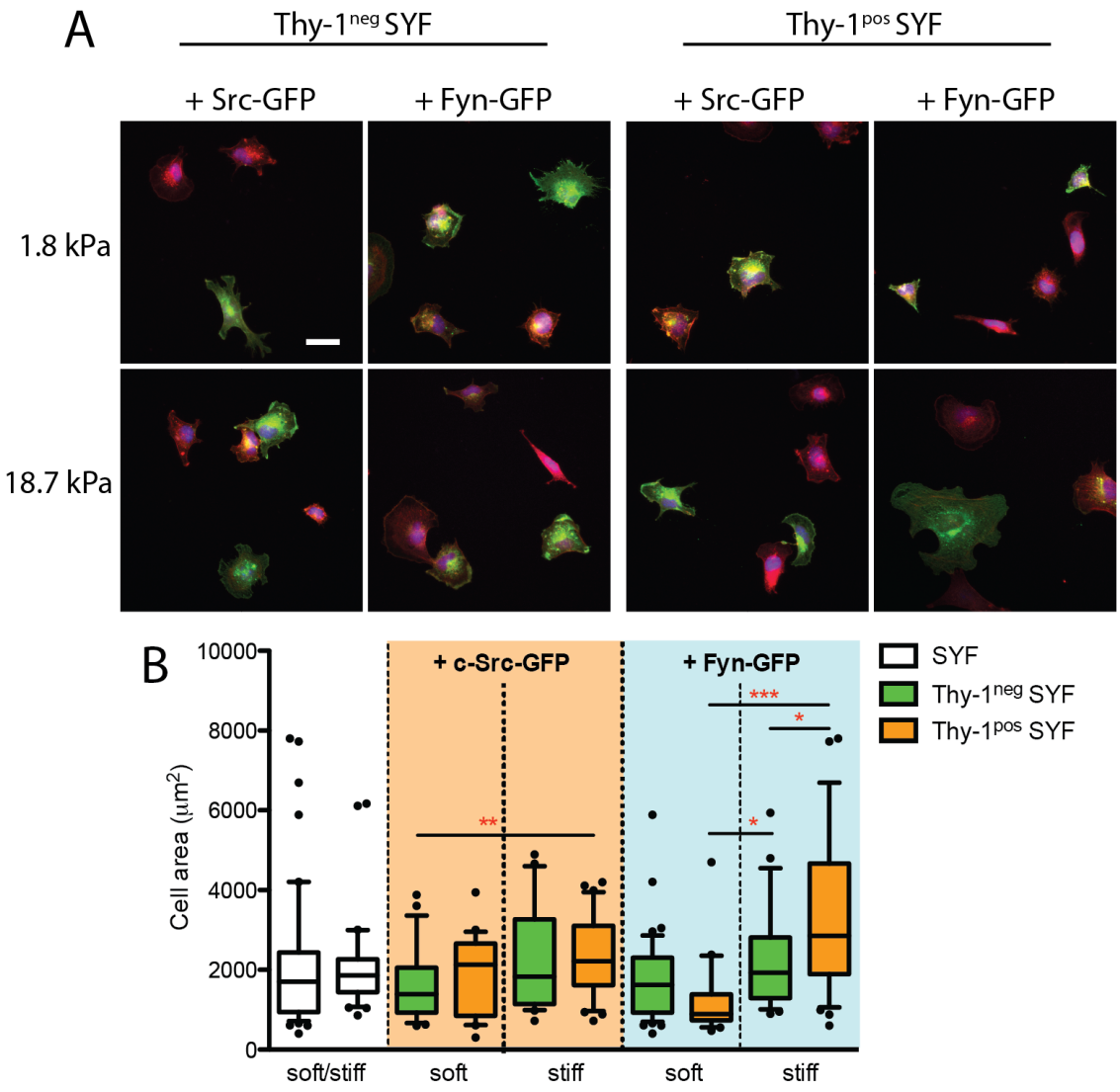

Figure 13: Analysis of c-Src- and Fyn-mediated SYF cell spreading in Thy-1^{pos} and Thy-1^{neg} SYF subpoplations. (A) Confocal micrographs of actin (red), GFP (green), and nuclei (blue) for Thy-1^{neg} (left) and Thy-1^{pos} (right) SYFs plated on the indicated stiffness Fn-coated pAAm substrate. Transiently transfected GFP-tagged SFKs are also indicated. Scale bar = 50 μm (B) Box plots of cell area for SYFs cells as indicated. Boxes indicate the lower and upper quartile and whiskers are 10-90 percentile. * = $p < 0.05$; ** = $p < 0.01$; *** = $p < 0.001$, as assessed by an unpaired, two-tailed Student's t-test.

4.3.7 Thy-1 regulates rigidity-dependent ECM assembly and remodeling

To assess the potential pro-fibrotic consequences of Thy-1^{neg} fibroblasts lack of sensitive rigidity sensing, we looked at ECM assembly and remodeling phenotypes in human lung fibroblasts. Assembly of Fn fibrils by fibroblasts in culture is dependent on cytoskeletal contractility, and inhibition of RhoA signaling or the downstream actomyosin system greatly inhibits Fn assembly (Zhang, Magnusson et al. 1997, Zhong, Chrzanowska-Wodnicka et al. 1998). Furthermore, ECM rigidity has recently been demonstrated to regulate Fn assembly, wherein cells on soft ECMs assemble significantly less Fn (Carraher and Schwarzbauer 2013). We analyzed the amount of cell-assembled Fn on soft vs. stiff matrices through quantitative immunofluorescence microscopy. Cont.shRNA fibroblasts on soft pAAm substrates did not assemble significant amounts of Fn initially, maintaining a rounded morphology, and this amount only slightly increased over 48 hrs in culture (Figure 14A,B). On stiff pAAm substrates however, cont.shRNAs dramatically increased the amount of Fn they assembled over 48 hrs. Thy-1.shRNA fibroblasts on stiff pAAm substrates exhibited a qualitatively similar level of Fn assembly as cont.shRNAs (Figure 14A,B). Uniquely, Thy-1.shRNAs were proficient at elaborating Fn matrix on soft pAAm substrates, indicating a pertinent phenotypic switch in the context of fibrotic ECM remodeling. Furthermore, Thy-1.shRNAs more efficiently contracted 1.0 mg/mL collagen matrices than did cont.shRNAs (Figure 14C,D). This enhanced contraction was mediated by ROCK signaling, as treatment with Y-27632 drastically inhibited gel contraction and normalized differences due to Thy-1 knockdown (Figure 14C,D). This data demonstrates a significantly enhanced Fn assembly/remodeling phenotype of Thy-1^{neg} fibroblasts, specifically in relatively soft ECM microenvironment.

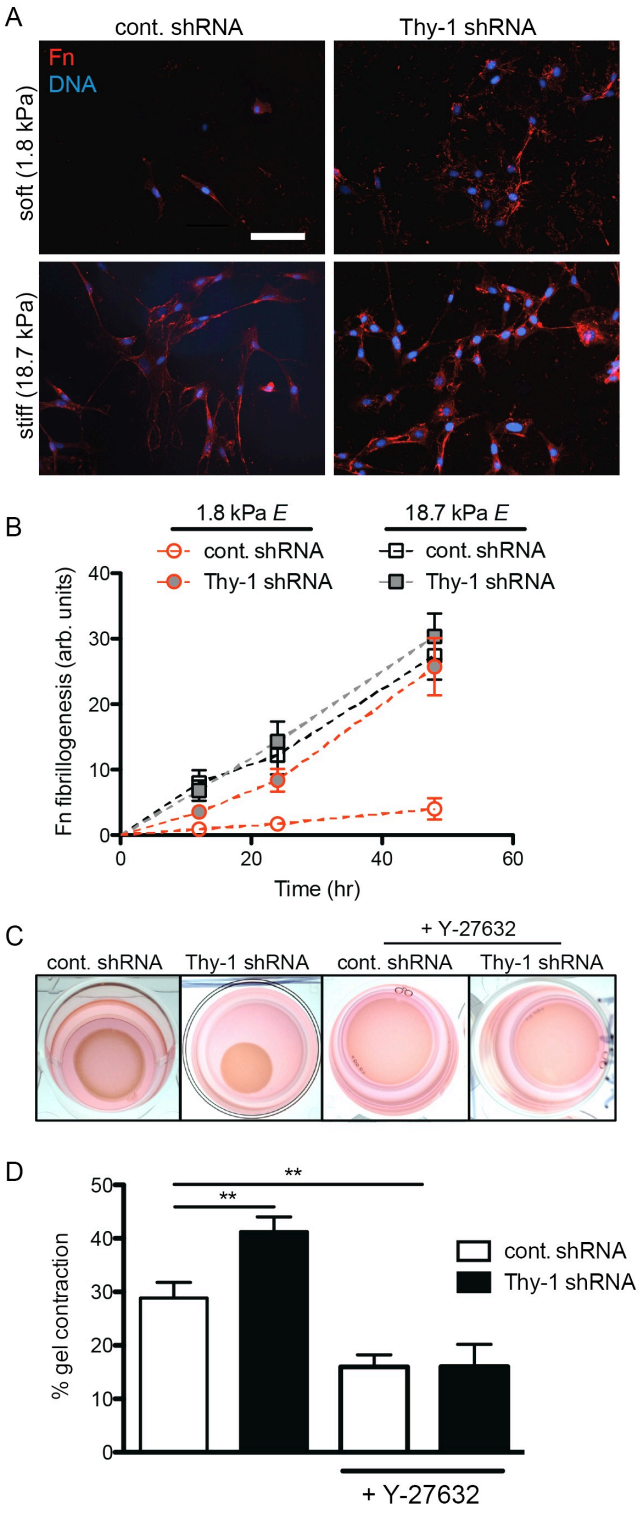

Figure 14: Thy-1 regulates Fn assembly and collagen gel contraction. (A) Immunofluorescence microscopy of extracellular Fn (red) and nuclei (blue) in

cont.shRNA- vs. Thy-1.shRNA-treated normal lung fibroblasts on soft (1.8 kPa) vs. stiff (18.7 kPa) pAAm substrates after 24 hrs. Scale bar = 10 μm. (B) Quantification of cell-associated Fn assembly (mean ± S.E.M.; area × intensity, arbitrary units) for cont.shRNA- vs. Thy-1.shRNA-treated normal lung fibroblasts on soft (1.8 kPa, red) vs. stiff (18.7 kPa, black) pAAm substrates for 12, 24, and 48 hrs. in culture. (C) Images of 1 mg/mL 3D collagen I gels contracted by fibroblasts after 48 hrs. in culture. (D) Quantification of gel contraction (percentage of the original gel diameter) for cont.shRNA- vs. Thy-1.shRNA-treated normal lung fibroblasts with and without 10 μM Y-27632 treatment. ** = $p < 0.01$ as assessed by unpaired, two-tailed Student's t-test.

4.4 Discussion

Rigid microenvironments promote cytoskeletal activation, ECM remodeling and myofibroblast differentiation, potentially resulting in a feed-forward loop of progressive fibrogenesis (Hinz 2010, Liu, Mih et al. 2010, Huang, Yang et al. 2012). However, how the initial wound environment evolves into a pathologic rigidity regime from a relatively compliant provisional matrix is not well understood. Here we analyzed the phenotype of lung fibroblasts in response to changes in ECM microenvironment, including substrate rigidity. We found that expression of the glycoprotein Thy-1 (CD90) at levels analogous to normal human lung fibroblasts, promotes sensitive cytoskeletal regulation in response to a changing ECM microenvironment, including alterations in substrate rigidity. This was observed in multiple cell systems including 1) both IPF and normal human lung fibroblasts, 2) RNAi-mediated Thy-1 gene repression in normal lung fibroblasts, 3) endogenous mouse lung fibroblast subpopulations, and 4) heterologous Thy-1 re-expression in a lung fibroblast cell line, demonstrating the robustness of this finding.

Furthermore, it demonstrates Thy-1 expression itself is required for the described phenotypic regulation. In contrast, cells lacking Thy-1 expression, either endogenously (including those isolated from heterogeneous IPF fibroblast isolates) or through genetic manipulation, are more refractory to changes in ECM rigidity. Consequently, Thy-1^{neg} cells exhibit significantly more mature actin cytoskeletons and FAs, higher cortical stiffness, and larger spread area in ECMs of rigidity not dissimilar from normal lung tissue, in contrast to the largely quiescent Thy-1^{pos} fibroblasts. This results in prominent Fn matrix assembly in soft ECMs and efficient contraction of floating collagen gels. Therefore, in soft ECMs, Thy-1^{neg} fibroblasts exhibit the pro-fibrotic phenotypes of enhanced cytoskeleton activation, ECM assembly, and ECM remodeling. This suggests an intriguing interpretation that, in a relatively healthy lung interstitium or in new provisional matrix following alveolar damage, the Thy-1^{neg} phenotype may contribute to elaboration of a fibrillar matrix consistent with tissue repair and fibrosis. Potential consequences of such phenotypic responses in the context of IPF are further elaborated in Chapter 6.

The Thy-1-dependent fibroblast phenotype is modulated by activation of the actomyosin regulator, RhoA. Consistent with ECM rigidity-dependent alterations in cytoskeletal phenotype, we find that Thy-1^{neg} fibroblasts have higher endogenous active RhoA on soft substrates (~2 kPa), whereas Thy-1^{pos} have higher active RhoA on stiff substrates (>10 kPa). As substrate rigidity is sensed through force-dependent adhesion signaling (i.e. mechanosignaling) pathways, we proceeded to directly investigate force-dependent adhesion signaling and if it was modulated by Thy-1. Intriguingly, RhoA activation in response to force application through Fn receptors was significantly diminished in the absence of Thy-1, demonstrating an important role for Thy-1 in efficient mechanosignaling of RhoA. Inhibition of RhoA downstream effector ROCK

disrupted Thy-1-dependent rigidity sensing, consistent with prior literature demonstrating the importance of this pathway in rigidity sensing.

We then took a targeted approach to look for interactions and molecules regulated by Thy-1 during force application; this was accomplished by isolating molecules associated with force-modulated adhesion complexes. Interestingly, we pulled out the SFK, Fyn, as a molecule whose localization is regulated by Thy-1 expression. Interestingly, its association with integrin-Fn complexes was largely independent of force, but as required by the assay, dependent on ligand binding (i.e. presentation of a Fn-coated bead). As Fyn has been previously demonstrated to be a critical early signaling element in force-dependent integrin signaling and adhesion reinforcement (von Wichert, Jiang et al. 2003, Kostic and Sheetz 2006), and it was recently discovered to be an upstream element in the force-activated RhoA pathway (Guilluy, Swaminathan et al. 2011), this suggests Thy-1 could modulate mechanosignaling via altering localization of Fyn with respect to integrin adhesion complexes. Interestingly, force-dependent activation of RhoA was found to result from parallel pathways emanating from integrins, namely Fyn-mediated activation of the RhoGEF, LARG, and activation of GEF-H1 by FAK/ERK, which are additive for full RhoA activation (Guilluy, Swaminathan et al. 2011). As force-mediated FAK activation is independent of Thy-1 expression, this may explain why partial RhoA activation in response to force is observed in the absence of Thy-1.

The activation of SFKs, as monitored by phosphorylation of Y418 within the activation motif, was modulated by Thy-1 in both a force-dependent and –independent manner. In the absence of Thy-1, both bead/ligand-induced (i.e. force-independent) and force-induced pY418-SFK adhesion association was abrogated. As association of the other fibroblast expressed, Fn-binding integrin-associated SFK, c-Src, is independent of Thy-1, this suggests that Thy-1 facilitates recruitment and activation of Fyn specifically.

Furthermore, this data demonstrates that both multivalent ligand binding and exogenous force application are capable of activating SFKs. This is in agreement with reports that multivalent ligands of both β1 and β3 integrins are able to activate SFKs in cells in suspension (Wary, Mariotti et al. 1998, Arias-Salgado, Lizano et al. 2003). Additionally, when optical tweezers were used to apply directional force via a fibronectin-coated bead, ligation of the probe bead, in the absence of the external forces imposed by the trap, was sufficient to locally activate SFKs independent of the actin cytoskeleton (Wang, Botvinick et al. 2005). This data has been used to support a model whereby ligand-induced clustering of integrin receptors is sufficient for co-clustering of SFKs, enabling trans-autophosphorylation within the SFK activation motif by proximal SFKs and promoting kinase activation (Arias-Salgado, Lizano et al. 2003, Shattil 2005). Thus, Thy-1 appears to facilitate Fn receptor clustering-induced SFK activation. Downstream of ligand binding and potential clustering mechanisms, direct force application via integrins further activates SFKs through a yet unknown mechanism (Wang, Botvinick et al. 2005, Na, Collin et al. 2008, Guilluy, Swaminathan et al. 2011). In the same optical tweezer study, Wang et al. demonstrated that 300 pN force caused actin cytoskeleton-dependent directional and long-range activation of SFKs using of a FRET biosensor. Intriguingly, the activity of their biosensor construct was sensitive to c-Src and Fyn (approximately 50% activity), however the N-terminal residues of Lyn kinase was used for membrane-targeting (Wang, Botvinick et al. 2005). As the N-terminal region of Lyn is both palmitoylated and myristolated, targeting the kinase to lipid raft domains where it interacts with GPI-anchored proteins, this suggests their biosensor was equally targeted to such domains. Further work from this group indeed verified differential SFK biosensor targeting to sub-membrane domains via targeting motifs (i.e. K-Ras vs. Lyn), which regulates the observed signaling responses (Seong, Lu et al. 2009). This demonstrates that the activity of their biosensor is sensitive to the local membrane environment, and as such, targeting to membrane domains occupied by dually acyl chain-modified SFKs (i.e.

Fyn, Lyn) vs. myristate only-modified (i.e. c-Src) likely reflects the relevant activity of these molecules. Furthermore, Guilluy et al. showed genetically that force-dependent activation of RhoA and adhesion reinforcement was mediated specifically by Fyn. These data support the importance of Fyn in force-dependent SFK activation during mechanostransduction through integrin-Fn bonds. However, due to a paucity of reagents with specificity for Fyn versus other SFK members, we took a similar genetic approach to investigate the requirement of Fyn vs. c-Src in Thy-1-dependent mechanotransduction responses. Consistently, both Thy-1 and exogenous Fyn expression were required for robust SYF cell spreading on stiff ECMs. The observed data support a mechanism for Thy-1 regulating Fyn localization and activation in response to force, which facilitates RhoA activation and remodeling of the cytoskeleton in response to force or substrate rigidity, providing a likely mechanism for Thy-1-mediated mechanotransduction. It will be the goal of further studies to understand how Thy-1 regulates the localization of Fyn during mechanotransduction.

CHAPTER 5 IDENTIFICATION OF A THY-1/$\alpha_V\beta_3$ INTEGRIN/FYN/RHOA SIGNALING AXIS REGULATING LUNG FIBROBLAST MECHANOTRANSDUCTION

5.1 Introduction

At present date, no effective treatments for idiopathic pulmonary fibrosis (IPF) exist. This is likely due to a lack of detailed knowledge of the pathogenesis of the disease, highlighting the complexity of persistent tissue remodeling disorders, wherein the tissue microenvironment is constantly evolving with disease progression. In our previous chapters, we quantitatively determined the extent of tissue stiffening that occurs due to fibrogenesis, and we discovered a known fibrosis-suppressor, Thy-1, regulates the mechanotransduction of normal- and fibrosis-associated tissue rigidity in lung fibroblasts. This raises the intriguing possibility that 1) loss of Thy-1 and its associated phenotypic regulation of mechanotransduction play a critical pathophysiologic role in IPF, and 2) understanding the mechanism of this phenotypic regulation may yield novel therapeutic targets for the treatment of IPF. In this chapter, we aim to address the latter by deciphering a mechanism by which Thy-1 modulates integrin signaling and mechanotransduction.

As the primary receptors for ECM, integrins are critical first responders to ECM-derived instructive cues. Integrins form complexes (focal adhesions, FAs) with associated signaling and scaffolding molecules that enable biochemical signal generation and propagation from the outside environment into the cell (Geiger and Yamada 2011). FAs also contain a plethora of structural proteins that link the ECM to the cytoskeleton, thereby allowing bidirectional transmission of mechanical forces. In this way, FAs are primary sites of cell-ECM force modulation and signal generation, and are capable of

transducing such forces into biochemical signals, i.e. mechanotransduction (Geiger, Spatz et al. 2009). For this reason, FAs have gained considerable interest as sites for focus in determining the molecular mechanisms that underlie this phenomenon.

Obfuscating the molecular mechanisms that regulate mechanosensing and mechanotransduction within FAs is the large number of FA-associated proteins and interactions. Recent proteomics analysis points to upwards of 900 proteins that may associate with integrin-ECM complexes at some point during their lifecycle (Humphries, Byron et al. 2009, Kuo, Han et al. 2011). How these proteins associate in space and time is critical for overall FA function and, thus, biochemical signal generation, force transmission, and mechanotransduction. For example, the scaffolding molecule paxillin is prominent during initial complex formation (i.e. nascent adhesions), as is the integrin-activating and actin-bridging protein talin, whereas other structural molecules such as α-actinin, zyxin, and tensin associate later in the FA assembly process (Gardel, Schneider et al. 2010, Geiger and Yamada 2011). Whereas the structural molecule vinculin is present in nascent adhesions, in more mature adhesions it can switch to an active conformation, linking talin and actin to stabilize force transmission (Dumbauld, Lee et al. 2013, Thievessen, Thompson et al. 2013). In space, these dynamic but coordinated interactions build a hierarchical network of proteins that link the cytoskeleton to the ECM, resembling a stratified structure of protein-protein interactions wherein innumerous opportunities for mechanotransductory events exist (Kanchanawong, Shtengel et al. 2010).

What are less well known are processes that mediate FA assembly and mechanotransduction upstream of integrin-ECM binding. However, as these complexes assemble in a rapid yet well-organized manner, additional regulatory mechanisms that contribute to the timing and configuration of these complexes are not surprising. Once integrins bind an immobilized ligand, FA assembly proceeds from a relatively stable position, microscopically, although FA translocation or frictional slippage does occur

(Smilenov, Mikhailov et al. 1999, Aratyn-Schaus and Gardel 2010). However preceding immobilization, integrin complexes are ambulatory within the plasma membrane, where they can undergo directional mobility at the leading edge to "probe" for ligand-binding sites or undergo Brownian motion within membrane compartments (Wiseman, Brown et al. 2004, Galbraith, Yamada et al. 2007). For examples, α5 integrins group in clusters of 3-5 molecules in non-FA regions, where they are highly mobile (Wiseman, Brown et al. 2004). At the nanoscopic level, single integrins receptors are highly mobile even within FA structures, exhibiting intermittent modes of confinement, diffusion and immobilization depending on their tripartite interaction with the ECM and the cytoskeleton (Rossier, Octeau et al. 2012). Furthermore, it is known that simply clustering integrins in the absence of ligation or force recruits downstream signaling molecules requisite for early ligand-induced signal generation, such as Src family kinases (SFKs) (Shattil 2005, Boettiger 2012). Intriguingly, not all early signaling intermediates directly bind to integrin receptors, necessitating alternate scaffolding molecules to bridge these interactions.

Integrins are dynamic molecular machines, existing in multiple conformations that control ligand recognition and affinity, cytoplasmic binding partner accessibility, and forces transmitted through the receptor-ligand complex. In a low-affinity state, integrin is bent, resulting in close juxtaposition of the ligand-recognizing headpiece to the plasma membrane (Takagi, Petre et al. 2002, Luo, Carman et al. 2007). A cytoplasmic salt bridge between Asp-723 in the β integrin subunit and Arg-995 in the α integrin subunit (i.e. membrane-proximal clasp) forms to stabilize this conformation and competes for the binding of cytoplasmic integrin-activating proteins (Vinogradova, Velyvis et al. 2002). In a simple description, when integrin-activating proteins, such as talin, bind to the cytoplasmic face and disrupt inter-subunit bonds, they facilitate global conformation changes (e.g. extension) of the protein (Calderwood, Zent et al. 1999, Garcia-Alvarez, de

Pereda et al. 2003). Interestingly, this global conformation change is linked to enhanced ligand-binding affinity, coupling global conformational changes to local conformation shifts within the ligand recognition site (Takagi, Petre et al. 2002, Kim, Ye et al. 2011). Although this is an over-simplification of the system – as local conformational changes and ligand recognition can exist in the absence of integrin extension, and lower-affinity states exist in the extended conformation – this illustrates the dynamic nature of integrin's recognition of ligand and regulation of downstream molecular responses.

As an increasing number of molecules that directly associate with integrin are identified, it is clear that they evolved to share or overlap in their binding motifs, resulting in adapter-binding 'hot-spots' (Legate and Fassler 2009). Intriguingly, like talin and other integrin-activating proteins, some partner molecules bind motifs cryptic to the active (i.e. extended) conformation and vice versa. For instance, a subset of molecules, known as integrin-activation inhibitors, directly bind to the juxtamembrane region of integrin and stabilize clasp formation (Pouwels, Nevo et al. 2012). Also, important scaffolding/signaling molecules paxillin and Fyn bind to the membrane-proximal clasp region, suggesting this motif is only accessible for adapter binding following separation of the two integrin tails and thus, integrin activation (Reddy, Smith et al. 2008, Legate and Fassler 2009).

In the pursuit of a molecular mechanism linking Thy-1 to intracellular mechanosignaling, we have chosen to focus on FAs as a likely target of Thy-1-associated signal transduction. Previous work by Barker et al. demonstrated that fibroblast Thy-1 surface expression is sufficient to alter SFK activation, p190 RhoGAP phosphorylation and downstream Rho signaling, leading to differential FA and stress fiber formation (Barker, Grenett et al. 2004). Furthermore, they established a critical role for the Thy-1/SFK signaling axis in thrombospondin-mediated FA disassembly (Barker, Pallero et al. 2004). Multiple groups have helped to establish SFKs as a key Thy-1-mediated signaling

effector (Ley, Marsh et al. 1994, Barker, Pallero et al. 2004, Cohen, Breuer et al. 2009, Shan, Hagood et al. 2010, Herrera-Molina, Frischknecht et al. 2012). Importantly, Thy-1's GPI anchor is critical to these signaling responses due to its ability to localize the Thy-1 to lipid rafts, where it interacts with SFKs (Stefanova, Horejsi et al. 1991, Draberova and Draber 1993, Tiveron, Nosten-Bertrand et al. 1994, Barboni, Rivero et al. 1995, Rege, Pallero et al. 2006). As an outer leaflet-associated molecule, Thy-1 requires extracellular binding partners for its polypeptide structure. Intriguingly, integrins have been identified as a Thy-1 binding partner, although these findings explicitly focus on integrin as a trans-acting (i.e. cell-cell) receptor (Leyton, Schneider et al. 2001, Wetzel, Chavakis et al. 2004, Saalbach, Wetzel et al. 2005, Avalos, Valdivia et al. 2009, Shan, Hagood et al. 2010). These prior findings along with the results from the previous chapter demonstrating 1) Thy-1 facilitates fibroblast mechanotransduction of ECM rigidity, 2) Thy-1 is required for efficient force-dependent RhoA activation, 3) Thy-1 mediates the localization of Fyn kinase to adhesion complexes, 4) Thy-1 regulates the force-activation of SFKs, and 5) efficient mechanotransduction of ECM rigidity requires both Thy-1 and Fyn expression, motivate us to investigate how Thy-1 may be regulating these phenomena.

5.2 Materials and Methods

5.2.1.1 Inhibitor treatments

Cholesterol oxidase (CholOx) from *Streptomyces sp.* (Sigma) was used at a concentration of 1 U/mL. Cells were treated for 1 hr. prior to the start of magnetic tweezing and complex precipitation assays, and CholOx was maintained in the media during assays. 2 mM Mn^{2+} or 10 μg/mL LIBS2 were added to cultures for 60 min. prior to fixation and PLA assays.

5.2.2 Protein complex identification assays

5.2.2.1 Immunoprecipitations

Cells were maintained in suspension or plated at $1x10^4/cm^2$ in a 10 cm diameter dish. Cells were lysed in 50 mM Tris, pH 8.0, 150 mM NaCl, 5 mM EDTA, 5% glycerol, 1% Triton X-100, 25 mM NaF, and supplemented with 1× protease inhibitor cocktail and phosphatase inhibitor cocktails (Roche). Lysates were clarified by centrifugation for 10 min at 12,000 rpm, 4 °C and pre-cleared with Dynabeads (M280, Invitrogen) for 1 hr. at 4 °C. Complexes were captured with antibody-conjugated (αv integrin, AB1930; Millipore) and BSA-blocked Dynabeads for 2 hr. at 4 °C. Beads were washed in lysis buffer, and proteins were eluted in sample buffer (2x Laemmli). Samples were probed by Western blotting with antibodies to αv integrin (AB1930) and Thy-1 (5E10, BD Pharmingen).

5.2.2.2 Proximity ligation assays (PLA)

Cells on No. 1.5 coverglass were fixed with 4% formaldehyde with 0.2% glutaraldehyde for 15 min. at 25°C. Samples were blocked with 5% normal goat serum (NGS) with 0.1% Tween-20, prior to primary antibody incubation. Primary antibodies used were Thy-1 (EPR3132, Abcam; Cambridge, MA), αvβ3 integrin (23C6, Chemicon International; Temecula, CA), αvβ3 integrin (LM609, Millipore), anti-LIBS2 epitode β3 integrin subunit (ab62, Millipore), αvβ3 integrin (WOW-1, a kind gift of Sanford Shattil, University of California, San Diego), β1 integrin (K20, BD Pharmingen), and β1 integrin (HUTS-4, Chemicon International). All antibodies were used at between 0.5-1.0 μg/mL in blocking buffer. Proximity ligation assays were performed according to the manufacturer's instructions (Olink Biosciences; Uppsala, Sweden).

5.2.3 Assays of cytoskeletal phenotype

5.2.3.1 Preparation of polyacryamide (pAAm) gel substrates

Polyacrylamide (pAAm) hydrogels with varying bisacrylamide concentrations were fabricated on amino-silanated coverslips, as previously described. (Tse and Engler 2010) Briefly, PA gel solutions were produced by combining acrylamide and bisacrylamide (Biorad; Hercules, CA) to final concentrations of 8% acrylamide and 0.045%, 0.102%, 0.146%, or 0.239% bisacrylamide to obtain gels with final elastic moduli of 1.8 kPa, 6.7 kPa, 10.6 kPa, or 18.7 kPa, respectively. 50 µl of each solution was polymerized by the addition of 1% (v/v) ammonium persulfate (VWR; West Chester, PA) and 1% (v/v) N,N,N',N'-tetramethylethylenediamine (Biorad). Human plasma fibronectin (Fn) was purified from blood plasma and covalently attached to the surface using the heterobifunctional crosslinker sulfosuccinimidyl-6-(4'-azido-2' nitrophenyl-amino)hexanoate (sulfo-SANPAH, Pierce Chemical Co.; Rockford, IL). Following overnight incubation with Fn, gels were then washed and stored in PBS.

5.2.3.2 Immunofluorescence staining

Thy-1 mouse lung fibroblast subpopulations or RFL-6 lines were plated on Fn-coated PAAm substrates of varying rigidity at a seeding density of 1,000 cells/cm^2. Cells plated in 10% FBS-containing growth media were allowed to attach and spread for 4 hours at 37°C, 5% CO_2. Samples were then fixed using 4% formaldehyde, permeabilized in 0.2% Triton X-100 for 5 minutes, and blocked with 10% normal goat serum (NGS). Primary antibodies including V284 (vinculin, Millipore; Billerica, MA), 8d4 (talin, Sigma), 53-2.1 (Thy-1, BD Pharmingen), 5E10 (Thy-1, BD Pharmingen), and AB2024 (Fn, Millipore) along with AlexaFluor-labeled secondary antibodies were used for

staining (Invitrogen). AlexaFluor-conjugated phalloidin (Invitrogen) was used to stain F-actin, and samples were counterstained with Hoechst 33528 (Invitrogen). Images were acquired at 20x (Plan-fluor, 0.5 N.A.) or 60x (Plan-apochromat, 1.4 N.A.) magnification with a Nikon TiE epifluorescence microscope (Nikon; Tokyo, Japan) and CoolSNAP HQ2 monochromatic CCD camera (Photometrics; Tucson, AZ), or using a Zeiss LSM700 confocal microscope (Carl Zeiss, Inc.; Jena, Germany) with a variable secondary dichroic and 20x (0.8 N.A.), 60x (1.4 N.A.) objectives. Cell area was measured with an intensity-based auto-detection algorithm to detect and highlight boarders and calculate pixel number. Quantitatively similar values of cell area are detected for membrane staining (DiI), actin, and vinculin immunostaining.

5.2.3.3 Quantification of cell and adhesion morphometrics

Immunostained vinculin image planes were extracted from 60x fluorescent micrographs and loaded into MATLAB. First, general background elimination was performed by averaging the intensity of a user-defined background polygon, and the average background pixel intensity was set to zero. Single cells within the field of view were masked and remaining pixels could be converted to cell area. A second mask, applied as a function of the standard deviated of the pixel intensity distribution, was used to select and convert adhesions to a binary sequence. Connected pixels were then grouped into bins based on size, converted to units (μm^2), and saved as the focal adhesion size data to the output structure.

5.2.3.4 AFM analysis of cortical stiffness

Cells were plated as for immunofluorescent staining and measured within 4-6 hours of plating. Using an MFP-3D-BIO atomic force microscope (AFM) (Asylum Research; Santa Barbara, CA), nanoindentation tests were performed in fluid conditions (DMEM + 10 mM HEPES, 10% FBS, 1% penicillin and streptomycin, pH 7.4) using a

4.74 μm diameter spherical tipped-silicon nitride cantilever (Bruker; Camarillo, CA). Cantilever spring constants were measured prior to sample analysis using the thermal fluctuation method, with nominal values of 40-60 pN/nm. Single force points taken from at least 3 peri-nuclear regions of greater than 300 nm in height were averaged to determine a cell's average cortical stiffness. Similarly, regions of PAAm substrate surrounding measured cells were probed. Force-indentation curves were individually analyzed using a Hertzian model for spherical tips, from which Young's modulus was obtained. The sample Poisson's ratio was assumed as 0.33, and a power law of 1.5 was used to model tip geometry. AFM measurements were made using a 2 nN force set point and an indentation rate of 22.85 μm/s.

5.2.4 Assays of force-dependent signaling

5.2.4.1 RhoA activity assay

RFL-6 or CCL-210 cells were plated on pAAm substrates at $5x10^3/cm^2$. After 4 hours, cells were washed once with ice-cold PBS and the RhoA G-LISA assay (Cytoskeleton, Inc.; Denver, CO) was performed per manufacturer's instructions. After absorbance measurements were taken at 490 nm, buffer-only background levels were subtracted and normalized by the experimental group with lowest RhoA activity levels. For magnetic force application assays, cells were plated and subject to force application as described below and RhoA G-LISA was performed; relative RhoA activity values were obtained after normalizing to zero force RhoA activity signal per experimental group. Western blot for total RhoA protein was used to ensure protein expression of RhoA was equivalent between samples and treatment conditions.

5.2.4.2 Magnetic tweezing and complex precipitation assay

$2x10^6$ cells/dish were plated in a 10 cm tissue culture-treated polystyrene dish and made quiescent overnight in serum-free DMEM. 2.8 μm diameter magnetic beads (M280 Dynabead, Invitrogen) coated with full-length Fn, anti-transferrin receptor (CD71, H-300; Santa Cruz Biotechnology), bovine serum album (BSA) were added at a 10:1 ratio of beads per cell in serum-free plus 0.5% BSA. Following a 15 minute period to allow bead attachment, a neodymium permanent magnet with (surface field of 2451 Gauss, K & J Magnets, Inc.) was placed 6 mm from the dish surface. Following the prescribed time of magnetic force application, cells were lysed (10 mM HEPES (pH 7.6), 150 mM NaCl, 0.1% NP-40, 2 mM $MgCl_2$ plus protease inhibitor cocktail), the bead fraction was precipitated magnetically (DynaMag, Invitrogen). Following 3x wash with lysis buffer, co-precipitated proteins were either denatured in 2x Laemmli for immunoblot anaysis or stained with primary and secondary antibodies for flow cytometry. Force levels applied using this set-up were between 10-16 pN per bead as verified using COMSOL simulations and according to those published previously (Guilluy, Swaminathan et al. 2011).

5.2.4.3 Western blots

Cultured cells directly lysed in Laemmli buffer or bead-associated adhesion complexes were heat-denatured at 95°C for 5 min. Protein was separated electrophoretically on a 4-15% polyacrylamide gel (Biorad) according to standard procedures, then transferred to nitrocellulose membranes using a semi-dry transfer apparatus (Trans-Blot SD, Biorad), blocked with 5% nonfat dry milk in TBS or 5% BSA, then incubated with Thy-1 (9798, Cell Signaling Technology; Danvers, MA), Fyn (1S, Millipore), c-Src (32G6, Cell Signaling Technology), and pY418-SFK (2101, Cell

Signaling Technology) primary antibodies overnight at 4° C. Following washing with TBS + 0.1% Tween 20, membranes were incubated for 2 hours with IR secondary antibody (Licor; Lincoln, NE), washed, and imaged using the Odyssey IR scanner (Licor). Western blots were quantified using Image J image processing software and a minimum of n = 3 blots were quantified and averaged per group.

5.3 Results

5.3.1 Lipid raft stability and Thy-1's GPI anchor are required for Fyn recruitment, force-dependent RhoA activation, and rigidity sensing

In the previous chapter, we made the unique observation that Thy-1 is required for the acute recruitment of the SFK member Fyn to Fn-associated adhesion complexes. It has been previously shown that Thy-1 interacts with Fyn in specialized membrane subdomains, termed lipid rafts. This association between the GPI-anchored outer leaflet molecules and inner leaflet-associated intracellular signaling molecules, via the local plasma membrane environment, is critical for the biological activity of many GPI-anchored molecules. This is the case for Thy-1, where almost all studies of Thy-1-medated intracellular signaling, including in antibody-induced activation of murine T cells, anti-Thy-1-induced glomerulonephritis, and thrombospondin-induced FA disassembly are critically dependent on its association with SFKs via lipid rafts. Disrupting the stability of lipid rafts inhibits these interactions and subsequent signaling; common methods of disruption are pharmacological agents that perturb membrane cholesterol, such the cholesterol-sequestering agent methyl-β-cyclodextran (MβCD) or cholesterol-modifying enzymes such as cholesterol oxidase (CholOx). To reduce the off-target effects associated with MβCD, we treated RFL-$6^{Thy\text{-}1}$ cells with CholOx, which

oxidizes cholesterol molecules to cholestenone and perturbs their interaction with sphingomyelin and associated liquid-ordered domains, thus disrupting such domains (Rouquette-Jazdian, Cellular Signaling 2006). CholOx treatment dramatically inhibited the ability of Thy-1 to recruit Fyn to adhesion complexes, and it also largely abrogated the force-induced SFK activation that was dependent on Thy-1 (Figure 15A,B). Lipid raft disruption similarly affected efficient force-dependent RhoA activation enabled by Thy-1 expression. These results demonstrate that lipid raft stability is required for Thy-1-mediated Fyn recruitment and SFK activation, and RhoA activation in response to force (Figure 15C).

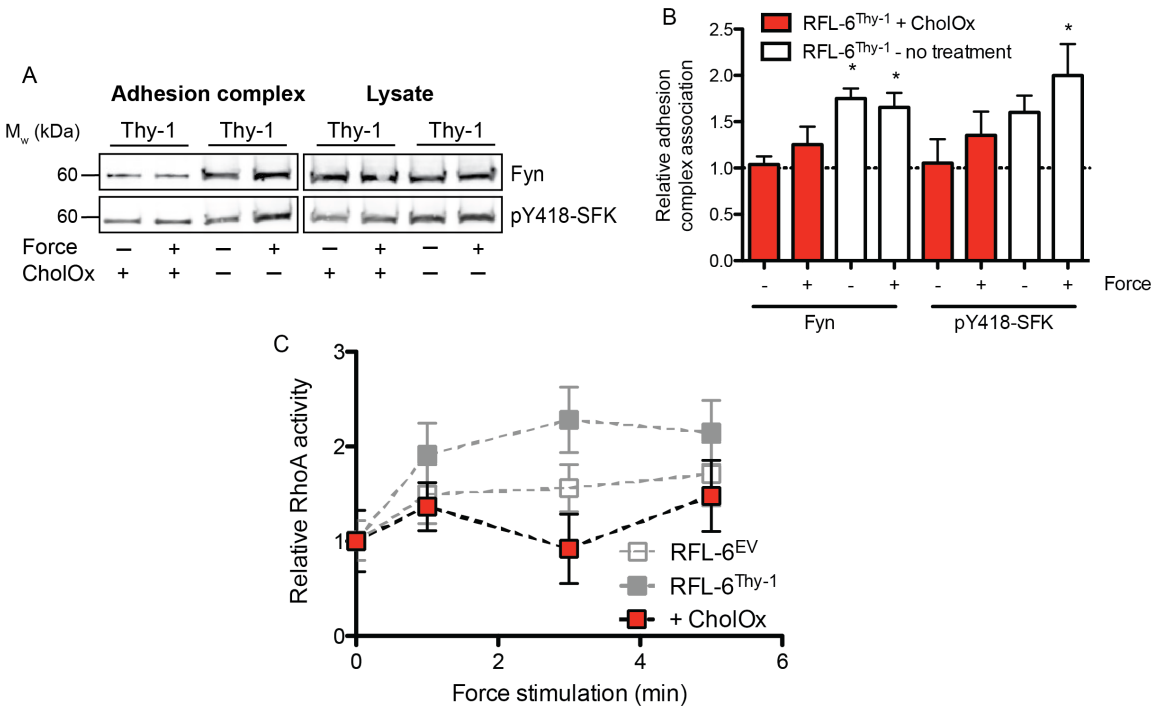

Figure 15: Lipid raft stability is required for Thy-1-mediated Fyn recruitment and force-dependent RhoA activation. (A) Western blots of indicated proteins within the adhesion complex or total cell lysate for RFL-6^{Thy-1} with and without treatment with 1.0 U/mL CholOx . Absence or presence of 5 min. continual force application is indicated. (B) Quantification of Western blots via densitomtery for a minimum of n

= 3 blots. Density measurements for each molecule is represented relative to the levels of RFL-6^{Thy-1} in the presence of CholOx; * = p < 0.05 as assessed by an unpaired, two-tailed Student's t-test. (C) RhoA activity (mean ± S.E.M.) of RFL-6^{Thy-1} + CholOx (red) probed with Fn-coated beads for varied duration of magnetic force application. RFL-6^{EV} and RFL-6^{Thy-1} are underlaid in gray.

To further explore the dependence of lipid rafts on Thy-1-mediated signaling, we used a chimeric mutant of Thy-1 in which the GPI anchor was substituted with the transmembrane domain and a short cytoplasmic tail of mouse CD8 (RFL-6$^{Thy-1/CD8}$). This mutation alters the localization of the Thy-1 ectodomian to regions of the plasma membrane distinct from its endogenous lipid raft sites (Tiveron, Nosten-Bertrand et al. 1994). Using this mutant, we verified that the Thy-1's GPI anchor was critical for Fyn recruitment and force-dependent SFK activation, suggesting lipid raft localization is required (Figure 16A,B). We also found this mutant was unable to mediate force-dependent RhoA activation and phenocopied the Thy-1^{neg} control (RFL-6^{EV}) (Figure 16 D). Next, we investigated the effect of the Thy-1$^{/CD8}$ chimera on cell-level cytoskeletal responses to substrate rigidity. Cortical stiffness and cell area increased with a similar slope as RFL-6^{EV} (k = 1.378 ± 0.393 kPa/kPa and 623.26 ± 95.7 μm^2/kPa for cortical stiffness and cell area, respectively) (Figure 16 E,F). These responses were significantly less sensitive substrate E than RFL-6^{Thy-1}. Furthermore, although some substrate E-dependent changes in FA size were observed, FAs were significantly larger on soft 2.2 kPa substrates in RFL-6$^{Thy-1/CD8}$ compared to RFL-6^{Thy-1} (0.882 ± 0.051 vs. 0.624 ± 0.051 μm^2) (Figure 16 G). This demonstrates that Thy-1's GPI anchor, presumably its localization to lipid rafts, and the stability of lipid rafts are critical for the function of Thy-1 in mechanosignaling and mechanotransduction.

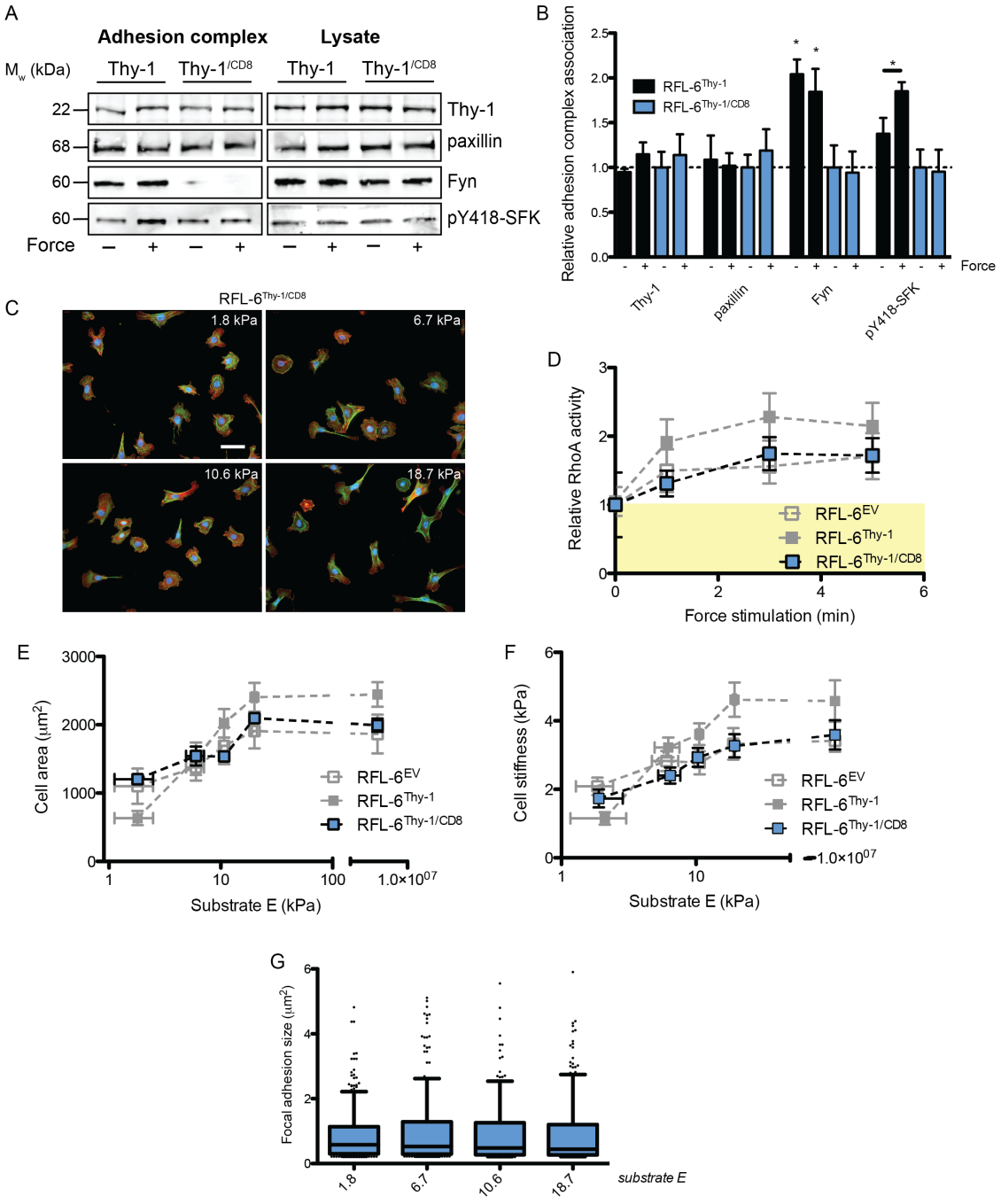

Figure 16: Thy-1's GPI anchor is required for Fyn recruitment, force-dependent RhoA activation, and rigidity sensing. (A) Western blots of indicated proteins within the adhesion complex or total cell lysate for RFL-6^{Thy-1} and RFL-6$^{Thy-1/CD8}$. Absence or presence of 5 min. continual force application is indicated. (B) Quantification of Western blots via densitomtery for a minimum of n = 3 blots from

two independent experiments. Density measurements for each molecule is represented relative to the levels of RFL-6$^{Thy\text{-}1/CD8}$ without force application; * = p < 0.05 as assessed by an unpaired, two-tailed Student's t-test. (C) Immunofluorescence micrographs of vinculin (red), actin (green), and nuclei (blue) for RFL-6$^{Thy\text{-}1/CD8}$ on Fn-coated pAAm substrates of varying rigidity (indicated in top right, white). (D) RhoA activity (mean ± S.E.M.) of RFL-6$^{Thy\text{-}1/CD8}$ (pink) probed with Fn-coated beads for varied duration of magnetic force application. RFL-6^{EV} and RFL-6$^{Thy\text{-}1}$ are underlaid in gray, and yellow box inidicates the approximate RhoA activity in untreated cells. Cell area (E) and cell stiffness (F) vs. substrate *E* (mean ± S.E.M.) in RFL-6$^{Thy\text{-}1/CD8}$ (pink) with RFL-6^{EV} and RFL-6$^{Thy\text{-}1}$ underlaid in gray. (G) Box plots of adhesion size for RFL-6$^{Thy\text{-}1/CD8}$ cells for various substrate rigidities (indicated below). Boxes indicate the lower and upper quartile and whiskers are 10-90 percentile. * = p < 0.05, as assessed by the Mann-Whitney test.

5.3.2 Thy-1 associates with αvβ3 integrin via the Arg-Leu-Asp motif

To further explore how Thy-1 facilitates lipid raft-mediated coupling of Fyn to adhesion complexes, we turned to the literature for evidence of alternate Thy-1 binding partners. It has been reported that Thy-1 binds integrins in a variety of tissue-specific contexts, including $\alpha_M\beta_2$ (Mac-1) on leukocytes (Saalbach, Haustein et al. 2000, Saalbach, Hildebrandt et al. 2002, Wetzel, Chavakis et al. 2004), $\alpha_v\beta_3$ on melanoma cells and neurons (Leyton, Schneider et al. 2001, Saalbach, Wetzel et al. 2005, Hermosilla, Munoz et al. 2008, Avalos, Valdivia et al. 2009), and $\alpha_v\beta_5$ on lung fibroblasts (Zhou, Hagood et al. 2010). We first asked if Thy-1 forms a complex with αv integrins in human lung fibroblasts. To accomplish this, we immunoprecipitated αv integrin via a C-terminal antibody in cell lysates and looked for co-precipitation of Thy-1. As demonstrated in Figure 11A, αv was specifically pulled-down by the anti-C-terminal αv antibody, whereas a control IgG antibody did not (Figure 17A). When immunoblotted

for Thy-1, we saw that indeed Thy-1 was co-precipitated as part of a complex with αv. Interestingly, when compared to cells spreading on Fn for 30 min. or overnight, cells in suspension demonstrated a greater amount of Thy-1 pulled-down with αv, indicating that Thy-1 preferentially forms complexes with αv in suspended cells.

Binding to α_v integrins and α5β1 is direct and mediated by Thy-1's Arg-Leu-Asp (RLD) motif, as mutation to non-functional Arg-Leu-Glu (RLE) abolishes binding (Hermosilla, Munoz et al. 2008, Avalos, Valdivia et al. 2009, unpublished data). We next asked if the complex formed between Thy-1 and αv integrins was mediated by the purported RLD binding motif. We made the Asp to Glu substitution within the RLD motif (Thy-1^{D37E}) of human Thy-1, which renders the molecule unable to directly bind αv and α5β1 integrins. In CHO.B2 cells stably expressing human αvβ3 integrin, this mutation completely abolished Thy-1 association by co-immunoprecipitation (Figure 17B). Interestingly, Thy-$1^{/CD8}$ was similarly unable to complex with αv integrin, implicating proper membrane localization as critical in Thy-1-αv association. This further suggests that post-lysis interactions were not significantly present in our experimental assay.

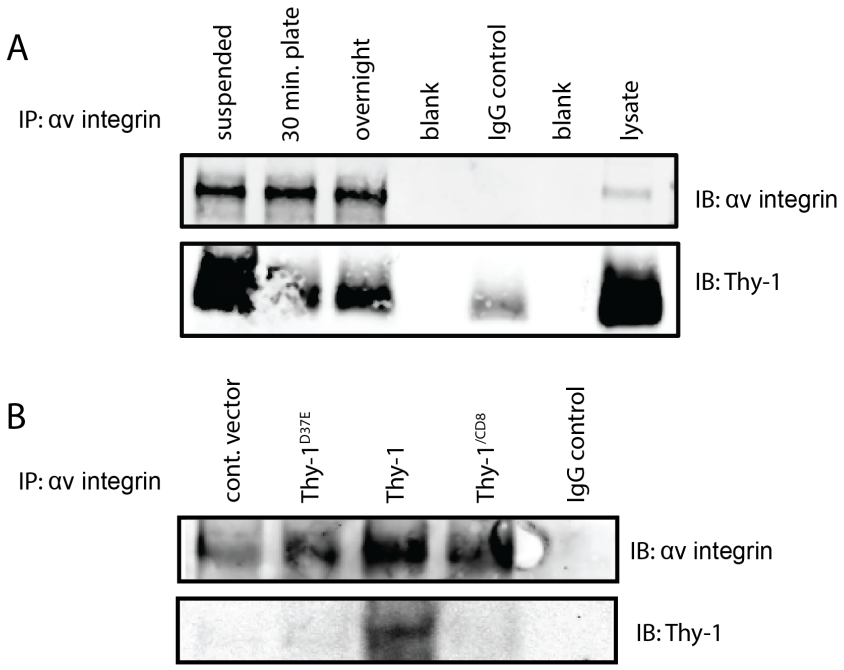

Figure 17: Co-immunoprecipitation of Thy-1 with αvβ3. (A) Immunoprecipitation of αv integrin from normal human lung fibroblasts in suspension vs. spread on Fn, and immunoblots of αv and Thy-1. IgG control antibody and total cell lysates are shown for compasion. (B) Immunoprecipitation of αv integrin from CHO.B2(hαvβ3) cells expressing various Thy-1 and mutant contructs, and immunblots of αv and Thy-1.

5.3.3 Thy-1 binds αvβ3 integrin in *cis* and is dependent on integrin conformation and Thy-1's RLD motif

There are several limitations of co-immunoprecipitation for analyzing molecular complexes including disruption of the endogenous cell compartmentalization and structure, an inability to assess spatial localization, difficulty in determining direct binding interactions within a ternary complex, and the possibility for post-lysis artifacts. We were critically interested in if Thy-1 might bind to αvβ3 within the plane of the plasma membrane (we term in *cis*), as in our previous studies, we have been assaying for

cell interactions with the ECM largely in the absence of transcellular contacts. Thus, to look at endogenous protein-protein interactions, we used a proximity-based ligation assay (PLA), which utilizes oligonucleotide-linked antibodies to form a hybridized DNA molecule capable of amplification and detection. This assay is capable of discriminating antigen interaction distances on the order of 40 nm *in situ* (Soderberg, Gullberg et al. 2006). To start, we probed multiple anti-αvβ3 antibodies for PLA with Thy-1 on the cell surface of human lung fibroblasts. Interestingly, we were only able to observed PLA signal with two antibodies: LM609, which binds to the βA domain of β3 and allosterically inhibits binding of ECM ligands and 23C6, which is a non-functional antibody (Figure 18A,B) (Lin, Carron et al. 1998). In contrast the LIBS2 antibody, which recognizes a site within the juxtamembrane β-tail domain and cooperatively binds with ligand by a propagating long-range conformation change within β3 (Du, Gu et al. 1993), or WOW-1, which is a ligand-mimetic antibody showing high affinity to extended αvβ3, and thus has been used to report the extended conformer, did not complex with Thy-1 (Pampori, Hato et al. 1999) (Figure 18A,B). A similar finding was observed with α5β1 integrin, where non-functional antibody K20 gave PLA signal, whereas the swung-out hybrid domain and high affinity-associated HUTS-4 did not (Mould, Barton et al. 2003). In total, these results suggest that proximity between Thy-1 and integrin is preferential for integrins not in the high-affinity or extended conformer.

To further examine this hypothesis, we tested whether directly perturbing integrin conformation would influence the proximity of αvβ3 and Thy-1 as detected by PLA. We incubated lung fibroblasts in culture with LIBS2 antibody or Mn^{2+}, which has been demonstrated both at the single-molecule and cell-level to promote extension of integrin molecules and ligand binding (Vinogradova, Velyvis et al. 2002, Askari, Tynan et al. 2010). In response to these treatments, PLA signal between Thy-1 and αvβ3 (LM609 antibody; similar results obtained with 23C6) was completely abolished (Figure 18C).

These results further demonstrate that Thy-1-αvβ3 interactions are preferential to the low-affinity or bent integrin conformation, and that ligation of ECM ligands, presumably by the high-affinity receptor, disrupts the interaction between Thy-1 and αvβ3 (Figure 16A).

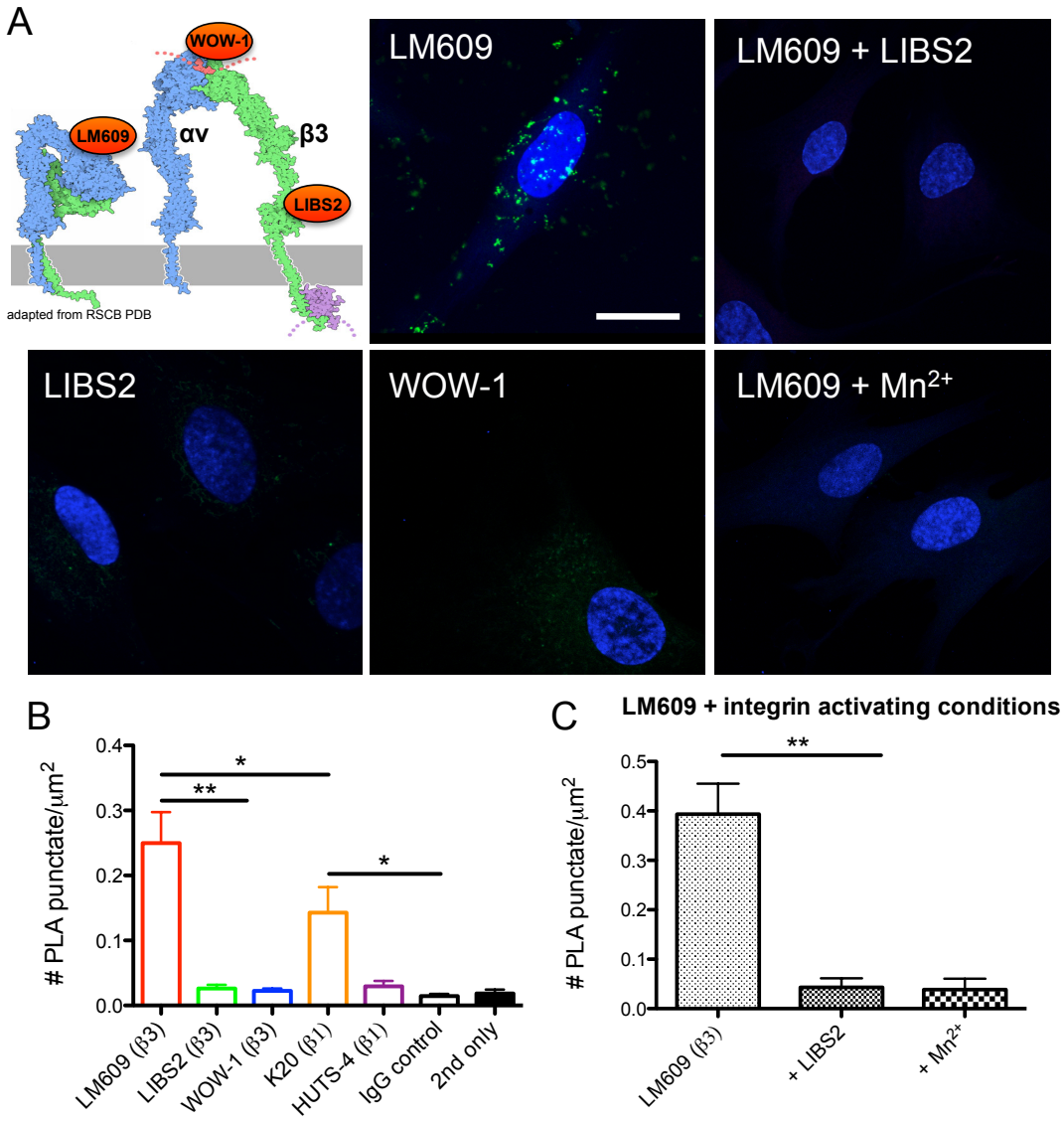

Figure 18: Thy-1 associates with integrin αvβ3 in *cis* and is dependent on integrin conformation. (A) Cartoon diagram of αvβ3 integrin adapted from RSCB Protein Data Bank Normal indicating the approximate binding sites for antibodies LM609, LIBS2, and WOW-1 (top left panel). PLA between Thy-1 and αvβ3 integrin in normal human lung fibroblasts for the antibodies and conditions indicated in white

lettering. PLA punta (green) and cell nuclei (blue) shown; scale bar = 10 µm. (B) Quantification of PLA signal (mean ± S.E.M.) for various antibodies and integrins with Thy-1. (C) Quantification of PLA signal (mean ± S.E.M.) between αvβ3 (LM609) and Thy-1 for Mn^{2+} and LIBS2 integrin activating conditions. * = p < 0.05, ** = p < 0.01 as assessed by unpaired, two-tailed Student's t-test.

Last we wanted to determine if the interaction reported by PLA was dependent on the RLD integrin-binding motif in Thy-1. To test this, we expressed Thy-1 and the RLD mutant (Thy-1^{D37E}) mutant, along with the GPI anchor mutant form (Thy-$1^{/CD8}$), in CHO.B2(hαvβ3) and performed PLA assays. Indeed, mutation to the RLD motif completely abolished PLA between Thy-1 and αvβ3 (Figure 19A,B). Interestingly, the GPI anchor mutant of Thy-1 still retained some binding activity to αvβ3 in this assay, although it was significantly abrogated. Therefore, we conclude that Thy-1 binding to αvβ3 integrin in *cis* is via Thy-1's RLD integrin-binding motif, and this interaction is facilitated by GPI-anchored membrane localization of Thy-1.

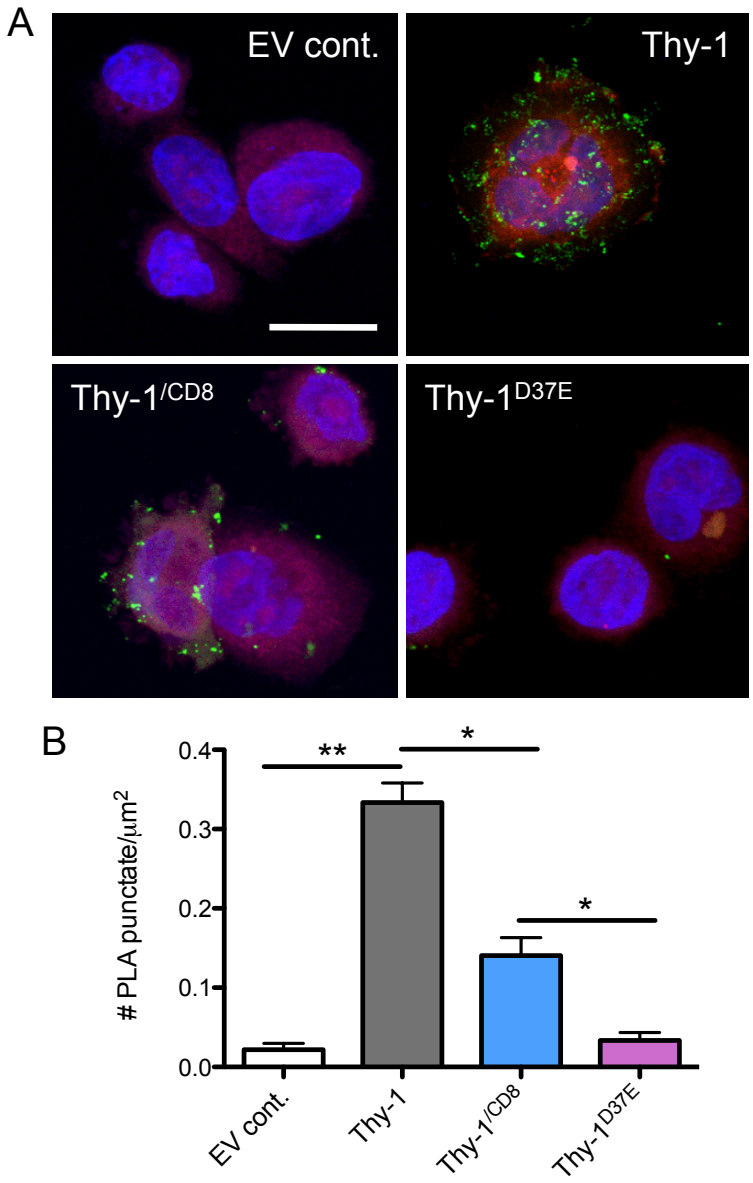

Figure 19: Thy-1 association with integrin αvβ3 in *cis* is dependent on Thy-1's RLD motif. PLA between Thy-1 and αvβ3 integrin in CHO(hαvβ3) cells. (A) PLA punta (green), mCherry (red), and cell nuclei (blue) shown with various Thy-1 contructs indicated in white lettering; scale bar = 10 μm. (B) Quantification of PLA signal (mean ± S.E.M.) for various Thy-1 contructs with αvβ3. * = $p < 0.05$, ** = $p < 0.01$ as assessed by unpaired, two-tailed Student's t-test.

5.3.4 Thy-1's RLD motif is required for Fyn recruitment, force-dependent RhoA activation, and rigidity sensing

Lastly, we investigated whether the RLD motif was necessary for Thy-1's mechanosignaling and mechanotransduction phenotypes. We expressed Thy-1^{D37E} in RFL-6 cells (RFL-$6^{Thy\text{-}1(D37E)}$) and investigated whether this molecule was able to support Fyn recruitment to adhesion complexes. Indeed, this mutant form was unable to recruit Fyn, and force- and Thy-1-dependent SFK activation was significantly abrogated (Figure 20A,B). Enhanced force-dependent RhoA activation mediated by Thy-1 was also not observed in RFL-$6^{Thy\text{-}1(D37E)}$ cells, demonstrating this motif is critical in Thy-1 mechanosignaling (Figure 20D). We investigated cell-level cytoskeletal responses to substrate E in the presence of Thy-1^{D37E}. Cortical stiffness and cell area increased with a similar slope as RFL-6^{EV} (k = 1.839 ± 0.441 kPa/kPa and 901.9 ± 108.9 μm^2/kPa for cortical stiffness and cell area, respectively) (Figure 20E,F). These responses were significantly less sensitive substrate E than RFL-$6^{Thy\text{-}1}$. Furthermore, substrate E-dependent changes in FA size was greatly abrogated in RFL-$6^{Thy\text{-}1(D37E)}$ cells, with a trend of larger mean FA size on soft substrates than RFL-$6^{Thy\text{-}1}$ (0.810 ± 0.059 vs. 0.624 ± 0.051 μm^2), but smaller on stiff substrates (0.973 ± 0.062 vs. 1.254 ± 0.084 μm^2) (Figure 20G). These data demonstrate that Thy-1's integrin-binding motif is critical for the function of Thy-1 in mechanosignaling and mechanotransduction, specifically in recruitment of Fyn to Fn-mediated adhesion complexes and facilitation of force-dependent SFK activation and RhoA mechanosignaling. Further discussion on the potential mechanisms underlying these phenomena is elaborated below.

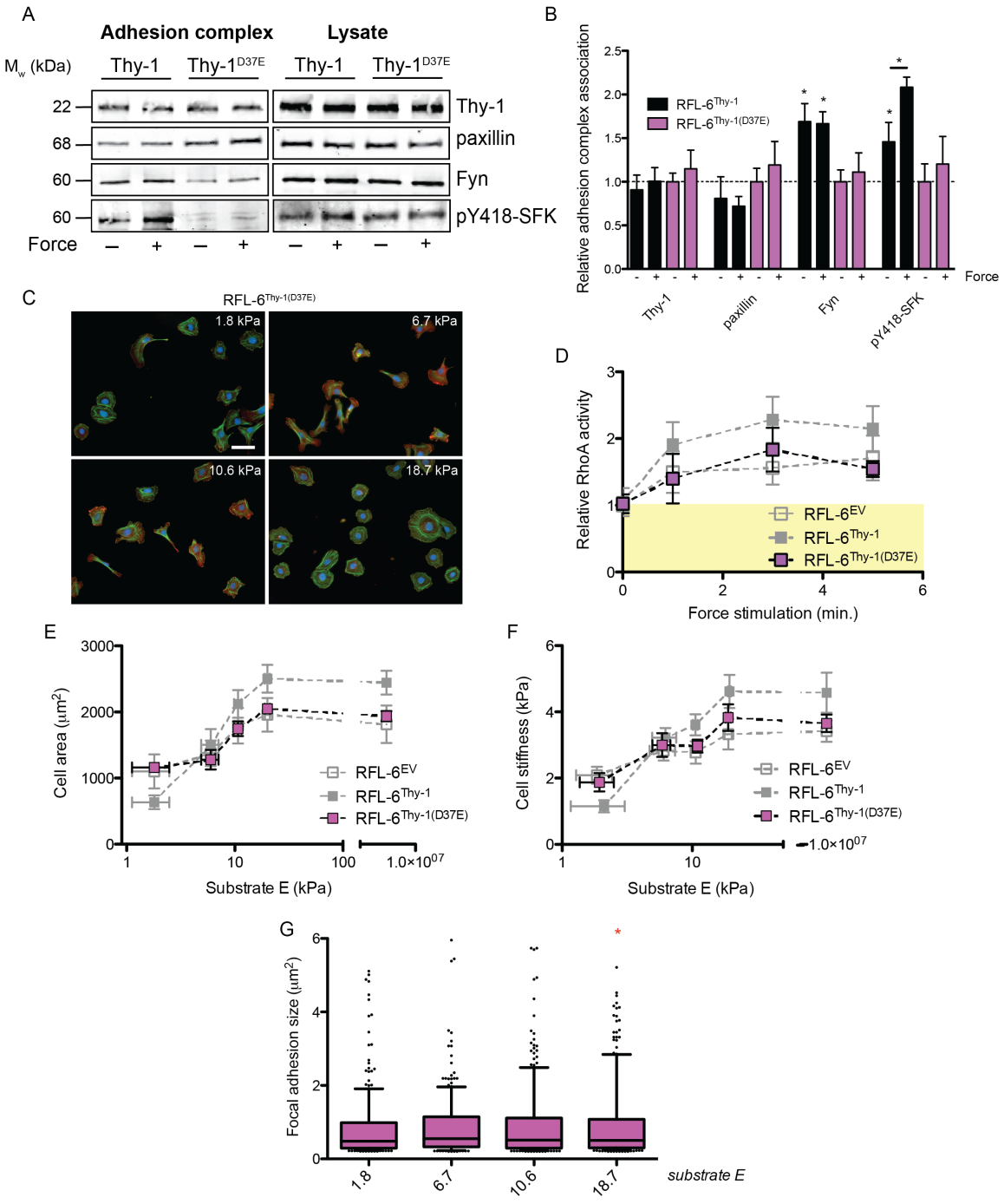

Figure 20: Thy-1's RLD motif is required for Fyn recruitment, force-dependent RhoA activation, and rigidity sensing. (A) Western blots of indicated proteins within the adhesion complex or total cell lysate for RFL-6^{Thy-1} and RFL-6$^{Thy-1(D37E)}$. Absence or presence of 5 min. continual force application is indicated. (B) Quantification of Western blots via densitomtery for a minimum of n = 3 blots.

Density measurements for each molecule is represented relative to the levels of RFL-6$^{Thy\text{-}1(D37E)}$ without force application; * = $p < 0.05$ as assessed by an unpaired, two-tailed Student's t-test. (C) Immunofluorescence micrographs of vinculin (red), actin (green), and nuclei (blue) for RFL-6$^{Thy\text{-}1(D37E)}$ on Fn-coated pAAm substrates of varying rigidity (indicated in top right, white). (D) RhoA activity (mean ± S.E.M.) of RFL-6$^{Thy\text{-}1(D37E)}$ (pink) probed with Fn-coated beads for varied duration of magnetic force application. RFL-6^{EV} and RFL-6$^{Thy\text{-}1}$ are underlaid in gray, and yellow box inidicates the approximate RhoA activity in untreated cells. Cell area (E) and cell stiffness (F) vs. substrate *E* (mean ± S.E.M.) in RFL-6$^{Thy\text{-}1(D37E)}$ (pink) with RFL-6^{EV} and RFL-6$^{Thy\text{-}1}$ underlaid in gray. (G) Box plots of adhesion size for RFL-6$^{Thy\text{-}1(D37E)}$ cells for various substrate rigidities (indicated below). Boxes indicate the lower and upper quartile and whiskers are 10-90 percentile. * = $p < 0.05$, as assessed by the Mann-Whitney test.

5.4 Discussion

In Chapter 4, we found that Thy-1 expression regulates mechanotransduction of ECM rigidity via a RhoA-mediated pathway, and that Thy-1 modulates the localization and activation of Fyn and SFKs, respectively, within adhesion complexes. In this chapter, we attempted to decipher how Thy-1 achieves these effects at the cell membrane. By substituting Thy-1's endogenous GPI anchor with an alternate receptor's transmembrane segment, we find that Thy-1's GPI anchor is critical in mediating mechanosignaling through Fyn and RhoA, and to modulate the mechanostransductory response to ECM rigidity. GPI-anchored Thy-1 interacts with Fyn within cholesterol-rich lipid rafts, suggesting this interaction is critical for Fyn recruitment to adhesion complexes. In support of this, treatment of wild-type Thy-1-expressing cells with

CholOx, which disrupts lipid rafts by altering cholesterol partitioning within the membrane, disrupted Fyn recruitment and SFK activation. Furthermore, downstream signaling through RhoA was altered, further validating the requirement of proper Fyn recruitment for mechanosignaling through RhoA.

We also find that Thy-1 complexes with αvβ3 integrins on the cell surface, and this interaction requires the Arg-Leu-Asp integrin binding motif of Thy-1. To determine if these molecules interact within the plasma membrane, or *in cis*, we used PLA to look for endogenous complexes on the cell surface. In doing this assay, we also found that only specific conformations of integrin were efficient in forming complexes with Thy-1. In particular, antibodies that bind with high-affinity to the active or extended integrin conformer did not complex with Thy-1, whereas those that either promote the low-affinity conformation or are insensitive to conformation state were proficient to bind. This was seen with both α5β1 and αvβ3 integrins, however the interaction was more robust with αvβ3, and so was further investigated. In support of the conformational sensitivity of this interaction, promoting integrin into the extended conformation using Mn^{2+} or activating antibody, LIBS2, again disrupted complex formation between αvβ3 and Thy-1. This data suggests that Thy-1 is only proficient at binding αvβ3 when it is in the bent state. This is sensible, as Thy-1 is only a single Ig domain of approximately 2 nm in diameter plus a compact glycan chain, and thus when lipidated and partitioned into the outer leaflet of the plasma membrane, would be unlikely to span the 20 nm distance integrin projects from the membrane in its extended conformation (Barboni, Rivero et al. 1995, Luo, Carman et al. 2007). However, we are not able to exclude alternative configurations of low-affinity αvβ3 binding to Thy-1 about the topographically complex cell surface.

We then investigated a mutated form of Thy-1, in which an Asp to Glu substitution within the integrin-binding motif rendered it unable to complex with αvβ3

integrin, demonstrated both by immunoprecipitation and PLA. This mutant form of Thy-1 was unable to support Fyn recruitment, force-dependent or -independent SFK activation, efficient force-dependent RhoA activation, or Thy-1-mediated rigidity sensing. Together with data establishing αvβ3 integrin as a *cis*-acting binding partner for Thy-1, specifically via the Arg-Leu-Asp sequence, and the known clustering/recruitment of αvβ3 integrins during recognition of a multivalent Fn substrate, this suggests a likely mechanism by which Thy-1 mediates Fyn recruitment to adhesion complexes and downstream signaling. Namely that binding of low-affinity αvβ3 integrin to Thy-1 could act as a molecular bridge for integrin and Fyn molecules, via Thy-1 and Fyn's association within lipid rafts. Disruption of the Thy-1's integrin-binding site, prevention of its localization to lipid rafts, or direct disruption of lipid rafts would all inhibit such a tripartite interaction between αvβ3, Fyn and Thy-1. Thus, such complexes would likely be preformed in the cell membrane prior to ECM ligand binding; subsequently, Fn binding and clustering of integrin promotes the local accumulation of Fyn in a Thy-1-dependent manner. In this way, Thy-1 acts as an adapter protein for integrin and Fyn, while being sensitive to their conformational states. As integrin clustering is sufficient to promote SFK priming and trans-activation, this may contribute the initial Thy-1- and Fn bead-dependent activation of SFKs (Arias-Salgado, Lizano et al. 2003). Furthermore, as Fyn is now localized to sites of local force application, force-mediated activation can now occur. As it has been well-demonstrated that Fyn activity is critically important in mechanotransduction (von Wichert, Jiang et al. 2003, Kostic and Sheetz 2006), and multiple pathways link Fyn to RhoA activation during force-dependent signaling (Thomas, Soriano et al. 1995, Giannone and Sheetz 2006, Moore, Roca-Cusachs et al. 2010, Guilluy, Swaminathan et al. 2011), this suggests a likely connection between the cell surface activity of Thy-1 and downstream modulation of mechanotransductory cytoskeleton remodeling through RhoA activity.

It is known that SFKs also exist in a series of conformations related to their activation state. Interactions between the SH3 domain and flexible linker region stabilize inactive SFKs in a clamped and sterically inaccessible state (Brown and Cooper 1996, Thomas and Brugge 1997). However, binding of the SH3 domain to associating adapters relieves the auto-inhibitory conformation, thus priming the molecule for further activation (Brown and Cooper 1996, Shattil 2005). In the case of c-Src and β3 integrin, this auto-inhibition is relieved by SH3 domain binding to the C-terminal Arg-Gly-Thr motif, which is sufficient for subsequent integrin-clustering-mediated trans-autoactivation of c-Src and downstream signaling (Arias-Salgado, Lizano et al. 2003, Arias-Salgado, Lizano et al. 2005). Intriguingly, the specific binding motif for Fyn is within the membrane-proximal HDRK motif, which is also the site for α/β integrin inter-subunit salt bridge formation (Reddy, Smith et al. 2008). This suggests that in the bent and membrane-proximal clasp-stabilized integrin, Fyn cannot access its SH3 domain binding site; whereas in the active and extended integrin conformation, Fyn is able to gain access to its SH3 binding site and relieve its auto-inhibitory conformation. Thereby, Thy-1 may enable coupling of inactive (i.e. clamped) Fyn molecules in close proximity to low-affinity integrin molecules (i.e. bent conformation), supporting temporally efficient signal transduction (i.e. SFK priming and activation) in response to integrin ligation and clustering and/or mechanical forces, while simultaneously facilitating the use of SFK's multiple regulatory mechanisms. Temporally efficient activation of RhoA, which is critically dependent on Thy-1, helps further this hypothesis. Support or disproval of this model should be a topic for future studies.

It has been long hypothesized that lipid rafts play a critical role in integrin signaling and FAs, as many adhesion-associated signaling molecules, such as SFKs, FAK, and Rac associate with detergent-resistant membrane (DRM) fractions (Shima, Nada et al. 2003, del Pozo, Alderson et al. 2004, Palazzo, Eng et al. 2004). FAs also

have a higher level of liquid-ordered membrane than do surrounding regions of the FA, suggesting a significant presence of cholesterol-rich membrane domains (Gaus, Le Lay et al. 2006). Intriguingly, the majority of integrins in the non-stimulated or ligated state are in non-raft fractions (Leitinger and Hogg 2002). It was recently demonstrated using superresolution microscopy that inactive integrins exist in nanodomains that are spatially separate, but adjacent to nanodomains of GPI-anchored proteins (van Zanten, Cambi et al. 2009). These domains coalesce upon integrin binding and are disrupted by cholesterol depletion, which also functionally impairs integrin. Therefore, it appears that under basal conditions, integrins have some affinity towards nanodomains of GPI-anchored proteins, but are not continuous. Thy-1 can bind integrin in its low-affinity state, and this interaction is greatly abrogated by substitution of Thy-1's GPI-anchor, suggesting that proximity between integrin and lipid raft nanodomains is critical. Furthermore, as perturbing the Thy-1-αvβ3 interaction inhibits recruitment of other lipid raft-associated molecules, this suggests that such a proximity between Thy-1 and αvβ3 (or other integrin and lipid raft nanodomains) is functional. However, such hypotheses wait further testing.

The preceding findings demonstrating that 1) Thy-1 is a critical regulator of fibroblast spreading, cortical actin stiffening, and FA maturation in response to matrix rigidity, 2) both Thy-1's GPI anchor and integrin-binding motif are required for Fyn recruitment, mechanosignaling, and rigidity sensing, and 3) evidence of a Thy-1-αvβ3 integrin *cis* interaction within the plasma membrane strongly support a αvβ3/Thy-1/Fyn/RhoA mechanotransduction signaling axis in lung fibroblasts.

CHAPTER 6 CONCLUSIONS AND FUTURE DIRECTIONS

In this thesis, we began by asking what the endogenous mechanical environment of lung parenchyma is and how it changes during disease. As such we were able to accurately describe the rigidity of the microenvironment for cell types residing within the lung, including epithelial, vascular, immune, and stromal cells such as fibroblasts. This work has informed multiple *in vitro* studies on the role of ECM rigidity in modulating lung cell phenotype, by using accurate values for mimicking cells *in situ*. With the field's continuing knowledge of the biological importance of mechanics in controlling cell fate, we then took a similar approach to specifically assess the contribution of ECM rigidity to fibroblast phenotype *in vitro*.

We found that Thy-1 expression, at levels corresponding to normal lung fibroblasts from healthy patients, promotes sensitive cytoskeletal regulation in response to a changing ECM microenvironment, including alterations in substrate rigidity from the level of normal lung tissue to fibrotic regimes (i.e. ~1-20 kPa). In contrast, cells lacking Thy-1 expression, either endogenously or through genetic manipulation, are more refractory to this changing parameter. In consequence, Thy-1^{neg} cells exhibit significantly more mature actin cytoskeletons and FAs, in contrast to largely quiescent Thy-1^{pos} fibroblasts, in rigidity environments not dissimilar from normal lung tissue. This results in pronounced Fn matrix assembly in soft ECMs and efficient contraction of floating collagen gels. Therefore, in soft ECMs, Thy-1^{neg} fibroblasts exhibit the pro-fibrotic phenotypes of enhanced cytoskeleton activation, ECM assembly, and ECM remodeling. This provides the intriguing interpretation that in a relatively healthy lung interstitium or in new provisional matrix following alveolar damage, the Thy-1^{neg} phenotype may contribute to elaboration of a fibrillar matrix consistent with tissue repair and fibrosis. Together with enhanced migratory and mitogenetic capabilities, this positions the Thy-1^{neg} phenotype as critical during early wound repair processes.

Whereas Thy-1^{pos} cells are capable of more fully maturing their cytoskeleton and FAs in a rigid environment, similar to fibrotic regions *in vivo* – potentially contributing to the continued evolution of scar tissue – they are also susceptible to apoptotic cues present in healing wounds. Akin to the physiologic establishment of robust scar tissue followed by apoptosis of myofibroblasts in response to injury, the Thy-1^{pos} phenotype may play a critical role in reparative fibrosis, namely the eventual cessation of fibrogenesis, which is lacking in IPF. This also suggests that persistence of the Thy-1^{neg} subpopulation, resulting in continual and largely ECM rigidity-independent ECM assembly and remodeling, may be pathologically relevant to the formation and persistence of fibroblastic foci. Together with the *in vivo* knowledge of repressed Thy-1 expression due to promoter hypermethylation specifically within fibroblastic foci versus both adjacent normal and mature fibrotic tissue, this suggests an intriguing "cause and effect" of Thy-1 regulation, specifically within fibroblastic foci (Sanders, Pardo et al. 2008). Although the *in vivo* consequences of the established phenotypes are speculative, this represents a radical paradigm shift in the phenotypes and microenvironmental cues implicated in progressive fibrotic disorders. Namely, this suggests that investigation of pro-fibrotic phenotypes within microenvironments not associated with mature or previously established fibrosis, but instead with recent wound healing or new/ongoing fibrosis, is essential. This suggests that fibroblast phenotypes investigated in rigid environments, even those between 7-20 kPa (on the low end of the *in vivo* fibrotic regime), may not reveal mechanisms critical to IPF pathogenesis (i.e. fibroblastic foci), but instead mechanisms reactive to *de novo* fibrotic remodeling. Thus phenotypes should be studied in soft environments, similar to normal tissue and early provisional matrices, to discover potentially causative mechanisms in fibroblastic foci formation and IPF pathogenesis. This represents a drastic change in the field, as most research is currently focused on understanding the mechanisms by which stiff ECM promotes fibroblast activation. In contrast, understanding how changes in fibroblast phenotype within soft ECMs results in

ECM assembly, remodeling, and eventual stiffening of the microenvironment should be a focus of future research.

In this work we also identify a unique complex formed between the GPI-anchored glycoprotein Thy-1 and αvβ3 integrin. This complex was formed via Thy-1's Arg-Leu-Asp integrin-binding motif in *cis* within the plasma membrane of fibroblasts. Furthermore, this interaction did not take place with extended or active integrin, and was preferential for cells not binding to ECM (i.e. more Thy-1-αvβ3 association with cells in suspension vs. spreading on Fn). These data, together with the knowledge that ECM binding and mechanosignaling is associated with extended integrin within FAs, this suggests that the Thy-1-integrin complex is formed upstream of ECM binding. Furthermore, experiments analyzing the spatial localization of Thy-1-αvβ3 complexes with respect to paxillin-marked FAs demonstrate that, indeed, such complexes appear to be preferentially formed outside FAs. Together with the role of Thy-1's integrin-binding motif and lipid raft targeting in mediating Fyn recruitment, force-dependent RhoA activation, and rigidity sensing, this suggests a functional importance for this upstream complex. Thus, we suggest this constitutes a protein complex upstream of integrin-ECM bonds that modulates downstream mechanosignaling. One importance for such a complex might be to spatially couple associated signaling molecules to inactive receptors, such that in response to ligand-induced activation, receptors can rapidly generate downstream signals; potentially critical for receptors that lack intrinsic enzymatic activity, such as integrins. Intriguingly, multiple lipid raft-associated outer membrane proteins, including uPAR, GPI-80, and CD47, have been shown to associate with integrin in *cis* and alter its signaling function (Wei, Lukashev et al. 1996, Brown and Frazier 2001, Yoshitake, Takeda et al. 2003, Wei, Czekay et al. 2005). Although the molecular details of these complexes are not known, it invites questions as to whether these complexes have a similar structure-function, and why lipid raft-associated (more

specifically GPI-anchored proteins) are utilized in this function? Intriguingly, as many of these interactions appear sensitive to integrin conformation, this provides a mechanism to switch from the composition and activity of upstream complexes (i.e. prior to ECM ligation), via conformational changes in integrin and integrin-associated proteins, to specific downstream associations.

Thy-1 also binds heparin sulfate proteoglycans, including syndecan-4, through a conserved polycationic motif in the C-C' strand loop motif (Avalos, Valdivia et al. 2009). We have discovered a novel *trans* interaction between syndecan-4 and Thy-1 involving α5β1 integrin (V. Fiore and L. Ju, unpublished data). Both receptors independently bind to Thy-1; however in the presence of both $\alpha_5\beta_1$ and syndecan-4, the two receptors bind cooperatively to Thy-1 to form a trimolecular complex. This complex displays prolongation of bond lifetimes under force, or catch bonds, and a unique phenomenon characterized by abrupt bond stiffening. Both α5β1 and syndecan-4 receptors are proficient at supporting adhesion and myosin II contractility-dependent signaling of melanoma cells on Thy-1 *in vitro*. Thus, it appears that complex and so far under-appreciated interactions between Thy-1 (and potentially other *cis*/*trans*-acting integrin-binding proteins), integrins and their co-receptors exist. This is especially intriguing in the context of syndecans as co-receptors of integrins, as these receptors bind a similar repertoire of ligands and are known to signal in a coordinated fashion. However, the molecular details of this synergy are as yet unknown. As trimolecular complexes between integrin, syndecan, and Thy-1 can form under short timescales, Thy-1 may be hypothetically viewed as a molecular bridge between these co-receptors. In contrast, during stable and close contact between integrins and the substratum, the large size of heparin sulfate glycosaminoglycan chains are expected to segregate syndecans from the integrin core, acting as an additional control element for spatial and temporal signaling sensitivity (Paszek, Boettiger et al. 2009, Roper, Williamson et al. 2012). As are the

bonds between integrins and their ligands, FA-associated molecules during their assembly and turnover, and the mobility of membrane-tethered proteins, these interactions are likely to be quite dynamic. Thus the further study and mechanistic understanding of these complexes should be undertaken at nano spatial- and sub-second time-scales, which is already underway.

With this work, we aimed at interrogating multiple length scales relevant to complex multi-cellular organisms, namely the tissue, cell and molecule. While the goal of connecting molecular mechanisms guiding cell phenotype *in vitro* to tissue-level regulators of cell phenotype *in vivo* (and *vice versa*) exists, mechanistically validating such connections among diverse length scales and microenvironmental inputs (i.e. mechanical, chemical) is a challenge. However, this challenge is worthy of approach. For example, in this study – although we were able to characterize the phenotype of one histologically-validated marker of disease-associated fibroblast subpopulation within the context of the *in vivo* microenvironment, and to describe a mechanism demonstrating Thy-1 as regulator of mechanotransductory phenotype – we have not thoroughly validated *in vitro* findings to the *in vivo* pathophysiology. Further studies should thoroughly validate Thy-1^{neg} IPFLFs as the *bona fide* fibroblastic foci-resident cell phenotype; this should be approached using laser capture microdissection of *in vivo* histologic features, along with gene expression profiling for comparison with *in vitro* cultures. In general, this approach can help validate or disprove certain *in vitro* culture methods and/or models as reliable predictors of *in vivo* physiology. Furthermore, investigation of the mechanical properties specific to fibroblastic foci and other unique histological features, via correlative histology and AFM force mapping, should be done to further connect cell and tissue phenotype with microenvironmental mechanics. Acknowledging the challenge of describing such processes at the multi-scale and multi-

parameter levels, this is a necessary undertaking for the future progress in human physiology and medicine.

REFERENCES

Alland, L., S. M. Peseckis, R. E. Atherton, L. Berthiaume and M. D. Resh (1994). "Dual myristylation and palmitylation of Src family member p59fyn affects subcellular localization." J Biol Chem **269**(24): 16701-16705.

Aratyn-Schaus, Y. and M. L. Gardel (2010). "Transient frictional slip between integrin and the ECM in focal adhesions under myosin II tension." Curr Biol **20**(13): 1145-1153.

Aratyn-Schaus, Y., P. W. Oakes and M. L. Gardel (2011). "Dynamic and structural signatures of lamellar actomyosin force generation." Mol Biol Cell **22**(8): 1330-1339.

Arias-Salgado, E. G., S. Lizano, S. Sarkar, J. S. Brugge, M. H. Ginsberg and S. J. Shattil (2003). "Src kinase activation by direct interaction with the integrin beta cytoplasmic domain." Proc Natl Acad Sci U S A **100**(23): 13298-13302.

Arias-Salgado, E. G., S. Lizano, S. J. Shattil and M. H. Ginsberg (2005). "Specification of the direction of adhesive signaling by the integrin beta cytoplasmic domain." J Biol Chem **280**(33): 29699-29707.

Askari, J. A., C. J. Tynan, S. E. Webb, M. L. Martin-Fernandez, C. Ballestrem and M. J. Humphries (2010). "Focal adhesions are sites of integrin extension." J Cell Biol **188**(6): 891-903.

Avalos, A. M., A. D. Valdivia, N. Munoz, R. Herrera-Molina, J. C. Tapia, S. Lavandero, M. Chiong, K. Burridge, P. Schneider, A. F. Quest and L. Leyton (2009). "Neuronal Thy-1 induces astrocyte adhesion by engaging syndecan-4 in a cooperative interaction with alphavbeta3 integrin that activates PKCalpha and RhoA." J Cell Sci **122**(Pt 19): 3462-3471.

Balaban, N. Q., U. S. Schwarz, D. Riveline, P. Goichberg, G. Tzur, I. Sabanay, D. Mahalu, S. Safran, A. Bershadsky, L. Addadi and B. Geiger (2001). "Force and focal adhesion assembly: a close relationship studied using elastic micropatterned substrates." Nat Cell Biol **3**(5): 466-472.

Balestrini, J. L., S. Chaudhry, V. Sarrazy, A. Koehler and B. Hinz (2012). "The mechanical memory of lung myofibroblasts." Integr Biol (Camb) **4**(4): 410-421.

Barboni, E., B. P. Rivero, A. J. George, S. R. Martin, D. V. Renoup, E. F. Hounsell, P. C. Barber and R. J. Morris (1995). "The glycophosphatidylinositol anchor affects the conformation of Thy-1 protein." J Cell Sci **108 (Pt 2)**: 487-497.

Barker, T. H., H. E. Grenett, M. W. MacEwen, S. G. Tilden, G. M. Fuller, J. Settleman, A. Woods, J. Murphy-Ullrich and J. S. Hagood (2004). "Thy-1 regulates fibroblast focal adhesions, cytoskeletal organization and migration through modulation of p190 RhoGAP and Rho GTPase activity." Exp Cell Res **295**(2): 488-496.

Barker, T. H. and J. S. Hagood (2009). "Getting a grip on Thy-1 signaling." Biochim Biophys Acta **1793**(5): 921-923.

Barker, T. H., M. A. Pallero, M. W. MacEwen, S. G. Tilden, A. Woods, J. E. Murphy-Ullrich and J. S. Hagood (2004). "Thrombospondin-1-induced focal adhesion disassembly in fibroblasts requires Thy-1 surface expression, lipid raft integrity, and Src activation." J Biol Chem **279**(22): 23510-23516.

Barry-Hamilton, V., R. Spangler, D. Marshall, S. McCauley, H. M. Rodriguez, M. Oyasu, A. Mikels, M. Vaysberg, H. Ghermazien, C. Wai, C. A. Garcia, A. C. Velayo, B. Jorgensen, D. Biermann, D. Tsai, J. Green, S. Zaffryar-Eilot, A. Holzer, S. Ogg, D. Thai, G. Neufeld, P. Van Vlasselaer and V. Smith (2010). "Allosteric inhibition of lysyl oxidase-like-2 impedes the development of a pathologic microenvironment." Nat Med **16**(9): 1009-1017.

Bhadriraju, K., M. Yang, S. Alom Ruiz, D. Pirone, J. Tan and C. S. Chen (2007). "Activation of ROCK by RhoA is regulated by cell adhesion, shape, and cytoskeletal tension." Exp Cell Res **313**(16): 3616-3623.

Bitterman, P. B. and C. A. Henke (1991). "Fibroproliferative disorders." Chest **99**(3 Suppl): 81S-84S.

Boettiger, D. (2012). "Mechanical control of integrin-mediated adhesion and signaling." Curr Opin Cell Biol **24**(5): 592-599.

Booth, A. J., R. Hadley, A. M. Cornett, A. A. Dreffs, S. A. Matthes, J. L. Tsui, K. Weiss, J. C. Horowitz, V. F. Fiore, T. H. Barker, B. B. Moore, F. J. Martinez, L. E. Niklason and E. S. White (2012). "Acellular normal and fibrotic human lung matrices as a culture system for in vitro investigation." Am J Respir Crit Care Med **186**(9): 866-876.

Bradley, J. E., G. Ramirez and J. S. Hagood (2009). "Roles and regulation of Thy-1, a context-dependent modulator of cell phenotype." Biofactors **35**(3): 258-265.

Brown, A. C., V. F. Fiore, T. A. Sulchek and T. H. Barker (2013). "Physical and chemical microenvironmental cues orthogonally control the degree and duration of fibrosis-associated epithelial-to-mesenchymal transitions." J Pathol **229**(1): 25-35.

Brown, E. J. and W. A. Frazier (2001). "Integrin-associated protein (CD47) and its ligands." Trends Cell Biol **11**(3): 130-135.

Brown, M. T. and J. A. Cooper (1996). "Regulation, substrates and functions of src." Biochim Biophys Acta **1287**(2-3): 121-149.

Butcher, D. T., T. Alliston and V. M. Weaver (2009). "A tense situation: forcing tumour progression." Nat Rev Cancer **9**(2): 108-122.

Butler, J. P., M. Nakamura, H. Sasaki, T. Sasaki and T. Takishima (1986). "Poissons' ratio of lung parenchyma and parenchymal interaction with bronchi." Jpn J Physiol **36**(1): 91-106.

Calderwood, D. A., R. Zent, R. Grant, D. J. Rees, R. O. Hynes and M. H. Ginsberg (1999). "The Talin head domain binds to integrin beta subunit cytoplasmic tails and regulates integrin activation." J Biol Chem **274**(40): 28071-28074.

Campbell, D. G., J. Gagnon, K. B. Reid and A. F. Williams (1981). "Rat brain Thy-1 glycoprotein. The amino acid sequence, disulphide bonds and an unusual hydrophobic region." Biochem J **195**(1): 15-30.

Carraher, C. L. and J. E. Schwarzbauer (2013). "Regulation of matrix assembly through rigidity-dependent fibronectin conformational changes." J Biol Chem **288**(21): 14805-14814.

Chang, H. Y., J. T. Chi, S. Dudoit, C. Bondre, M. van de Rijn, D. Botstein and P. O. Brown (2002). "Diversity, topographic differentiation, and positional memory in human fibroblasts." Proc Natl Acad Sci U S A **99**(20): 12877-12882.

Chen, Y., W. R. Thelin, B. Yang, S. L. Milgram and K. Jacobson (2006). "Transient anchorage of cross-linked glycosyl-phosphatidylinositol-anchored proteins depends on cholesterol, Src family kinases, caveolin, and phosphoinositides." J Cell Biol **175**(1): 169-178.

Choi, C. K., M. Vicente-Manzanares, J. Zareno, L. A. Whitmore, A. Mogilner and A. R. Horwitz (2008). "Actin and alpha-actinin orchestrate the assembly and maturation of nascent adhesions in a myosin II motor-independent manner." Nat Cell Biol **10**(9): 1039-1050.

Choquet, D., D. P. Felsenfeld and M. P. Sheetz (1997). "Extracellular matrix rigidity causes strengthening of integrin-cytoskeleton linkages." Cell **88**(1): 39-48.

Chrzanowska-Wodnicka, M. and K. Burridge (1996). "Rho-stimulated contractility drives the formation of stress fibers and focal adhesions." J Cell Biol **133**(6): 1403-1415.

Cohen, P. Y., R. Breuer and S. B. Wallach-Dayan (2009). "Thy1 up-regulates FasL expression in lung myofibroblasts via Src family kinases." Am J Respir Cell Mol Biol **40**(2): 231-238.

Crouch, E. (1990). "Pathobiology of pulmonary fibrosis." Am J Physiol **259**(4 Pt 1): L159-184.

Cukierman, E., R. Pankov, D. R. Stevens and K. M. Yamada (2001). "Taking cell-matrix adhesions to the third dimension." Science **294**(5547): 1708-1712.

del Pozo, M. A., N. B. Alderson, W. B. Kiosses, H. H. Chiang, R. G. Anderson and M. A. Schwartz (2004). "Integrins regulate Rac targeting by internalization of membrane domains." Science **303**(5659): 839-842.

del Rio, A., R. Perez-Jimenez, R. Liu, P. Roca-Cusachs, J. M. Fernandez and M. P. Sheetz (2009). "Stretching single talin rod molecules activates vinculin binding." Science **323**(5914): 638-641.

Discher, D. E., P. Janmey and Y. L. Wang (2005). "Tissue cells feel and respond to the stiffness of their substrate." Science **310**(5751): 1139-1143.

Dolhnikoff, M., T. Mauad and M. S. Ludwig (1999). "Extracellular matrix and oscillatory mechanics of rat lung parenchyma in bleomycin-induced fibrosis." Am J Respir Crit Care Med **160**(5 Pt 1): 1750-1757.

Draberova, L. and P. Draber (1993). "Thy-1 glycoprotein and src-like protein-tyrosine kinase p53/p56lyn are associated in large detergent-resistant complexes in rat basophilic leukemia cells." Proc Natl Acad Sci U S A **90**(8): 3611-3615.

Driskell, R. R., B. M. Lichtenberger, E. Hoste, K. Kretzschmar, B. D. Simons, M. Charalambous, S. R. Ferron, Y. Herault, G. Pavlovic, A. C. Ferguson-Smith and F. M. Watt (2013). "Distinct fibroblast lineages determine dermal architecture in skin development and repair." Nature **504**(7479): 277-281.

Du, X., M. Gu, J. W. Weisel, C. Nagaswami, J. S. Bennett, R. Bowditch and M. H. Ginsberg (1993). "Long range propagation of conformational changes in integrin alpha IIb beta 3." J Biol Chem **268**(31): 23087-23092.

Dumbauld, D. W., T. T. Lee, A. Singh, J. Scrimgeour, C. A. Gersbach, E. A. Zamir, J. Fu, C. S. Chen, J. E. Curtis, S. W. Craig and A. J. Garcia (2013). "How vinculin regulates force transmission." Proc Natl Acad Sci U S A **110**(24): 9788-9793.

Ebihara, T., N. Venkatesan, R. Tanaka and M. S. Ludwig (2000). "Changes in extracellular matrix and tissue viscoelasticity in bleomycin-induced lung fibrosis. Temporal aspects." Am J Respir Crit Care Med **162**(4 Pt 1): 1569-1576.

Eggeling, C., C. Ringemann, R. Medda, G. Schwarzmann, K. Sandhoff, S. Polyakova, V. N. Belov, B. Hein, C. von Middendorff, A. Schonle and S. W. Hell (2009). "Direct observation of the nanoscale dynamics of membrane lipids in a living cell." Nature **457**(7233): 1159-1162.

Ehrlicher, A. J., F. Nakamura, J. H. Hartwig, D. A. Weitz and T. P. Stossel (2011). "Mechanical strain in actin networks regulates FilGAP and integrin binding to filamin A." Nature **478**(7368): 260-263.

Engler, A. J., M. A. Griffin, S. Sen, C. G. Bonnemann, H. L. Sweeney and D. E. Discher (2004). "Myotubes differentiate optimally on substrates with tissue-like stiffness:

pathological implications for soft or stiff microenvironments." J Cell Biol **166**(6): 877-887.

Engler, A. J., S. Sen, H. L. Sweeney and D. E. Discher (2006). "Matrix elasticity directs stem cell lineage specification." Cell **126**(4): 677-689.

Fehrenbach, H. (2001). "Alveolar epithelial type II cell: defender of the alveolus revisited." Respir Res **2**(1): 33-46.

Friedland, J. C., M. H. Lee and D. Boettiger (2009). "Mechanically activated integrin switch controls alpha5beta1 function." Science **323**(5914): 642-644.

Fries, K. M., T. Blieden, R. J. Looney, G. D. Sempowski, M. R. Silvera, R. A. Willis and R. P. Phipps (1994). "Evidence of fibroblast heterogeneity and the role of fibroblast subpopulations in fibrosis." Clin Immunol Immunopathol **72**(3): 283-292.

Fritsch, C., V. Orian-Rousseaul, O. Lefebvre, P. Simon-Assmann, J. M. Reimund, B. Duclos and M. Kedinger (1999). "Characterization of human intestinal stromal cell lines: response to cytokines and interactions with epithelial cells." Exp Cell Res **248**(2): 391-406.

Fuchs, E. and S. Raghavan (2002). "Getting under the skin of epidermal morphogenesis." Nat Rev Genet **3**(3): 199-209.

Fust, A., J. H. Bates and M. S. Ludwig (2004). "Mechanical properties of mouse distal lung: in vivo versus in vitro comparison." Respir Physiol Neurobiol **143**(1): 77-86.

Galbraith, C. G., K. M. Yamada and J. A. Galbraith (2007). "Polymerizing actin fibers position integrins primed to probe for adhesion sites." Science **315**(5814): 992-995.

Galbraith, C. G., K. M. Yamada and M. P. Sheetz (2002). "The relationship between force and focal complex development." J Cell Biol **159**(4): 695-705.

Garcia-Alvarez, B., J. M. de Pereda, D. A. Calderwood, T. S. Ulmer, D. Critchley, I. D. Campbell, M. H. Ginsberg and R. C. Liddington (2003). "Structural determinants of integrin recognition by talin." Mol Cell **11**(1): 49-58.

Gardel, M. L., I. C. Schneider, Y. Aratyn-Schaus and C. M. Waterman (2010). "Mechanical integration of actin and adhesion dynamics in cell migration." Annu Rev Cell Dev Biol **26**: 315-333.

Gaus, K., S. Le Lay, N. Balasubramanian and M. A. Schwartz (2006). "Integrin-mediated adhesion regulates membrane order." J Cell Biol **174**(5): 725-734.

Geiger, B., J. P. Spatz and A. D. Bershadsky (2009). "Environmental sensing through focal adhesions." Nat Rev Mol Cell Biol **10**(1): 21-33.

Geiger, B. and K. M. Yamada (2011). "Molecular architecture and function of matrix adhesions." Cold Spring Harb Perspect Biol **3**(5).

Ghosh, A. K., S. E. Quaggin and D. E. Vaughan (2013). "Molecular basis of organ fibrosis: potential therapeutic approaches." Exp Biol Med (Maywood) **238**(5): 461-481.

Giannone, G. and M. P. Sheetz (2006). "Substrate rigidity and force define form through tyrosine phosphatase and kinase pathways." Trends Cell Biol **16**(4): 213-223.

Goetz, J. G., S. Minguet, I. Navarro-Lerida, J. J. Lazcano, R. Samaniego, E. Calvo, M. Tello, T. Osteso-Ibanez, T. Pellinen, A. Echarri, A. Cerezo, A. J. Klein-Szanto, R. Garcia, P. J. Keely, P. Sanchez-Mateos, E. Cukierman and M. A. Del Pozo (2011). "Biomechanical remodeling of the microenvironment by stromal caveolin-1 favors tumor invasion and metastasis." Cell **146**(1): 148-163.

Goffin, J. M., P. Pittet, G. Csucs, J. W. Lussi, J. J. Meister and B. Hinz (2006). "Focal adhesion size controls tension-dependent recruitment of alpha-smooth muscle actin to stress fibers." J Cell Biol **172**(2): 259-268.

Goswami, D., K. Gowrishankar, S. Bilgrami, S. Ghosh, R. Raghupathy, R. Chadda, R. Vishwakarma, M. Rao and S. Mayor (2008). "Nanoclusters of GPI-anchored proteins are formed by cortical actin-driven activity." Cell **135**(6): 1085-1097.

Guilluy, C., V. Swaminathan, R. Garcia-Mata, E. T. O'Brien, R. Superfine and K. Burridge (2011). "The Rho GEFs LARG and GEF-H1 regulate the mechanical response to force on integrins." Nat Cell Biol **13**(6): 722-727.

Gurtner, G. C., S. Werner, Y. Barrandon and M. T. Longaker (2008). "Wound repair and regeneration." Nature **453**(7193): 314-321.

Hagood, J. S., J. A. Lasky, J. E. Nesbitt and P. Segarini (2001). "Differential expression, surface binding, and response to connective tissue growth factor in lung fibroblast subpopulations." Chest **120**(1 Suppl): 64S-66S.

Hagood, J. S., A. Mangalwadi, B. Guo, M. W. MacEwen, L. Salazar and G. M. Fuller (2002). "Concordant and discordant interleukin-1-mediated signaling in lung fibroblast thy-1 subpopulations." Am J Respir Cell Mol Biol **26**(6): 702-708.

Hagood, J. S., P. J. Miller, J. A. Lasky, A. Tousson, B. Guo, G. M. Fuller and J. C. McIntosh (1999). "Differential expression of platelet-derived growth factor-alpha receptor by Thy-1(-) and Thy-1(+) lung fibroblasts." Am J Physiol **277**(1 Pt 1): L218-224.

Hagood, J. S., P. Prabhakaran, P. Kumbla, L. Salazar, M. W. MacEwen, T. H. Barker, L. A. Ortiz, T. Schoeb, G. P. Siegal, C. B. Alexander, A. Pardo and M. Selman (2005). "Loss of fibroblast Thy-1 expression correlates with lung fibrogenesis." Am J Pathol **167**(2): 365-379.

Hardie, W. D., S. W. Glasser and J. S. Hagood (2009). "Emerging concepts in the pathogenesis of lung fibrosis." Am J Pathol **175**(1): 3-16.

Hermosilla, T., D. Munoz, R. Herrera-Molina, A. Valdivia, N. Munoz, S. U. Nham, P. Schneider, K. Burridge, A. F. Quest and L. Leyton (2008). "Direct Thy-1/alphaVbeta3 integrin interaction mediates neuron to astrocyte communication." Biochim Biophys Acta **1783**(6): 1111-1120.

Herrera-Molina, R., R. Frischknecht, H. Maldonado, C. I. Seidenbecher, E. D. Gundelfinger, C. Hetz, L. Aylwin Mde, P. Schneider, A. F. Quest and L. Leyton (2012). "Astrocytic alphaVbeta3 integrin inhibits neurite outgrowth and promotes retraction of neuronal processes by clustering Thy-1." PLoS One **7**(3): e34295.

Hinz, B. (2010). "The myofibroblast: paradigm for a mechanically active cell." J Biomech **43**(1): 146-155.

Hinz, B., G. Celetta, J. J. Tomasek, G. Gabbiani and C. Chaponnier (2001). "Alpha-smooth muscle actin expression upregulates fibroblast contractile activity." Mol Biol Cell **12**(9): 2730-2741.

Hinz, B., S. H. Phan, V. J. Thannickal, M. Prunotto, A. Desmouliere, J. Varga, O. De Wever, M. Mareel and G. Gabbiani (2012). "Recent developments in myofibroblast biology: paradigms for connective tissue remodeling." Am J Pathol **180**(4): 1340-1355.

Hu, K., L. Ji, K. T. Applegate, G. Danuser and C. M. Waterman-Storer (2007). "Differential transmission of actin motion within focal adhesions." Science **315**(5808): 111-115.

Huang, X., N. Yang, V. F. Fiore, T. H. Barker, Y. Sun, S. W. Morris, Q. Ding, V. J. Thannickal and Y. Zhou (2012). "Matrix stiffness-induced myofibroblast differentiation is mediated by intrinsic mechanotransduction." Am J Respir Cell Mol Biol **47**(3): 340-348.

Hudon-David, F., F. Bouzeghrane, P. Couture and G. Thibault (2007). "Thy-1 expression by cardiac fibroblasts: lack of association with myofibroblast contractile markers." J Mol Cell Cardiol **42**(5): 991-1000.

Humphries, J. D., A. Byron, M. D. Bass, S. E. Craig, J. W. Pinney, D. Knight and M. J. Humphries (2009). "Proteomic analysis of integrin-associated complexes identifies RCC2 as a dual regulator of Rac1 and Arf6." Sci Signal **2**(87): ra51.

Hynes, R. O. (2002). "Integrins: bidirectional, allosteric signaling machines." Cell **110**(6): 673-687.

Hynes, R. O. (2009). "The extracellular matrix: not just pretty fibrils." Science **326**(5957): 1216-1219.

Idiopathic Pulmonary Fibrosis Clinical Research, N., G. Raghu, K. J. Anstrom, T. E. King, Jr., J. A. Lasky and F. J. Martinez (2012). "Prednisone, azathioprine, and N-acetylcysteine for pulmonary fibrosis." N Engl J Med **366**(21): 1968-1977.

Ingber, D. E. (2003). "Tensegrity I. Cell structure and hierarchical systems biology." J Cell Sci **116**(Pt 7): 1157-1173.

Jiang, G., A. H. Huang, Y. Cai, M. Tanase and M. P. Sheetz (2006). "Rigidity sensing at the leading edge through alphavbeta3 integrins and RPTPalpha." Biophys J **90**(5): 1804-1809.

Johnson, C. P., H. Y. Tang, C. Carag, D. W. Speicher and D. E. Discher (2007). "Forced unfolding of proteins within cells." Science **317**(5838): 663-666.

Kanchanawong, P., G. Shtengel, A. M. Pasapera, E. B. Ramko, M. W. Davidson, H. F. Hess and C. M. Waterman (2010). "Nanoscale architecture of integrin-based cell adhesions." Nature **468**(7323): 580-584.

Katzenstein, A. L. and J. L. Myers (1998). "Idiopathic pulmonary fibrosis: clinical relevance of pathologic classification." Am J Respir Crit Care Med **157**(4 Pt 1): 1301-1315.

Kim, C., F. Ye and M. H. Ginsberg (2011). "Regulation of integrin activation." Annu Rev Cell Dev Biol **27**: 321-345.

King, T. E., Jr., A. Pardo and M. Selman (2011). "Idiopathic pulmonary fibrosis." Lancet **378**(9807): 1949-1961.

King, T. E., Jr., M. I. Schwarz, K. Brown, J. A. Tooze, T. V. Colby, J. A. Waldron, Jr., A. Flint, W. Thurlbeck and R. M. Cherniack (2001). "Idiopathic pulmonary fibrosis: relationship between histopathologic features and mortality." Am J Respir Crit Care Med **164**(6): 1025-1032.

Kis, K., X. Liu and J. S. Hagood (2011). "Myofibroblast differentiation and survival in fibrotic disease." Expert Rev Mol Med **13**: e27.

Klinghoffer, R. A., C. Sachsenmaier, J. A. Cooper and P. Soriano (1999). "Src family kinases are required for integrin but not PDGFR signal transduction." EMBO J **18**(9): 2459-2471.

Kong, F., A. J. Garcia, A. P. Mould, M. J. Humphries and C. Zhu (2009). "Demonstration of catch bonds between an integrin and its ligand." J Cell Biol **185**(7): 1275-1284.

Kong, F., Z. Li, W. M. Parks, D. W. Dumbauld, A. J. Garcia, A. P. Mould, M. J. Humphries and C. Zhu (2013). "Cyclic mechanical reinforcement of integrin-ligand interactions." Mol Cell **49**(6): 1060-1068.

Kostic, A. and M. P. Sheetz (2006). "Fibronectin rigidity response through Fyn and p130Cas recruitment to the leading edge." Mol Biol Cell **17**(6): 2684-2695.

Kuhn, C. and J. A. McDonald (1991). "The roles of the myofibroblast in idiopathic pulmonary fibrosis. Ultrastructural and immunohistochemical features of sites of active extracellular matrix synthesis." Am J Pathol **138**(5): 1257-1265.

Kuo, J. C., X. Han, C. T. Hsiao, J. R. Yates, 3rd and C. M. Waterman (2011). "Analysis of the myosin-II-responsive focal adhesion proteome reveals a role for beta-Pix in negative regulation of focal adhesion maturation." Nat Cell Biol **13**(4): 383-393.

Larsen, M., V. V. Artym, J. A. Green and K. M. Yamada (2006). "The matrix reorganized: extracellular matrix remodeling and integrin signaling." Curr Opin Cell Biol **18**(5): 463-471.

Legate, K. R. and R. Fassler (2009). "Mechanisms that regulate adaptor binding to beta-integrin cytoplasmic tails." J Cell Sci **122**(Pt 2): 187-198.

Leitinger, B. and N. Hogg (2002). "The involvement of lipid rafts in the regulation of integrin function." J Cell Sci **115**(Pt 5): 963-972.

Levental, K. R., H. Yu, L. Kass, J. N. Lakins, M. Egeblad, J. T. Erler, S. F. Fong, K. Csiszar, A. Giaccia, W. Weninger, M. Yamauchi, D. L. Gasser and V. M. Weaver (2009). "Matrix crosslinking forces tumor progression by enhancing integrin signaling." Cell **139**(5): 891-906.

Ley, S. C., M. Marsh, C. R. Bebbington, K. Proudfoot and P. Jordan (1994). "Distinct intracellular localization of Lck and Fyn protein tyrosine kinases in human T lymphocytes." J Cell Biol **125**(3): 639-649.

Leyton, L., P. Schneider, C. V. Labra, C. Ruegg, C. A. Hetz, A. F. Quest and C. Bron (2001). "Thy-1 binds to integrin beta(3) on astrocytes and triggers formation of focal contact sites." Curr Biol **11**(13): 1028-1038.

Lin, E. C., C. P. Carron, D. M. Meyer and J. W. Smith (1998). "A series of function blocking antibodies against the alpha v beta 3 integrin bind allosteric to the ligand binding site and induce ligand dissociation." Cell Adhes Commun **6**(6): 451-464.

Lingwood, D. and K. Simons (2007). "Detergent resistance as a tool in membrane research." Nat Protoc **2**(9): 2159-2165.

Lingwood, D. and K. Simons (2010). "Lipid rafts as a membrane-organizing principle." Science **327**(5961): 46-50.

Liu, F., J. D. Mih, B. S. Shea, A. T. Kho, A. S. Sharif, A. M. Tager and D. J. Tschumperlin (2010). "Feedback amplification of fibrosis through matrix stiffening and COX-2 suppression." J Cell Biol **190**(4): 693-706.

Luo, B. H., C. V. Carman and T. A. Springer (2007). "Structural basis of integrin regulation and signaling." Annu Rev Immunol **25**: 619-647.

Maaloum, M., P. Muller and M. P. Krafft (2002). "Monodisperse surface micelles of nonpolar amphiphiles in langmuir monolayers." Angew Chem Int Ed Engl **41**(22): 4331-4334.

Machacek, M., L. Hodgson, C. Welch, H. Elliott, O. Pertz, P. Nalbant, A. Abell, G. L. Johnson, K. M. Hahn and G. Danuser (2009). "Coordination of Rho GTPase activities during cell protrusion." Nature **461**(7260): 99-103.

Mapel, D. W., J. M. Samet and D. B. Coultas (1996). "Corticosteroids and the treatment of idiopathic pulmonary fibrosis. Past, present, and future." Chest **110**(4): 1058-1067.

McIntosh, J. C., J. S. Hagood, T. L. Richardson and J. W. Simecka (1994). "Thy1 (+) and (-) lung fibrosis subpopulations in LEW and F344 rats." Eur Respir J **7**(12): 2131-2138.

Miki, H., T. Mio, S. Nagai, Y. Hoshino, T. Nagao, M. Kitaichi and T. Izumi (2000). "Fibroblast contractility: usual interstitial pneumonia and nonspecific interstitial pneumonia." Am J Respir Crit Care Med **162**(6): 2259-2264.

Miyamoto, S., B. Z. Katz, R. M. Lafrenie and K. M. Yamada (1998). "Fibronectin and integrins in cell adhesion, signaling, and morphogenesis." Ann N Y Acad Sci **857**: 119-129.

Moore, S. W., P. Roca-Cusachs and M. P. Sheetz (2010). "Stretchy proteins on stretchy substrates: the important elements of integrin-mediated rigidity sensing." Dev Cell **19**(2): 194-206.

Mould, A. P., S. J. Barton, J. A. Askari, P. A. McEwan, P. A. Buckley, S. E. Craig and M. J. Humphries (2003). "Conformational changes in the integrin beta A domain provide a mechanism for signal transduction via hybrid domain movement." J Biol Chem **278**(19): 17028-17035.

Na, S., O. Collin, F. Chowdhury, B. Tay, M. Ouyang, Y. Wang and N. Wang (2008). "Rapid signal transduction in living cells is a unique feature of mechanotransduction." Proc Natl Acad Sci U S A **105**(18): 6626-6631.

Nicholson, A. G., L. G. Fulford, T. V. Colby, R. M. du Bois, D. M. Hansell and A. U. Wells (2002). "The relationship between individual histologic features and disease progression in idiopathic pulmonary fibrosis." Am J Respir Crit Care Med **166**(2): 173-177.

Nobes, C. D. and A. Hall (1995). "Rho, rac, and cdc42 GTPases regulate the assembly of multimolecular focal complexes associated with actin stress fibers, lamellipodia, and filopodia." Cell **81**(1): 53-62.

Oakes, P. W., Y. Beckham, J. Stricker and M. L. Gardel (2012). "Tension is required but not sufficient for focal adhesion maturation without a stress fiber template." J Cell Biol **196**(3): 363-374.

Palazzo, A. F., C. H. Eng, D. D. Schlaepfer, E. E. Marcantonio and G. G. Gundersen (2004). "Localized stabilization of microtubules by integrin- and FAK-facilitated Rho signaling." Science **303**(5659): 836-839.

Pampori, N., T. Hato, D. G. Stupack, S. Aidoudi, D. A. Cheresh, G. R. Nemerow and S. J. Shattil (1999). "Mechanisms and consequences of affinity modulation of integrin alpha(V)beta(3) detected with a novel patch-engineered monovalent ligand." J Biol Chem **274**(31): 21609-21616.

Pasapera, A. M., I. C. Schneider, E. Rericha, D. D. Schlaepfer and C. M. Waterman (2010). "Myosin II activity regulates vinculin recruitment to focal adhesions through FAK-mediated paxillin phosphorylation." J Cell Biol **188**(6): 877-890.

Paszek, M. J., D. Boettiger, V. M. Weaver and D. A. Hammer (2009). "Integrin clustering is driven by mechanical resistance from the glycocalyx and the substrate." PLoS Comput Biol **5**(12): e1000604.

Paszek, M. J. and V. M. Weaver (2004). "The tension mounts: mechanics meets morphogenesis and malignancy." J Mammary Gland Biol Neoplasia **9**(4): 325-342.

Paszek, M. J., N. Zahir, K. R. Johnson, J. N. Lakins, G. I. Rozenberg, A. Gefen, C. A. Reinhart-King, S. S. Margulies, M. Dembo, D. Boettiger, D. A. Hammer and V. M. Weaver (2005). "Tensional homeostasis and the malignant phenotype." Cancer Cell **8**(3): 241-254.

Pelham, R. J., Jr. and Y. Wang (1997). "Cell locomotion and focal adhesions are regulated by substrate flexibility." Proc Natl Acad Sci U S A **94**(25): 13661-13665.

Plotnikov, S. V., A. M. Pasapera, B. Sabass and C. M. Waterman (2012). "Force fluctuations within focal adhesions mediate ECM-rigidity sensing to guide directed cell migration." Cell **151**(7): 1513-1527.

Ponti, A., M. Machacek, S. L. Gupton, C. M. Waterman-Storer and G. Danuser (2004). "Two distinct actin networks drive the protrusion of migrating cells." Science **305**(5691): 1782-1786.

Pouwels, J., J. Nevo, T. Pellinen, J. Ylanne and J. Ivaska (2012). "Negative regulators of integrin activity." J Cell Sci **125**(Pt 14): 3271-3280.

Ramos, C., M. Montano, J. Garcia-Alvarez, V. Ruiz, B. D. Uhal, M. Selman and A. Pardo (2001). "Fibroblasts from idiopathic pulmonary fibrosis and normal lungs differ in growth rate, apoptosis, and tissue inhibitor of metalloproteinases expression." Am J Respir Cell Mol Biol **24**(5): 591-598.

Reddy, K. B., D. M. Smith and E. F. Plow (2008). "Analysis of Fyn function in hemostasis and alphaIIbbeta3-integrin signaling." J Cell Sci **121**(Pt 10): 1641-1648.

Rege, T. A. and J. S. Hagood (2006). "Thy-1 as a regulator of cell-cell and cell-matrix interactions in axon regeneration, apoptosis, adhesion, migration, cancer, and fibrosis." FASEB J **20**(8): 1045-1054.

Rege, T. A., M. A. Pallero, C. Gomez, H. E. Grenett, J. E. Murphy-Ullrich and J. S. Hagood (2006). "Thy-1, via its GPI anchor, modulates Src family kinase and focal adhesion kinase phosphorylation and subcellular localization, and fibroblast migration, in response to thrombospondin-1/hep I." Exp Cell Res **312**(19): 3752-3767.

Resh, M. D. (1994). "Myristylation and palmitylation of Src family members: the fats of the matter." Cell **76**(3): 411-413.

Ridley, A. J. and A. Hall (1992). "The small GTP-binding protein rho regulates the assembly of focal adhesions and actin stress fibers in response to growth factors." Cell **70**(3): 389-399.

Riveline, D., E. Zamir, N. Q. Balaban, U. S. Schwarz, T. Ishizaki, S. Narumiya, Z. Kam, B. Geiger and A. D. Bershadsky (2001). "Focal contacts as mechanosensors: externally applied local mechanical force induces growth of focal contacts by an mDia1-dependent and ROCK-independent mechanism." J Cell Biol **153**(6): 1175-1186.

Rolls, A., R. Shechter and M. Schwartz (2009). "The bright side of the glial scar in CNS repair." Nat Rev Neurosci **10**(3): 235-241.

Roper, J. A., R. C. Williamson and M. D. Bass (2012). "Syndecan and integrin interactomes: large complexes in small spaces." Curr Opin Struct Biol **22**(5): 583-590.

Rossier, O., V. Octeau, J. B. Sibarita, C. Leduc, B. Tessier, D. Nair, V. Gatterdam, O. Destaing, C. Albiges-Rizo, R. Tampe, L. Cognet, D. Choquet, B. Lounis and G. Giannone (2012). "Integrins beta1 and beta3 exhibit distinct dynamic nanoscale organizations inside focal adhesions." Nat Cell Biol **14**(10): 1057-1067.

Saalbach, A., U. F. Haustein and U. Anderegg (2000). "A ligand of human thy-1 is localized on polymorphonuclear leukocytes and monocytes and mediates the binding to activated thy-1-positive microvascular endothelial cells and fibroblasts." J Invest Dermatol **115**(5): 882-888.

Saalbach, A., G. Hildebrandt, U. F. Haustein and U. Anderegg (2002). "The Thy-1/Thy-1 ligand interaction is involved in binding of melanoma cells to activated Thy-1- positive microvascular endothelial cells." Microvasc Res **64**(1): 86-93.

Saalbach, A., A. Wetzel, U. F. Haustein, M. Sticherling, J. C. Simon and U. Anderegg (2005). "Interaction of human Thy-1 (CD 90) with the integrin alphavbeta3 (CD51/CD61): an important mechanism mediating melanoma cell adhesion to activated endothelium." Oncogene **24**(29): 4710-4720.

Saez, A., A. Buguin, P. Silberzan and B. Ladoux (2005). "Is the mechanical activity of epithelial cells controlled by deformations or forces?" Biophys J **89**(6): L52-54.

Sanders, Y. Y., P. Kumbla and J. S. Hagood (2007). "Enhanced myofibroblastic differentiation and survival in Thy-1(-) lung fibroblasts." Am J Respir Cell Mol Biol **36**(2): 226-235.

Sanders, Y. Y., A. Pardo, M. Selman, G. J. Nuovo, T. O. Tollefsbol, G. P. Siegal and J. S. Hagood (2008). "Thy-1 promoter hypermethylation: a novel epigenetic pathogenic mechanism in pulmonary fibrosis." Am J Respir Cell Mol Biol **39**(5): 610-618.

Sansores, R. H., A. Ramirez-Venegas, R. Perez-Padilla, M. Montano, C. Ramos, C. Becerril, M. Gaxiola, P. Pare and M. Selman (1996). "Correlation between pulmonary fibrosis and the lung pressure-volume curve." Lung **174**(5): 315-323.

Santhanam, L., E. C. Tuday, A. K. Webb, P. Dowzicky, J. H. Kim, Y. J. Oh, G. Sikka, M. Kuo, M. K. Halushka, A. M. Macgregor, J. Dunn, S. Gutbrod, D. Yin, A. Shoukas, D. Nyhan, N. A. Flavahan, A. M. Belkin and D. E. Berkowitz (2010). "Decreased S-nitrosylation of tissue transglutaminase contributes to age-related increases in vascular stiffness." Circ Res **107**(1): 117-125.

Schiller, H. B., M. R. Hermann, J. Polleux, T. Vignaud, S. Zanivan, C. C. Friedel, Z. Sun, A. Raducanu, K. E. Gottschalk, M. Thery, M. Mann and R. Fassler (2013). "beta1- and alphav-class integrins cooperate to regulate myosin II during rigidity sensing of fibronectin-based microenvironments." Nat Cell Biol **15**(6): 625-636.

Seong, J., S. Lu, M. Ouyang, H. Huang, J. Zhang, M. C. Frame and Y. Wang (2009). "Visualization of Src activity at different compartments of the plasma membrane by FRET imaging." Chem Biol **16**(1): 48-57.

Shan, B., J. S. Hagood, Y. Zhuo, H. T. Nguyen, M. MacEwen, G. F. Morris and J. A. Lasky (2010). "Thy-1 attenuates TNF-alpha-activated gene expression in mouse embryonic fibroblasts via Src family kinase." PLoS One **5**(7): e11662.

Sharma, P., R. Varma, R. C. Sarasij, Ira, K. Gousset, G. Krishnamoorthy, M. Rao and S. Mayor (2004). "Nanoscale organization of multiple GPI-anchored proteins in living cell membranes." Cell **116**(4): 577-589.

Shattil, S. J. (2005). "Integrins and Src: dynamic duo of adhesion signaling." Trends Cell Biol **15**(8): 399-403.

Shenoy-Scaria, A. M., L. K. Gauen, J. Kwong, A. S. Shaw and D. M. Lublin (1993). "Palmitylation of an amino-terminal cysteine motif of protein tyrosine kinases p56lck and p59fyn mediates interaction with glycosyl-phosphatidylinositol-anchored proteins." Mol Cell Biol **13**(10): 6385-6392.

Shima, T., S. Nada and M. Okada (2003). "Transmembrane phosphoprotein Cbp senses cell adhesion signaling mediated by Src family kinase in lipid rafts." Proc Natl Acad Sci U S A **100**(25): 14897-14902.

Simons, K. and M. J. Gerl (2010). "Revitalizing membrane rafts: new tools and insights." Nat Rev Mol Cell Biol **11**(10): 688-699.

Simons, K. and E. Ikonen (1997). "Functional rafts in cell membranes." Nature **387**(6633): 569-572.

Smilenov, L. B., A. Mikhailov, R. J. Pelham, E. E. Marcantonio and G. G. Gundersen (1999). "Focal adhesion motility revealed in stationary fibroblasts." Science **286**(5442): 1172-1174.

Soderberg, O., M. Gullberg, M. Jarvius, K. Ridderstrale, K. J. Leuchowius, J. Jarvius, K. Wester, P. Hydbring, F. Bahram, L. G. Larsson and U. Landegren (2006). "Direct observation of individual endogenous protein complexes in situ by proximity ligation." Nat Methods **3**(12): 995-1000.

Solon, J., I. Levental, K. Sengupta, P. C. Georges and P. A. Janmey (2007). "Fibroblast adaptation and stiffness matching to soft elastic substrates." Biophys J **93**(12): 4453-4461.

Sorrell, J. M. and A. I. Caplan (2004). "Fibroblast heterogeneity: more than skin deep." J Cell Sci **117**(Pt 5): 667-675.

Sorrell, J. M. and A. I. Caplan (2009). "Fibroblasts-a diverse population at the center of it all." Int Rev Cell Mol Biol **276**: 161-214.

Stefanova, I., V. Horejsi, I. J. Ansotegui, W. Knapp and H. Stockinger (1991). "GPI-anchored cell-surface molecules complexed to protein tyrosine kinases." Science **254**(5034): 1016-1019.

Stricker, J., Y. Aratyn-Schaus, P. W. Oakes and M. L. Gardel (2011). "Spatiotemporal constraints on the force-dependent growth of focal adhesions." Biophys J **100**(12): 2883-2893.

Swift, J., I. L. Ivanovska, A. Buxboim, T. Harada, P. C. Dingal, J. Pinter, J. D. Pajerowski, K. R. Spinler, J. W. Shin, M. Tewari, F. Rehfeldt, D. W. Speicher and D. E. Discher (2013). "Nuclear lamin-A scales with tissue stiffness and enhances matrix-directed differentiation." Science **341**(6149): 1240104.

Takagi, J., B. M. Petre, T. Walz and T. A. Springer (2002). "Global conformational rearrangements in integrin extracellular domains in outside-in and inside-out signaling." Cell **110**(5): 599-511.

Tee, S. Y., J. Fu, C. S. Chen and P. A. Janmey (2011). "Cell shape and substrate rigidity both regulate cell stiffness." Biophys J **100**(5): L25-27.

Thievessen, I., P. M. Thompson, S. Berlemont, K. M. Plevock, S. V. Plotnikov, A. Zemljic-Harpf, R. S. Ross, M. W. Davidson, G. Danuser, S. L. Campbell and C. M. Waterman (2013). "Vinculin-actin interaction couples actin retrograde flow to focal adhesions, but is dispensable for focal adhesion growth." J Cell Biol **202**(1): 163-177.

Thomas, S. M. and J. S. Brugge (1997). "Cellular functions regulated by Src family kinases." Annu Rev Cell Dev Biol **13**: 513-609.

Thomas, S. M., P. Soriano and A. Imamoto (1995). "Specific and redundant roles of Src and Fyn in organizing the cytoskeleton." Nature **376**(6537): 267-271.

Tiveron, M. C., E. Barboni, F. B. Pliego Rivero, A. M. Gormley, P. J. Seeley, F. Grosveld and R. Morris (1992). "Selective inhibition of neurite outgrowth on mature astrocytes by Thy-1 glycoprotein." Nature **355**(6362): 745-748.

Tiveron, M. C., M. Nosten-Bertrand, H. Jani, D. Garnett, E. M. Hirst, F. Grosveld and R. J. Morris (1994). "The mode of anchorage to the cell surface determines both the function and the membrane location of Thy-1 glycoprotein." J Cell Sci **107 (Pt 7)**: 1783-1796.

Tomasek, J. J., G. Gabbiani, B. Hinz, C. Chaponnier and R. A. Brown (2002). "Myofibroblasts and mechano-regulation of connective tissue remodelling." Nat Rev Mol Cell Biol **3**(5): 349-363.

Trichet, L., J. Le Digabel, R. J. Hawkins, S. R. Vedula, M. Gupta, C. Ribrault, P. Hersen, R. Voituriez and B. Ladoux (2012). "Evidence of a large-scale mechanosensing mechanism for cellular adaptation to substrate stiffness." Proc Natl Acad Sci U S A **109**(18): 6933-6938.

Tschumperlin, D. J., F. Liu and A. M. Tager (2013). "Biomechanical regulation of mesenchymal cell function." Curr Opin Rheumatol **25**(1): 92-100.

Tse, J. R. and A. J. Engler (2010). "Preparation of hydrogel substrates with tunable mechanical properties." Curr Protoc Cell Biol **Chapter 10**: Unit 10 16.

van den Bogaart, G., K. Meyenberg, H. J. Risselada, H. Amin, K. I. Willig, B. E. Hubrich, M. Dier, S. W. Hell, H. Grubmuller, U. Diederichsen and R. Jahn (2011). "Membrane protein sequestering by ionic protein-lipid interactions." Nature **479**(7374): 552-555.

van Zanten, T. S., A. Cambi, M. Koopman, B. Joosten, C. G. Figdor and M. F. Garcia-Parajo (2009). "Hotspots of GPI-anchored proteins and integrin nanoclusters function as nucleation sites for cell adhesion." Proc Natl Acad Sci U S A **106**(44): 18557-18562.

Vinogradova, O., A. Velyvis, A. Velyviene, B. Hu, T. Haas, E. Plow and J. Qin (2002). "A structural mechanism of integrin alpha(IIb)beta(3) "inside-out" activation as regulated by its cytoplasmic face." Cell **110**(5): 587-597.

Visscher, D. W. and J. L. Myers (2006). "Histologic spectrum of idiopathic interstitial pneumonias." Proc Am Thorac Soc **3**(4): 322-329.

von Wichert, G., G. Jiang, A. Kostic, K. De Vos, J. Sap and M. P. Sheetz (2003). "RPTP-alpha acts as a transducer of mechanical force on alphav/beta3-integrin-cytoskeleton linkages." J Cell Biol **161**(1): 143-153.

Wang, N., J. P. Butler and D. E. Ingber (1993). "Mechanotransduction across the cell surface and through the cytoskeleton." Science **260**(5111): 1124-1127.

Wang, Y., E. L. Botvinick, Y. Zhao, M. W. Berns, S. Usami, R. Y. Tsien and S. Chien (2005). "Visualizing the mechanical activation of Src." Nature **434**(7036): 1040-1045.

Wary, K. K., A. Mariotti, C. Zurzolo and F. G. Giancotti (1998). "A requirement for caveolin-1 and associated kinase Fyn in integrin signaling and anchorage-dependent cell growth." Cell **94**(5): 625-634.

Watanabe, N., P. Madaule, T. Reid, T. Ishizaki, G. Watanabe, A. Kakizuka, Y. Saito, K. Nakao, B. M. Jockusch and S. Narumiya (1997). "p140mDia, a mammalian homolog of Drosophila diaphanous, is a target protein for Rho small GTPase and is a ligand for profilin." EMBO J **16**(11): 3044-3056.

Wei, Y., R. P. Czekay, L. Robillard, M. C. Kugler, F. Zhang, K. K. Kim, J. P. Xiong, M. J. Humphries and H. A. Chapman (2005). "Regulation of alpha5beta1 integrin conformation and function by urokinase receptor binding." J Cell Biol **168**(3): 501-511.

Wei, Y., M. Lukashev, D. I. Simon, S. C. Bodary, S. Rosenberg, M. V. Doyle and H. A. Chapman (1996). "Regulation of integrin function by the urokinase receptor." Science **273**(5281): 1551-1555.

Wetzel, A., T. Chavakis, K. T. Preissner, M. Sticherling, U. F. Haustein, U. Anderegg and A. Saalbach (2004). "Human Thy-1 (CD90) on activated endothelial cells is a counterreceptor for the leukocyte integrin Mac-1 (CD11b/CD18)." J Immunol **172**(6): 3850-3859.

White, E. S., M. H. Lazar and V. J. Thannickal (2003). "Pathogenetic mechanisms in usual interstitial pneumonia/idiopathic pulmonary fibrosis." J Pathol **201**(3): 343-354.

White, E. S., V. J. Thannickal, S. L. Carskadon, E. G. Dickie, D. L. Livant, S. Markwart, G. B. Toews and D. A. Arenberg (2003). "Integrin alpha4beta1 regulates migration across basement membranes by lung fibroblasts: a role for phosphatase and tensin homologue deleted on chromosome 10." Am J Respir Crit Care Med **168**(4): 436-442.

Wipff, P. J., D. B. Rifkin, J. J. Meister and B. Hinz (2007). "Myofibroblast contraction activates latent TGF-beta1 from the extracellular matrix." J Cell Biol **179**(6): 1311-1323.

Wiseman, P. W., C. M. Brown, D. J. Webb, B. Hebert, N. L. Johnson, J. A. Squier, M. H. Ellisman and A. F. Horwitz (2004). "Spatial mapping of integrin interactions and

dynamics during cell migration by image correlation microscopy." J Cell Sci **117**(Pt 23): 5521-5534.

Wozniak, M. A., R. Desai, P. A. Solski, C. J. Der and P. J. Keely (2003). "ROCK-generated contractility regulates breast epithelial cell differentiation in response to the physical properties of a three-dimensional collagen matrix." J Cell Biol **163**(3): 583-595.

Wynn, T. A. (2007). "Common and unique mechanisms regulate fibrosis in various fibroproliferative diseases." J Clin Invest **117**(3): 524-529.

Xue, G. P., B. P. Rivero and R. J. Morris (1991). "The surface glycoprotein Thy-1 is excluded from growing axons during development: a study of the expression of Thy-1 during axogenesis in hippocampus and hindbrain." Development **112**(1): 161-176.

Yeung, T., P. C. Georges, L. A. Flanagan, B. Marg, M. Ortiz, M. Funaki, N. Zahir, W. Ming, V. Weaver and P. A. Janmey (2005). "Effects of substrate stiffness on cell morphology, cytoskeletal structure, and adhesion." Cell Motil Cytoskeleton **60**(1): 24-34.

Yoshitake, H., Y. Takeda, T. Nitto, F. Sendo and Y. Araki (2003). "GPI-80, a beta2 integrin associated glycosylphosphatidylinositol-anchored protein, concentrates on pseudopodia without association with beta2 integrin during neutrophil migration." Immunobiology **208**(4): 391-399.

Zhang, Q., M. K. Magnusson and D. F. Mosher (1997). "Lysophosphatidic acid and microtubule-destabilizing agents stimulate fibronectin matrix assembly through Rho-dependent actin stress fiber formation and cell contraction." Mol Biol Cell **8**(8): 1415-1425.

Zhong, C., M. Chrzanowska-Wodnicka, J. Brown, A. Shaub, A. M. Belkin and K. Burridge (1998). "Rho-mediated contractility exposes a cryptic site in fibronectin and induces fibronectin matrix assembly." J Cell Biol **141**(2): 539-551.

Zhou, Y., J. S. Hagood, B. Lu, W. D. Merryman and J. E. Murphy-Ullrich (2010). "Thy-1-integrin alphav beta5 interactions inhibit lung fibroblast contraction-induced latent transforming growth factor-beta1 activation and myofibroblast differentiation." J Biol Chem **285**(29): 22382-22393.

Zhou, Y., J. S. Hagood and J. E. Murphy-Ullrich (2004). "Thy-1 expression regulates the ability of rat lung fibroblasts to activate transforming growth factor-beta in response to fibrogenic stimuli." Am J Pathol **165**(2): 659-669.